ARR Nov. 1942

NATIONAL ADVISORY COMMITTEE FOR AERONAUTICS

WARTIME REPORT

ORIGINALLY ISSUED
November 1942 as
Advance Restricted Report

FULL-SCALE TUNNEL INVESTIGATION OF THE CONTROL AND STABILITY OF A TWIN-ENGINE MONOPLANE WITH PROPELLERS OPERATING

By Harold H. Sweberg

Langley Memorial Aeronautical Laboratory
Langley Field, Va.

130

NACA

WASHINGTON

NATIONAL ADVISORY COMMITTEE FOR AERONAUTICS

ADVANCE RESTRICTED REPORT

FULL-SCALE TUNNEL INVESTIGATION OF THE CONTROL AND STABILITY OF A TWIN-ENGINE MONOPLANE WITH PROPELLERS OPERATING

By Harold H. Sweberg

SUMMARY

Extensive force tests, covering a wide range of propeller thrust coefficients, have been made of a typical twin-engine tractor monoplane model with the horizontal tail surface removed and attached. Measurements were made with flaps retracted and deflected at various angles of attack with different stabilizer and elevator settings. The tests were made in the Committee's full-scale tunnel at the Langley Memorial Aeronautical Laboratory. The lift, drag, and pitching-moment characteristics of the model with propellers removed and operating are shown, together with values of the effective downwash angles at the tail obtained from the pitching-moment measurements. Values are also shown of the tail-surface effectiveness for the various model and propeller conditions. An attempt has been made to correlate the data of previous investigations of the isolated horizontal tail-surface characteristics and of the air flow in the region of the tail surfaces with the force measurements for the purpose of evaluating the various interference and slipstream effects.

INTRODUCTION

As part of a general investigation directed toward predicting the effects of propeller operation on the stability of various types of aircraft with various power-plant arrangements, extensive tests have been conducted in the NACA full-scale wind tunnel of a typical twin-engine tractor monoplane model. The tests included:

1. Air-flow surveys in the region of the tail plane (reference 1)

2. Force tests of the isolated horizontal tail surface (reference 2)

3. Force tests of the model with horizontal tail surfaces removed

4. Force tests of the complete model

The results of the force tests of the model with and without the horizontal tail are given in the present paper.

In the analysis, an attempt has been made to correlate the data of references 1 and 2 with the results presented herein for the purpose of evaluating the various interference and slipstream effects. Some comparisons of the experimental results with the existing theory of the phenomena involved are given.

SYMBOLS

L	lift
C_L	lift coefficient
c_l	section lift coefficient
C_m	pitching-moment coefficient
D'	propellers-removed drag
D_R	resultant drag with propellers operating
C_D	drag coefficient
C_n	yawing-moment coefficient
C_N	normal-force coefficient
C_c	chord-force coefficient
C_h	hinge-moment coefficient
T	propeller thrust
T_c	thrust coefficient $\left(\frac{\text{effective thrust}}{\rho V_o^2 D^2}\right)$

N_P	normal force acting on a propeller inclined to the air stream
C_{N_P}	propeller normal-force coefficient $\left(\frac{N_P}{\rho n^2 D^4}\right)$
a_o	lift-curve slope for infinite aspect ratio
ρ	air density
n	propeller rotational speed
V	local velocity
V_o	free-stream velocity
a	velocity-increment factor at propeller disk
s	velocity-increment factor back of the propeller disk
q	local dynamic pressure $\left(\frac{1}{2}\rho V^2\right)$
q_o	free-stream dynamic pressure $\left(\frac{1}{2}\rho V_o^2\right)$
$(q/q_o)_{av}$	ratio of average dynamic pressure at the tail, as found from air-flow surveys, to free-stream dynamic pressure
N	number of propellers
D	propeller diameter
S	wing area
b	span
$\bar{c}$	mean geometric chord
c_P	chord of wing directly behind the propeller axis
l_1	distance of quarter-chord line of horizontal tail surface from center of gravity of model, measured parallel to thrust axis
l_2	distance from elevator hinge line to the center of gravity of model, measured parallel to thrust axis

y	lateral distance from center line of model
x	distance from propeller disk to wing center of pressure
α	angle of attack
δ	deflection of movable tail surface
ϵ	downwash angle relative to free-stream direction
ϵ_{av}	average downwash angle at tail, as found from air-flow surveys
ϵ_{eff}	effective downwash angle at tail, as found by comparison of pitching moments with and without horizontal tail
χ	empirical factor used in formula for increase in lift of wing due to slipstream velocity

Subscripts:

w	wing
f	flap
P	propeller
T	thrust
s	slipstream
i	portion immersed in slipstream
t	tail
is	isolated tail surface
S	stabilizer
e	elevator
r	rudder
TR	trim

DESCRIPTION OF MODEL AND TESTS

The NACA full-scale tunnel is described in reference 3, and the methods by which the data were corrected for jet-boundary and blocking effects are discussed in references 4 and 5. The complete model is described in reference 1 and the isolated horizontal tail surface is described in reference 2, where it is referred to as the minimum-balance tail. A photograph of the model as mounted in the wind tunnel is given in figure 1. Sketches showing the important dimensions of the complete model are given in figure 2, and of the isolated horizontal tail surface in figure 3. The center-of-gravity location was arbitrarily assumed to be located along the fuselage center line at the wing-chord point. This assumption was necessary in order to obtain a reference point for the moment calculations.

The force tests included lift, drag, and pitching-moment measurements of the model both without the horizontal tail surface and with the horizontal tail surface with various settings of the stabilizer and elevator. Most of the tests included the effects of propeller operation and were made with flaps retracted and flaps deflected 50°. Some tests were made, with propellers removed, of the elevator hinge moments and rudder effectiveness. The effects of nacelles on the aerodynamic characteristics of the model with propellers removed were also investigated.

The thrust coefficient is defined as

$$T_c = \frac{\text{effective thrust}}{\rho V_o^2 D^2} = \frac{D' - D_R}{\rho V_o^2 D^2} \qquad (1)$$

where D' and D_R are both measured at zero lift coefficient. The thrust coefficient was determined as a function of V/nD for the flaps-retracted condition. Figure 4 shows the variation of propeller thrust coefficient with V/nD. For each angle of attack, the thrust was varied to include both high and low thrust coefficients; accordingly, the thrust coefficient at any particular angle of attack did not necessarily simulate a practical flight condition.

RESULTS AND DISCUSSION

The results of the tests have been analyzed in two parts. One part includes the effects of propeller operation on the forces of the wing-fuselage combination. The other part includes the effects of propeller operation on the forces and air flow at the tail and on the tail effectiveness. The second part also includes a discussion of the aerodynamic characteristics of the isolated horizontal tail surface and comparisons of the isolated and attached horizontal tail surface. The propeller forces have been taken into account in the discussion.

Effect of Propeller Operation on Wing-Fuselage Combination

The propellers-operating lift and pitching-moment coefficients for the model with the tail surfaces removed are plotted in figure 5 for the flaps-retracted condition and in figure 6 for the flaps-deflected condition. The effects of propeller operation on the forces of the wing-fuselage combination as shown in these figures include the direct effect of the propeller forces as well as the effects arising from the increased velocity and change in direction of the air flow at that part of the wing immersed in the slipstream.

Lift.- The increment of lift due to the components of the propeller forces acting in the lift direction is

$$\Delta L_p = T \sin \alpha_T + N_p \cos \alpha_T \qquad (2)$$

and

$$\Delta C_{L_p} = 2N \frac{D^2}{S} T_c \sin \alpha_T + 2N \frac{D^2}{S} \frac{C_{N_p} \cos \alpha_T}{\left(\frac{V}{nD}\right)^2} \qquad (3)$$

The second term of the right side of equation (3) (the lift increment due to the normal-force component of a propeller inclined in pitch) is usually negligible, although the pitching moment produced by it may be important. Methods for calculating this increment are given in reference 6.

For the increment of lift resulting from the passage

of the slipstream over a part of the wing, the semi-empirical formula of reference 7 has been found to give satisfactory results for a wing without flaps:

$$\Delta C_{L_s} = \frac{b_i c_p}{S} s \left[\lambda c_l - 0.6 a_o \epsilon_p \right] \tag{4}$$

In this expression c_l is the local lift coefficient, without slipstream, of the airfoil section at the propeller center line and b_i is the span of that portion of the wing immersed in the slipstream, which, for twin-engine operation, is taken here as

$$b_i = 2D \sqrt{\frac{1 + a}{1 + s}} \tag{5}$$

The velocity-increment factor back of the propeller disk, s, is given in reference 7 by the expression

$$s = a \left(1 + \frac{x}{\sqrt{\frac{D^2}{4} + x^2}} \right) \tag{6}$$

and the velocity-increment factor at the propeller disk, a, as determined from the momentum theory, is

$$a = -\frac{1}{2} + \frac{1}{2} \sqrt{1 + \frac{8T_c}{\pi}} \tag{7}$$

The term ϵ_p is the propeller downwash resulting from the inclination of the propeller axis to the direction of motion. If the effects of the viscous forces of the air stream are neglected, the propeller downwash angle is given in reference 7 as

$$\epsilon_p = \left(\frac{a}{1 + a} \right) \alpha_T \tag{8}$$

The factor λ, introduced because of the change in circulation over the wing, is plotted in figure 7 as a function of the aspect ratio of the part of the wing immersed in the slipstream. For twin-engine operation, the aspect ratio of the part of the wing immersed in the slipstream is taken, according to reference 7, as the ratio of the

distance between the outermost tips of the propellers and the chord of the wing directly behind the propeller center line. A comparison between the experimental lift coefficients and the values calculated from equations (3) and (4) for the flaps-retracted condition is given in figure 8. The agreement shown is good.

With flaps deflected, the values of λ shown in figure 7 do not hold, possibly because of the marked effect of the slipstream on the flapped-wing vortex system. It was noted in reference 7 that equation (4) gave good results for a model with flaps deflected if λ was multiplied by a factor of 1.4. Calculations of the propellers-operating lift coefficients using a value for λ from figure 7 multiplied by 1.4 showed satisfactory agreement with the experimental results at low angles of attack but were too high at the higher angles of attack (fig. 9).

Pitching moments.- Inasmuch as the thrust axis is slightly above the center of gravity, the thrust causes a small increment of diving moment (fig. 5) for the flaps-retracted condition. At high angles of attack this increment is neutralized to some extent by the positive moment due to the normal-force component of a propeller inclined in pitch. A few calculations showed that, for the flaps-retracted tail-removed condition, nearly all of the change of pitching moment could be accounted for by the propeller forces. The effect of the slipstream on the wing pitching-moment coefficient may therefore be considered negligible for this airplane.

Flap deflection caused a large increment of diving moment (fig. 6) which may be considered the result of the change in camber of the flapped portion of the wing. This increment of diving moment is further increased by propeller operation. The effect of slipstream on the pitching moment of the wing with flaps deflected may be considered as resulting from the change in wing lift and from the increase in the actual pitching moments of the flapped wing sections about their aerodynamic centers. The increment of lift due to the slipstream is assumed to be applied at the wing aerodynamic center, which for this model is approximately coincident with the assumed center-of-gravity location. The increment of pitching moment due to the wing-lift increment is therefore negligible. The effect of the slipstream on the wing pitching-moment coefficient with flaps deflected may be expressed as follows:

$$\Delta C_{m_s} = \Delta C_{m_f} \frac{S_{f_i}}{S_f} \frac{\bar{c}_{w_i}}{\bar{c}_w} \left(\frac{q}{q_o} - 1 \right) \qquad (9)$$

where ΔC_{m_f} is the propellers-removed increment of pitching-moment coefficient resulting from flap deflection and S_{f_i}/S_f is the ratio of the area of the flapped portion of the wing immersed in the slipstream to the flapped portion of the wing. If it is assumed that the velocity-increment factor back of the propeller disk is equal to 2a, equation (9) becomes

$$\Delta C_{m_s} = \Delta C_{m_f} \frac{S_{f_i}}{S_f} \frac{\bar{c}_{w_i}}{\bar{c}_w} \frac{8T_c}{\pi} \qquad (10)$$

A comparison is given in figure 10 of the experimental increment of pitching-moment coefficient due to the slipstream and the values calculated from equation (10) at $\alpha_T = 0^\circ$ and $\alpha_T = 10^\circ$ for $\delta_f = 50^\circ$. The agreement is good at $\alpha_T = 0^\circ$ but some discrepancy exists at $\alpha_T = 10^\circ$.

Forces and Air Flow at Tail

Tail surface characteristics, propellers removed.- The lift, drag, and pitching-moment coefficients of the model with the tail on and with the flaps retracted and deflected 50° are shown in figure 11. The results with the horizontal tail off are shown in figure 12.

For the complete model, tests were made to determine the effects of flaps, nacelles, and angle of attack on the elevator and stabilizer effectiveness. The results of the elevator-effectiveness tests are given in figures 13 through 16 and the results of the stabilizer-effectiveness tests are given in figures 17 and 18. The elevator effectiveness decreased or increased slightly with angle of attack as the horizontal tail advanced into or receded from the wake. An increase of about 7 percent of elevator effectiveness was measured when the flaps were deflected, which may be explained by the fact that the stronger downwash when the flaps are deflected carries the wake down so that the tail enters it only at the highest angle of attack. The stabilizer effectiveness showed no appreciable

change as a result of varying the angle of attack of the model or of deflecting the flaps, except at the stall. The addition of nacelles to the model resulted in little change of either stabilizer or elevator effectiveness.

The horizontal tail surface has an appreciable effect on the vertical tail-surface effectiveness. According to reference 8, the horizontal tail surface acts as an end plate for the vertical tail surface and increases the effective aspect ratio of the vertical tail. The variation of yawing-moment coefficient with rudder deflection is shown in figures 19 to 22 for the flaps-retracted and the flaps-deflected conditions and with the horizontal tail surface attached to the model and removed. The rudder effectiveness $dC_n/d\delta_r$ with the horizontal tail surface removed was estimated, according to reference 9, to be -0.00062 and, according to reference 8, to be increased to -0.00079 when the horizontal tail surface was attached to the model. These values are in close agreement with the experimental values. Flap deflection resulted in only a slight increase of rudder effectiveness.

The effect of deflecting one tail surface on the effectiveness of the other is shown in figures 23 and 24. The test results indicate that, for this type of empennage, the effectiveness of the horizontal tail surface is independent of the deflection of the vertical tail surface and vice versa.

The elevator angles for trim ($C_m = 0$) are shown in figure 25 for both the flaps-retracted and the flaps-deflected conditions. A maximum change of only about 2° elevator deflection was necessary to trim the model at any angle of attack as a result of deflecting the flaps. This small change of elevator deflection necessary to trim the model results from the increased downwash at the tail (caused by deflecting the flaps), which neutralized, to a large extent, the increment of negative pitching moment due to the flaps.

The horizontal tail surface used on this model was tested alone and the results of the tests have been reported in reference 2. A summary of the variation of normal-force coefficient and chord-force coefficient with tail angle of attack for elevator deflections from 0° to 30° is given in figure 26. The slopes $dC_{N_t}/d\delta_s$ and $dC_{N_t}/d\delta_e$ for the isolated horizontal tail surface were found to be 0.060 and 0.032, respectively.

A comparison of the isolated tail-surface parameters $dC_{N_t}/d\delta_e$ and $dC_{N_t}/d\delta_S$ with the corresponding values for the tail surface when attached to the model can be made by means of the following equations:

$$\frac{dC_{N_t}}{d\delta_S} = \frac{\frac{dC_m}{d\delta_S}}{\frac{q}{q_o}} \frac{S_w}{S_t} \frac{\bar{c}_w}{l_1} \tag{11}$$

and

$$\frac{dC_{N_t}}{d\delta_e} = \frac{\frac{dC_m}{d\delta_e}}{\frac{q}{q_o}} \frac{S_w}{S_t} \frac{\bar{c}_w}{l_2} \tag{12}$$

The distances l_1 and l_2 are, respectively, the distance from the quarter-chord point of the horizontal tail surface to the center of gravity of the model and the distance from the elevator hinge line to the center of gravity of the model. Values for the dynamic pressure ratio q/q_o have been obtained from the surveys of reference 1 and represent arithmetical averages. Table I gives values of $dC_{N_t}/d\delta_S$ and $dC_{N_t}/d\delta_e$ calculated from equations (11) and (12) for various angles of attack and model conditions, together with the corresponding values of $dC_m/d\delta_S$ and $dC_m/d\delta_e$ obtained from the test results. It will be noticed from table I that the values for the slope $dC_{N_t}/d\delta_e$ as calculated from the test results are in close agreement with the value measured for the isolated tail for most cases; the values, however, for $dC_{N_t}/d\delta_S$ are 4 to 20 percent lower than the value measured for the isolated tail. This discrepancy may be partly accounted for by the effective reduction of stabilizer area caused by the intersection of the fuselage and the stabilizer. A comparison of the experimental values of $dC_{N_t}/d\delta_S$ and $dC_{N_t}/d\delta_e$ for $\alpha_T = 0^\circ$ with values calculated from reference 10 is given in figures 27 and 28.

The variation of elevator hinge-moment coefficient with elevator deflection for the isolated and attached tail

($\alpha_T = 0^\circ$), together with the theoretical values computed from thin-airfoil theory, is shown in figure 29. The experimental values for the isolated and attached tail are in satisfactory agreement but are lower than the theoretical value.

Elevator effectiveness and dynamic pressure at tail, propellers operating.- The variation of pitching-moment coefficient with elevator angle for various angles of attack and thrust coefficients are given in figures 30 to 32 for the flaps-retracted condition and in figures 33 to 36 for the flaps-deflected condition. At constant thrust coefficient the elevator effectiveness increases with angle of attack. The reason for the increase of $dC_m/d\delta_e$ with angle of attack will be obvious when it is considered that the elevator hinge line is near the top of the slipstream at low angles of attack but progressively approaches the center of the slipstream as the angle of attack is increased (reference 1). The elevator effectiveness for the flaps-retracted condition is considerably higher than the elevator effectiveness for the flaps deflected condition. This result is due to the fact that the slipstream center line is depressed farther below the elevator hinge line with flaps deflected than with flaps retracted.

It has been shown that, with propellers removed, the elevator effectiveness is approximately proportional to the average dynamic-pressure ratio at the tail; that is,

$$\frac{dC_m}{d\delta_e} = \left(\frac{dC_m}{d\delta_e}\right)_{is} \left(\frac{q}{q_o}\right)_{av} \qquad (13)$$

Accordingly, for these conditions, the effective dynamic pressure approximately equals the average dynamic pressure. This proportionality no longer exists at the higher thrust coefficients; for such conditions, the effective dynamic pressure is less than the average found from the surveys. This effect is illustrated in table II, which gives a comparison between the measured $dC_m/d\delta_e$ and the values calculated from equation (13). The values of $(q/q_o)_{av}$ were obtained from the surveys of reference 1. Table II shows that the calculated values are about 10 percent higher than the experimental values for most cases. The difference between the measured and the calculated $dC_m/d\delta_e$ is probably due to the finite extent and nonuni-

formity of the slipstream. Previous tests of several types of airplanes (reference 11) showed a similar discrepancy between the measured elevator effectiveness and the elevator effectiveness calculated from equation (13) at high values of thrust coefficient. In figure 37 the measured $dC_m/d\delta_e$ has been plotted against the calculated value and a curve showing the relationship between the two has been obtained. This curve deviates from the theoretical 45° slope by approximately 11 percent.

Downwash at tail.- In reference 1 are given values of the average downwash at the tail, with propellers removed and operating, as determined from the surveys. From measurements of the pitching moments of the model with stabilizer set at various angles, a comparison has been made between the effective and the average downwash angles. The effective downwash angles were determined by comparing the values of angle of attack and stabilizer incidence for which the tail contributed zero pitching-moment coefficient.

Figures 17 and 18 give curves showing the variation of pitching-moment coefficient with stabilizer setting at various angles of attack for the propellers-removed condition. Values for ϵ_{eff} have been obtained from the curves of figures 17 and 18 and are compared with the values of ϵ_{av} obtained from the surveys of reference 1 for both the flaps-retracted and the flaps-deflected conditions in figure 38. The agreement between ϵ_{eff} and ϵ_{av} is good (within 1°).

The results of the stabilizer-effectiveness tests with propellers operating and with flaps retracted and deflected 50° are shown in figures 39 to 42. Table III gives a comparison between the effective downwash angles obtained from these figures and the average downwash angles obtained from the surveys of reference 1 for the flaps-retracted and flaps-deflected conditions. The agreement between the effective and the average downwash angles is satisfactory (within 1°) at low angles of attack; at high angles of attack, however, the effective downwash angles are somewhat lower than the average downwash angles. The reasons for the differences between ϵ_{eff} and ϵ_{av} at the high angles of attack are not very clear, but it is likely that the nonuniformity of the slipstream and the pulsation of the air flow may contribute to the low values of ϵ_{eff}.

A theoretical solution for the resultant downwash angle at the tail with propellers operating has been the subject of extensive research, but as yet no generally satisfactory method exists for its prediction. Several factors may influence the resultant angle of downwash at the tail, chief among which are the downwash due to the wing and the fuselage (propellers removed), the inclination of the thrust axis to the free-stream direction, the thrust, and the torque. From experimental data, an attempt has been made to study the order of magnitude of these various factors.

L-425

In references 1 and 12 comparisons are made between the average downwash angles at the tail as obtained from surveys (propellers removed) and the theoretical wing downwash angles computed from the charts of reference 13. The agreement shown between the average and the theoretical downwash angles was satisfactory, which indicates that the presence of the fuselage does not materially affect the downwash at the tail.

When propellers are operating, there exists an increment of downwash associated with the increment of lift at the wing and an increment of downwash associated with the vertical component of the propeller forces. The passage of slipstream over the wing may be considered to result in a change of the lift distribution over the wing, with a corresponding change of downwash. The vertical component of the propeller forces arises from the inclination of the propeller axis to the free-stream direction. Measurements by Stüper (reference 14) showed no appreciable variation in downwash as the angle of inclination of the propeller was varied with respect to the wing.

A further increment of downwash at the tail may exist as a result of the rotation imparted to the air stream by the propeller. For a twin-engine airplane operating at large torque coefficients, the slipstream rotation may have considerable influence on the downwash at the tail, depending on the direction of rotation of the propellers (references 15 and 16). For propellers rotating in the same direction (as for the case of this model), the downwash across one semispan of the horizontal tail surface will be greater than the downwash across the other semispan. The effect of slipstream rotation on the downwash distribution at the tail of this model is illustrated in figures 43 to 46 for the flaps-retracted and flaps-deflected conditions. The local downwash angles were ob-

tained from the surveys of reference 1. Since the span of the horizontal tail surface is approximately equal to the distance between propeller center lines, the horizontal tail is mainly affected by the flow from the inner halves of the two slipstreams. With flaps retracted, the downwash at the tail on the side affected by the upward strokes of the propeller blades was reduced, whereas the downwash at the tail on the side affected by the downward strokes of the propeller blades was increased. This effect was reversed when the flaps were deflected; that is, the downwash on the side of the upgoing blades was increased, whereas the downwash on the side of the downgoing blades was decreased. It appears, however, that the reduction of downwash on one side of the tail due to the upward components of the slipstream rotation is approximately equal to the increase of downwash on the other side due to the downward components of the slipstream rotation. The net effect of the slipstream rotation on the average downwash across the complete tail span of the model is therefore probably negligible.

Tail contribution, propellers operating.- The pitching-moment and the lift coefficients at various values of thrust coefficient for the tail-on conditions are plotted against angle of attack in figures 47 and 48. Figures 49 and 50 show the pitching-moment coefficients due to the horizontal tail surface, as obtained from tail-on and tail-off pitching-moment measurements, plotted against angle of attack for various values of thrust coefficient.

As a result of the increased downwash at the tail due to the thrust, the effect of propeller operation is to increase the downward force on the tail. With flaps retracted, the stalling moment resulting from the increased downwash at the tail counteracts the diving moment caused by the location of the thrust axis with respect to the center of gravity of the model. With flaps deflected, the increased downwash at the tail due to flap deflection and propeller thrust increases the downward force on the tail. This force results in a stalling moment, which neutralizes, to a large extent, the diving moment caused by deflecting the flaps. It must also be pointed out that there is a comparatively large change in the forces at the tail with angle of attack resulting from the fact that the tail advances into the slipstream with increasing angle of attack.

With flaps retracted, the effect of propeller operation on the slope of the curve of pitching moment against angle of attack (T_c = constant) is shown in figure 47. At positive angles of attack, the slope progressively increases with increase in thrust coefficient. Figure 47 also serves to show the effects of propeller operation on balance. Thus, with propellers removed, the model trims at $\alpha_T = 3.9^\circ$ and at $T_c = 1.20$, the angle of attack for trim is increased to $\alpha_T = 10.3^\circ$. This change of trim angle with thrust is attributed mainly to the increased downwash due to the thrust.

SUMMARY OF RESULTS

From tests of a twin-engine tractor monoplane model with propellers rotating in the same direction, the following results are summarized:

1. For most conditions, the stabilizer effectiveness of the isolated horizontal tail surface was reduced about 12 percent by attaching the tail surface to the model but the elevator effectiveness was not appreciably affected.

2. With propellers removed, deflecting the flaps 50° increased the elevator effectiveness about 7 percent; with propellers operating, however, deflecting the flaps decreased the elevator effectiveness considerably.

3. The horizontal tail surface acted as an end plate for the vertical tail surface, thus increasing its effective aspect ratio. With the horizontal tail surface removed, the rudder effectiveness was about -0.00062, which was increased to about -0.00077 when the horizontal tail surface was attached to the model.

4. The increment of lift at a wing with flaps retracted, caused by the passage of a slipstream over it, may be computed with satisfactory accuracy by the methods of reference 6.

5. The effect of the propeller slipstream on the wing pitching moment with flaps retracted was negligible for this model.

6. Deflecting the flaps caused a large diving moment

which increased with thrust coefficient. This diving moment was neutralized to a large extent, however, by the increased downwash at the tail due to flap deflection. As an example, with the horizontal tail surface removed and at zero angle of attack, deflecting the flaps caused an increment of pitching-moment coefficient of -0.140, which increased with thrust to -0.375 at a thrust coefficient of 1.2. With the horizontal tail surface attached to the model and at zero angle of attack, deflecting the flaps caused an increment of pitching-moment coefficient of -0.001, which increased with thrust to -0.093 at a thrust coefficient of 1.2.

7. With propellers removed, the elevator effectiveness was approximately proportional to the average dynamic pressure at the tail; this proportionality did not hold for the propellers-operating condition.

8. The dynamic pressure at the tail generally increased with angle of attack because, for this airplane, the tail was near the top of the slipstream at low angles of attack and advanced into it as the angle of attack increased.

9. With propellers removed, the effective downwash angles were in good agreement with the average downwash angles; with propellers operating, however, the effective downwash angles were somewhat lower than the average downwash angles at the higher angles of attack.

Langley Memorial Aeronautical Laboratory,
National Advisory Committee for Aeronautics,
Langley Field, Va.

REFERENCES

1. Sweberg, Harold H.: The Effect of Propeller Operation on the Air Flow in the Region of the Tail Plane for a Twin-Engine Tractor Monoplane. NACA A.R.R., Aug. 1942.

2. Goett, Harry J., and Reeder, J. P.: Effects of Elevator Nose Shape, Gap, Balance, and Tabs on the Aerodynamic Characteristics of a Horizontal Tail Surface. Rep. No. 675, NACA, 1939.

3. DeFrance, Smith J.: The N.A.C.A. Full-Scale Wind Tunnel. Rep. No. 459, NACA, 1933.

4. Silverstein, Abe, and Katzoff, S.: Experimental Investigation of Wind-Tunnel Interference on the Downwash behind an Airfoil. Rep. No. 609, NACA, 1937.

5. Theodorsen, Theodore, and Silverstein, Abe: Experimental Verification of the Theory of Wind-Tunnel Boundary Interference. Rep. No. 478, NACA, 1934.

6. Goett, Harry J., and Pass, H. R.: Effect of Propeller Operation on the Pitching Moments of Single-Engine Monoplanes. NACA A.C.R., May 1941.

7. Smelt, R., and Davies, H.: Estimation of Increase in Lift Due to Slipstream. R. & M. No. 1788, British A.R.C., 1937.

8. Katzoff, S., and Mutterperl, William: The End-Plate Effect of a Horizontal-Tail Surface on a Vertical-Tail Surface. T.N. No. 797, NACA, 1940.

9. Pass, H. R.: Analysis of Wind-Tunnel Data on Directional Stability and Control. T.N. No. 775, NACA, 1940.

10. Silverstein, Abe, and Katzoff, S.: Aerodynamic Characteristics of Horizontal Tail Surfaces. Rep. No. 688, NACA, 1940.

11. Katzoff, S.: Longitudinal Stability and Control with Special Reference to Slipstream Effects. Rep. No. 690, NACA, 1940.

12. Silverstein, Abe: Toward a Rational Method of Tail-Plane Design. Jour. Aero. Sci., vol. 6, no. 9, July 1939, pp. 361-369.

13. Silverstein, Abe, and Katzoff, S.: Design Charts for Predicting Downwash Angles and Wake Characteristics behind Plain and Flapped Wings. Rep. No. 648, NACA, 1939.

14. Stüper, J.: Effect of Propeller Slipstream on Wing and Tail. T.M. No. 874, NACA, 1938.

15. Stiess, W.: Über den Einfluss des Luftschraubendrehsinnes auf die Längsstabilität von sweimotorigen Flugzeugen. Jahrb. 1938 der deutschen Luftfahrtforschung, R. Oldenbourg (Munich), pp. 1206-1219.

16. Seiferth, R.: Windkanaluntersuchungen über den Einfluss des Schrauben-Drehsinns auf die Längsstabilität eines zweimotorigen Flugzeugs. Jahrb. 1938 der deutschen Luftfahrtforschung, R. Oldenbourg (Munich), pp. 1220-1225.

TABLE I

VALUES FOR HORIZONTAL TAIL SURFACE PARAMETERS

$dC_{N_t}/d\delta_S$ AND $dC_{N_t}/d\delta_e$

[Propellers removed]

Condition	a_T (deg)	$\left(\frac{q}{q_o}\right)_{av}$	$\left(\frac{dC_m}{d\delta_S}\right)_{exp}$	$\left(\frac{dC_{N_t}}{d\delta_S}\right)_{calc}$	$\left(\frac{dC_m}{d\delta_e}\right)_{exp}$	$\left(\frac{dC_{N_t}}{d\delta_e}\right)_{calc}$
Nacelles off; $\delta_f = 0°$	-2.3	0.93	-0.022	0.052	-0.0135	0.031
	3.2	.91	-.022	.053	-.0134	.031
	9.6	.93	-.021	.050	-.0137	.031
	16.0	.95	-.022	.051	-.0138	.031
Nacelles off; $\delta_f = 50°$	-2.7	.96	-.021	.048	-.0147	.032
	2.7	.95	-.022	.051	-.0144	.032
	8.9	.91	-.022	.053	-.0147	.034
	15.2	.76	-.020	.058	-.0137	.038
Nacelles on; $\delta_f = 0°$	-2.3	.94	-.022	.052	-.0137	.031
	3.2	.90	-.022	.054	-.0130	.030
	9.6	.92	-.022	.053	-.0136	.031
	16.0	.97	-.023	.052	-.0138	.030
Nacelles on; $\delta_f = 50°$	-2.7	.91	-.022	.053	-.0141	.033
	2.7	.92	-.022	.053	-.0141	.032
	8.9	.89	-.022	.055	-.0147	.035
	15.2	.67	-.017	.056	-.0128	.040

TABLE II

COMPARISON OF CALCULATED AND EXPERIMENTAL

ELEVATOR EFFECTIVENESS

[Propellers operating; nacelles off. Values of $(q/q_o)_{av}$ from reference 1]

T_c	a_T	$\left(\frac{q}{q_o}\right)_{av}$	$\left(\frac{dC_m}{d\delta_e}\right)_{calc}$	$\left(\frac{dC_m}{d\delta_e}\right)_{exp}$
		$\delta_f = 0°$		
0.2	-4.1	1.28	-0.0191	-0.0173
	1.4	1.41	-.0210	-.0182
	7.7	1.50	-.0223	-.0184
.4	-4.0	1.55	-.0231	-.0210
	1.4	1.78	-.0265	-.0244
	7.6	1.92	-.0286	-.0250
.6	-4.0	1.81	-.0270	-.0271
	1.4	2.15	-.0320	-.0277
	7.6	2.34	-.0348	-.0294
.8	-3.9	2.03	-.0302	-.0301
	1.4	2.46	-.0367	-.0321
	7.6	2.75	-.0410	-.0335
		$\delta_f = 50°$		
0.2	-4.7	1.00	-0.0149	-0.0142
	.7	1.06	-.0158	-.0152
	6.9	1.15	-.0171	-.0155
	13.2	1.15	-.0171	-.0150
.4	-4.7	1.00	-.0149	-.0140
	.6	1.12	-.0167	-.0156
	6.8	1.32	-.0197	-.0172
	13.0	1.32	-.0197	-.0166
.6	-4.9	1.05	-.0156	-.0128
	.5	1.18	-.0176	-.0162
	6.6	1.42	-.0212	-.0188
	12.8	1.42	-.0212	-.0174
.8	-4.9	1.02	-.0152	-.0127
	.4	1.23	-.0183	-.0168
	6.5	1.48	-.0220	-.0208
	12.6	1.48	-.0220	-.0186

TABLE III

COMPARISON OF EFFECTIVE AND AVERAGE DOWNWASH ANGLES AT TAIL

[Propellers operating; nacelles off]

T_c	a_T	ϵ_{eff}	ϵ_{av}
	$\delta_f = 0°$		
0.161	-4.1	-3.4	-3.2
	1.4	-.3	.2
	7.7	2.1	3.9
	14.0	5.3	5.3
.619	-4.0	-2.5	-3.2
	1.3	.4	.7
	7.7	3.2	5.0
	14.0	6.1	8.5
	$\delta_f = 50°$		
0.161	-4.7	-4.0	-3.4
	6.7	6.6	5.9
	13.2	7.8	9.6
	-4.8	9.3	11.1
.619	.6	5.4	5.0
	6.9	8.5	8.2
	13.3	9.7	11.9
		11.0	14.9

L-425

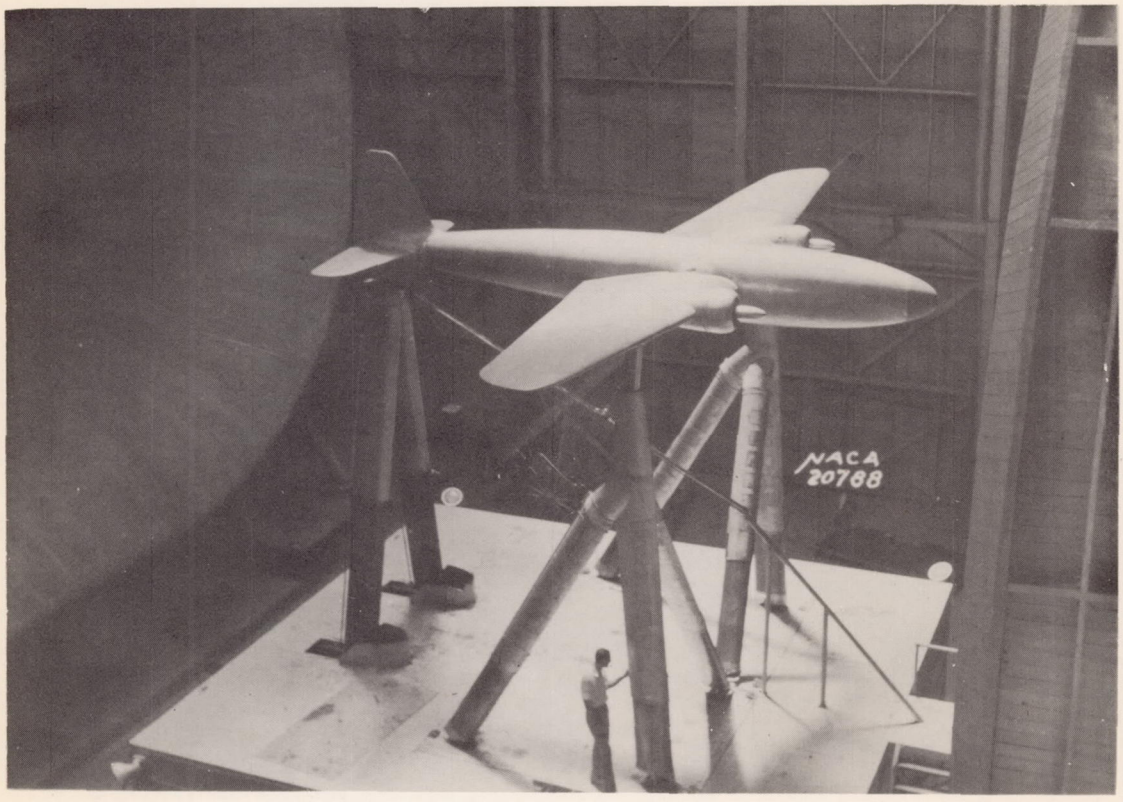

Figure 1.- Installation of stability model in the NACA full-scale wind tunnel.

L-42J

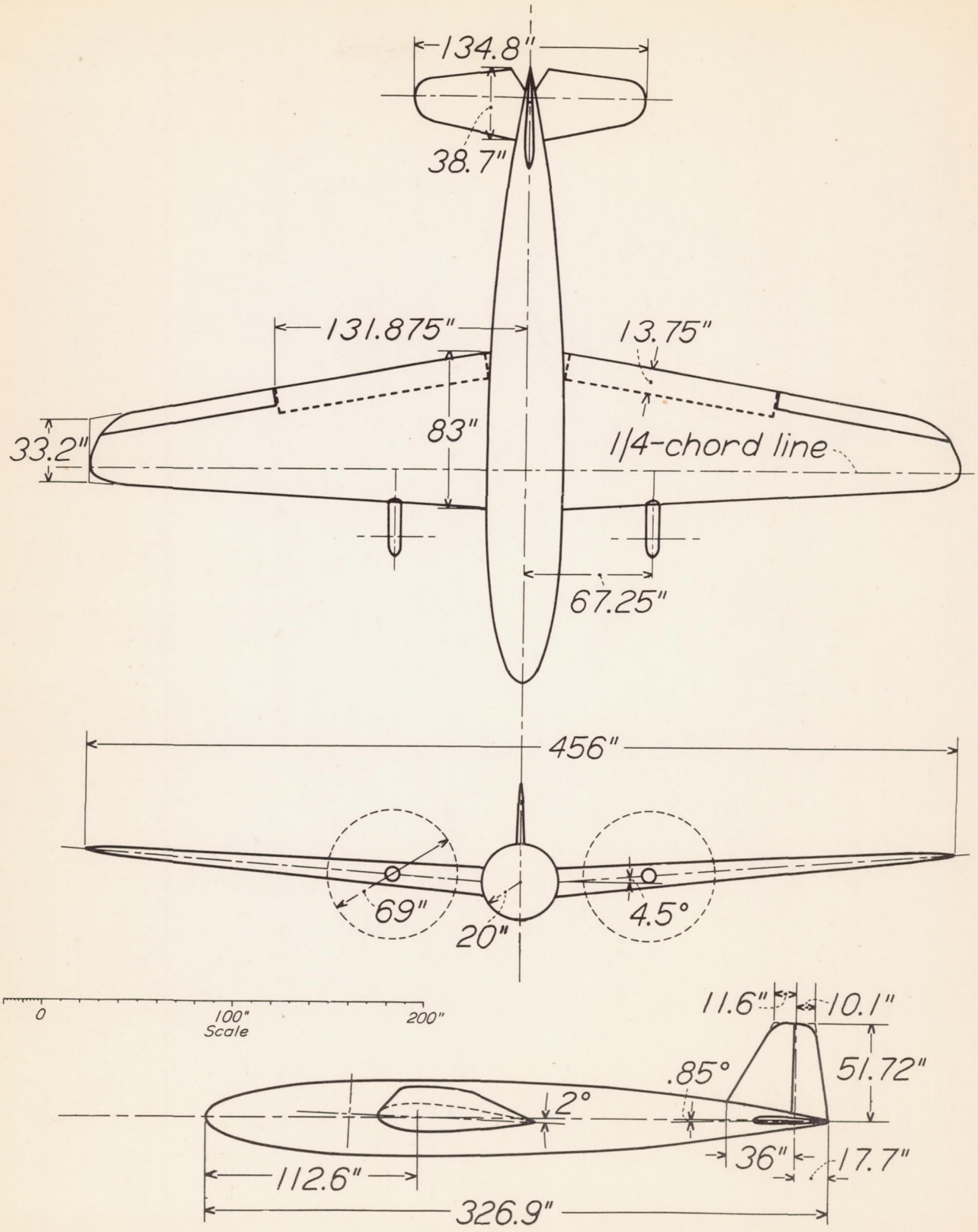

Figure 2.- Three-view drawing of stability model. Nacelles off.

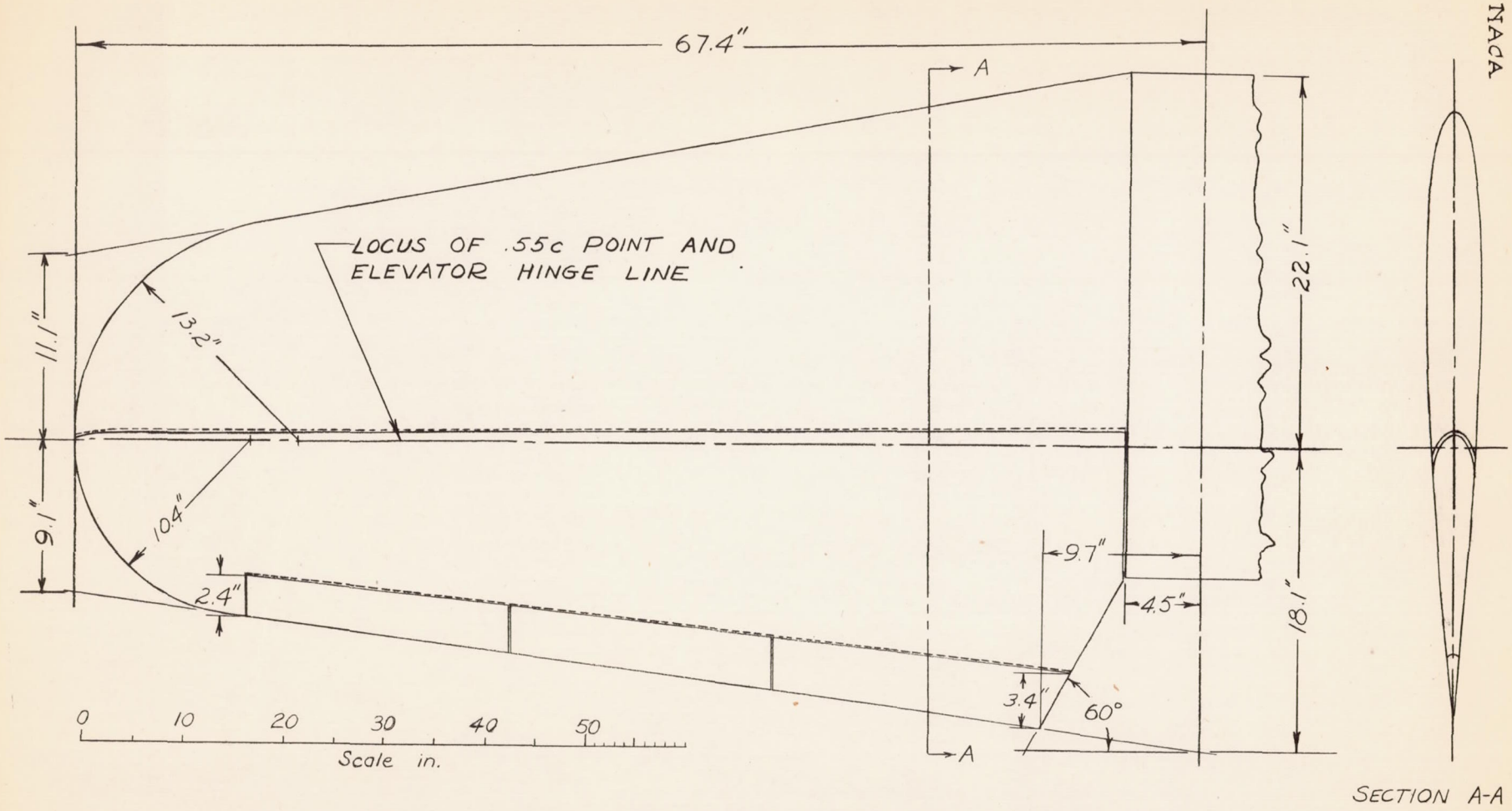

Figure 3.- Horizontal tail surface. Total area, 27 sq ft; stabilizer area, 15.9 sq ft; elevator area, 11.1 sq ft; taper ratio, 2:1; aspect ratio, 4.7; airfoil section, NACA 0009.

Fig. 3

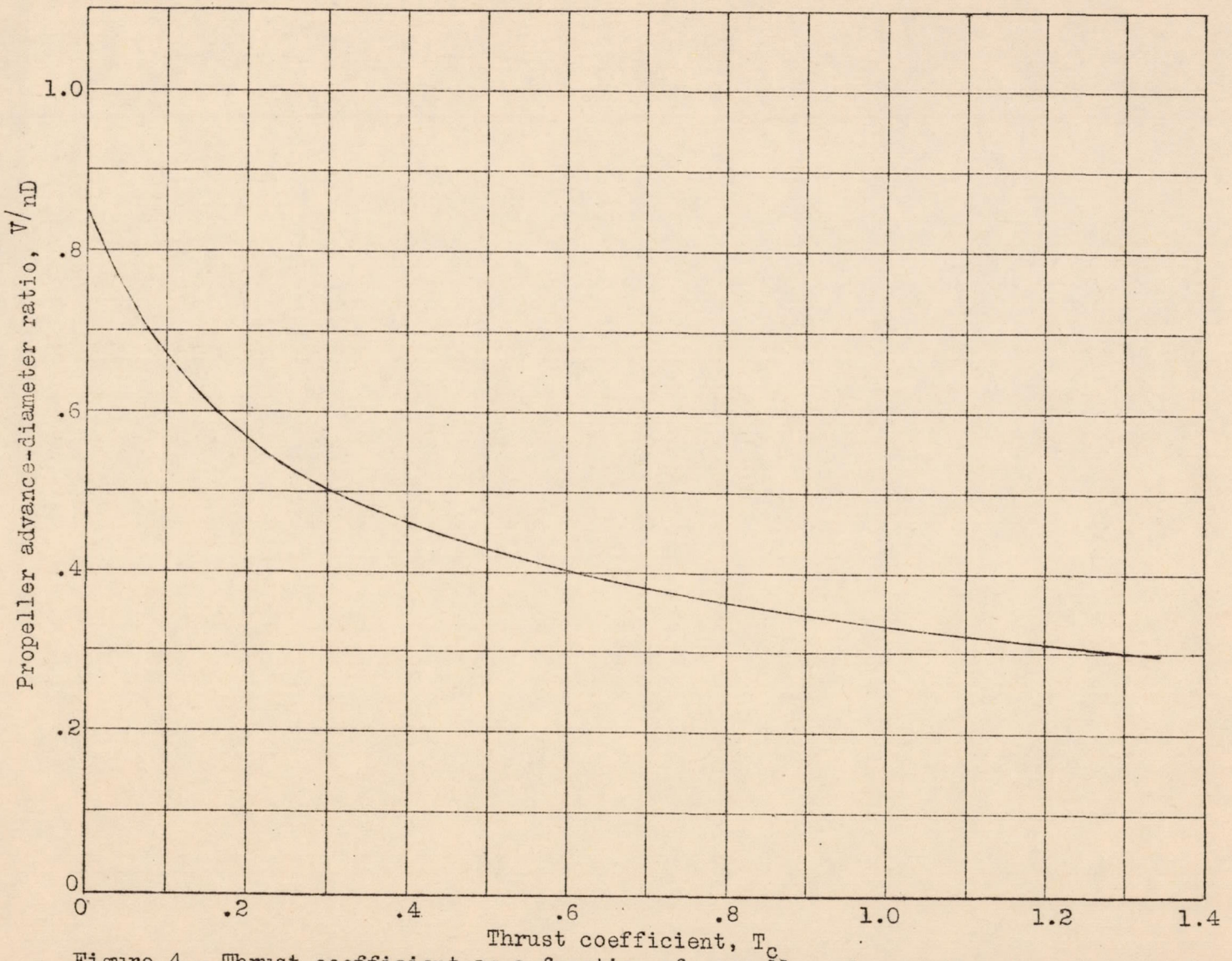

Figure 4.- Thrust coefficient as a function of propeller advance-diameter ratio.

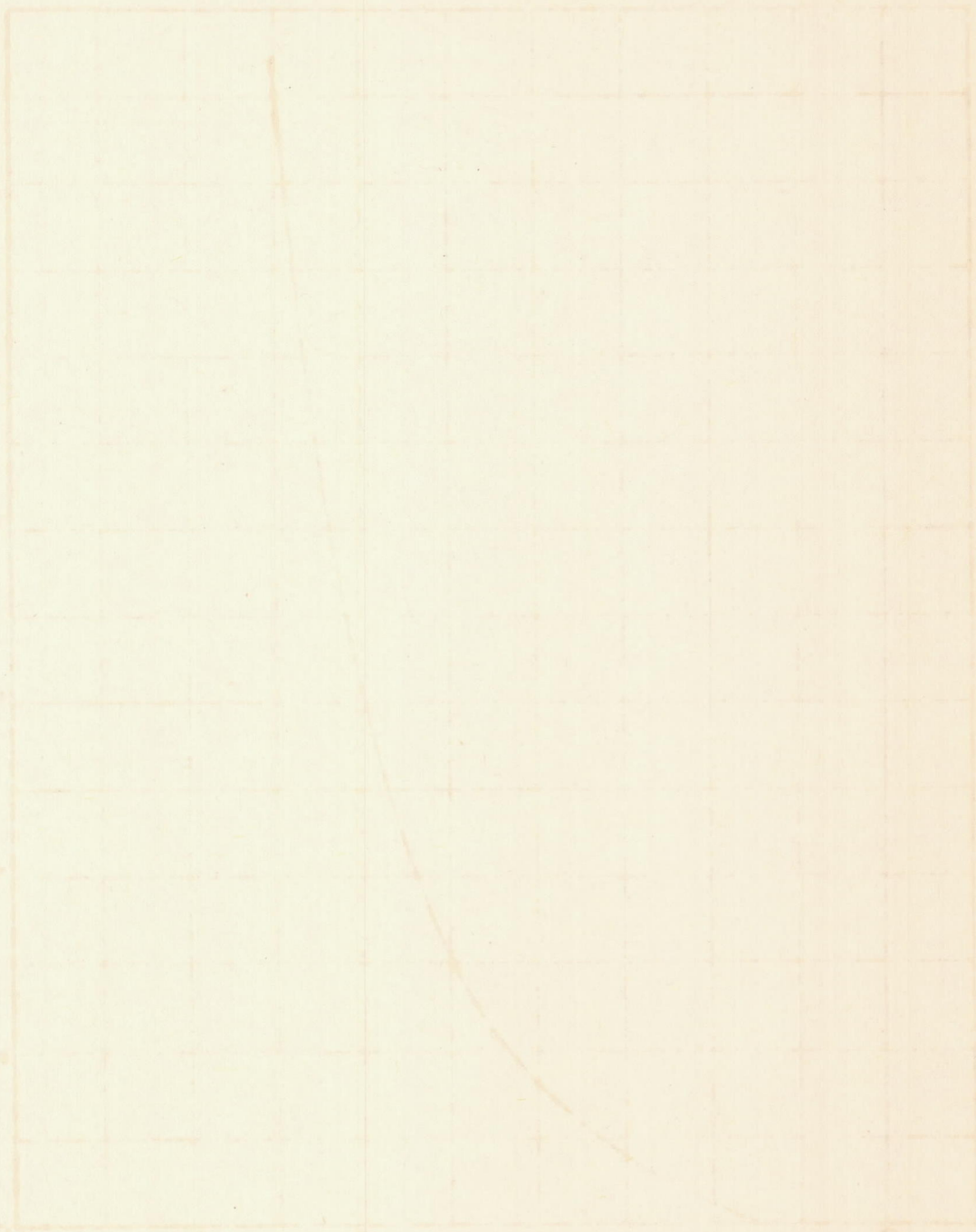

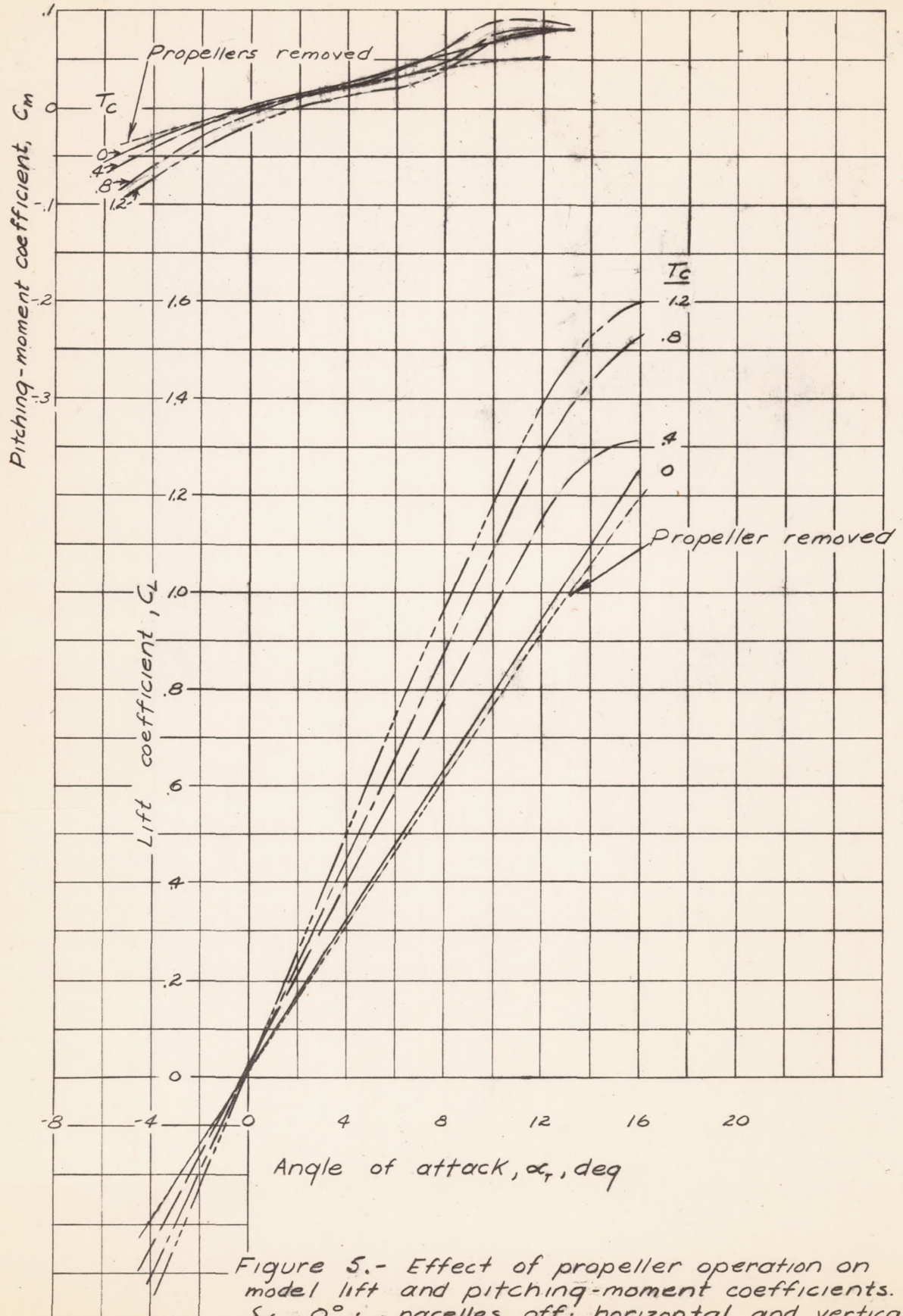

Figure 5.- Effect of propeller operation on model lift and pitching-moment coefficients. δ_f, 0°; nacelles off; horizontal and vertical tail surfaces removed.

L-425

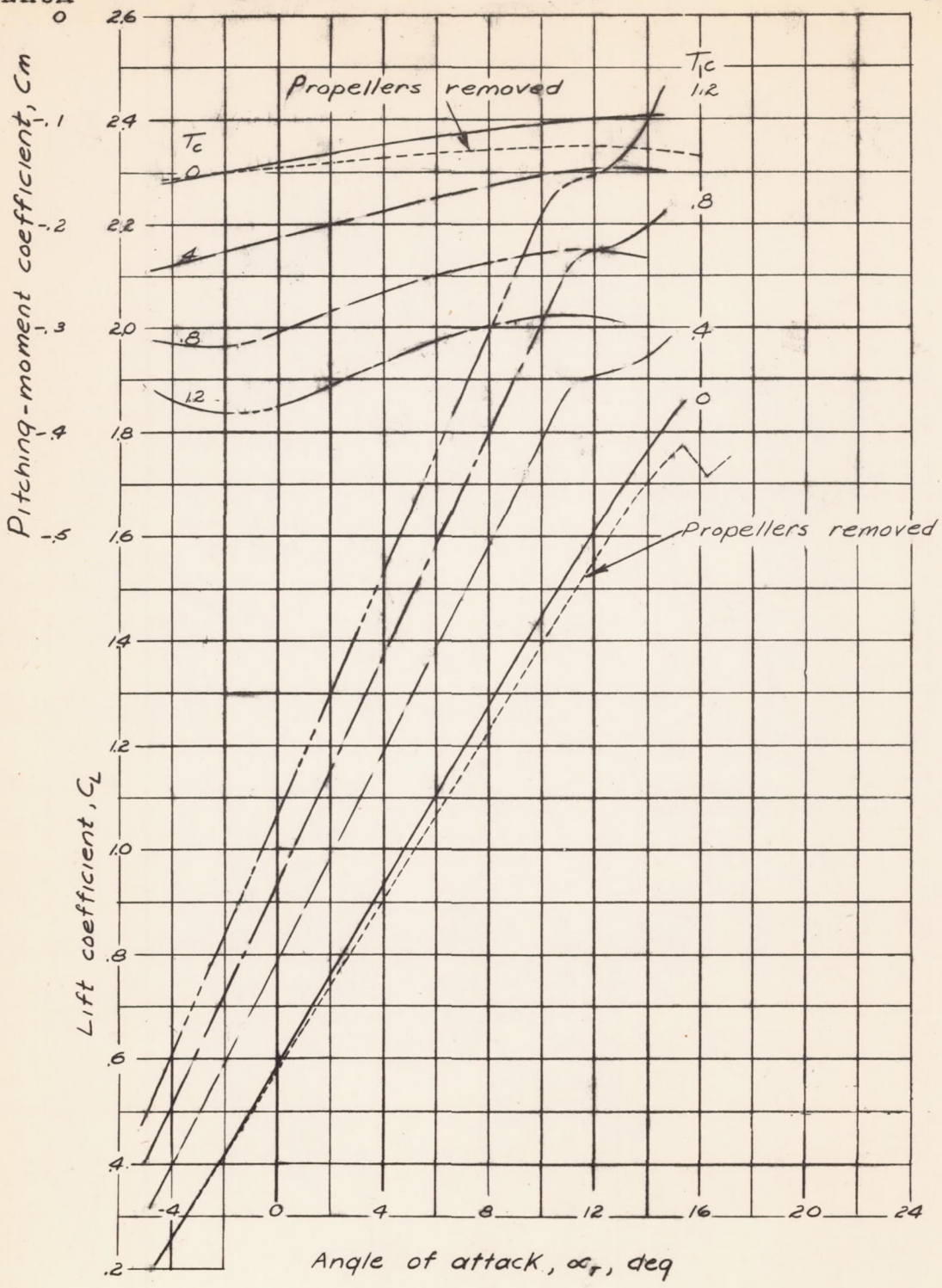

Figure 6 – Effect of propeller operation on model lift and pitching-moment coefficients. δ_f, 50°; nacelles off; horizontal and vertical tail surfaces removed.

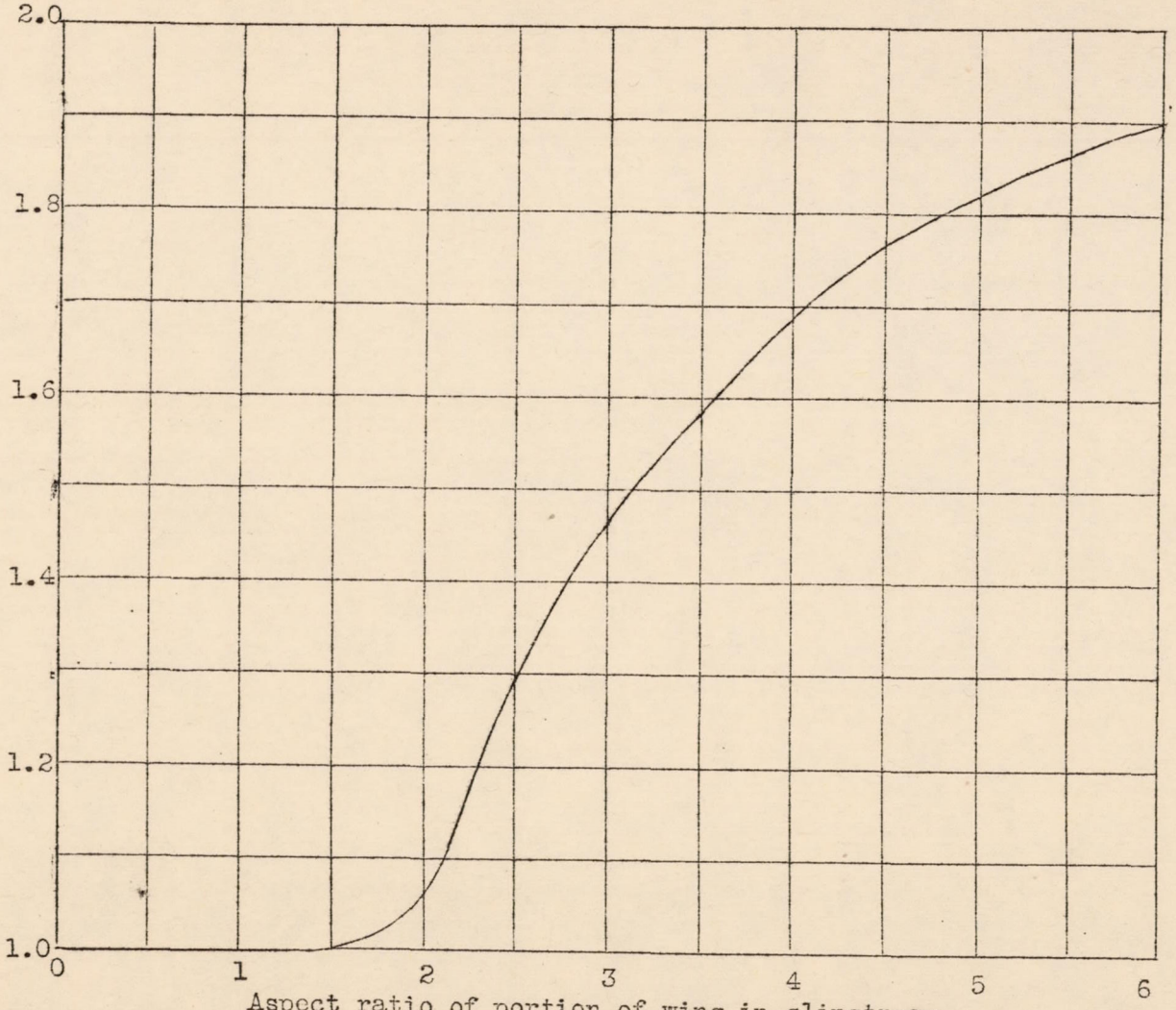

Figure 7.- Value of λ from reference 7 for estimating increase in wing lift due to slipstream.

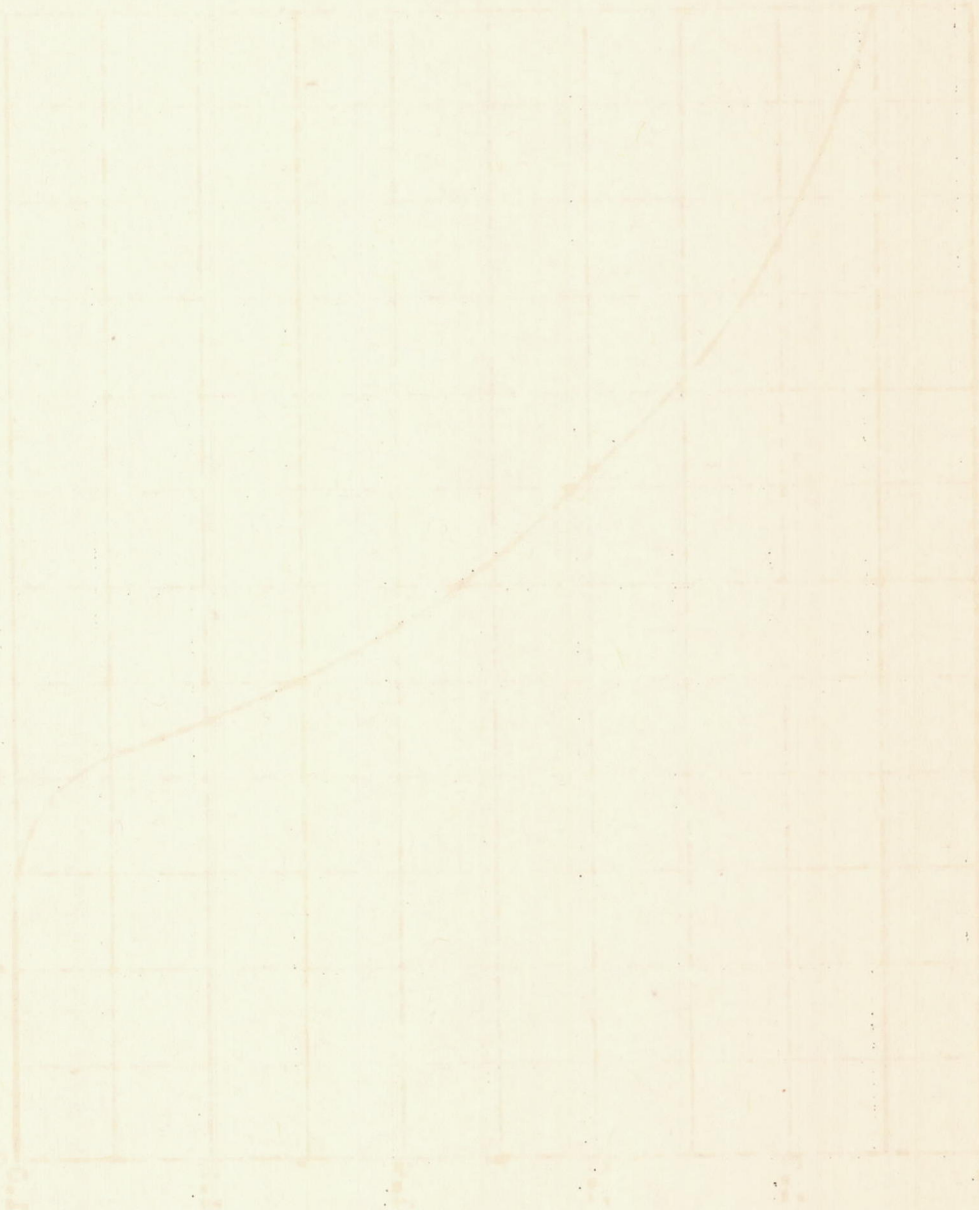

NACA

Fig. 8

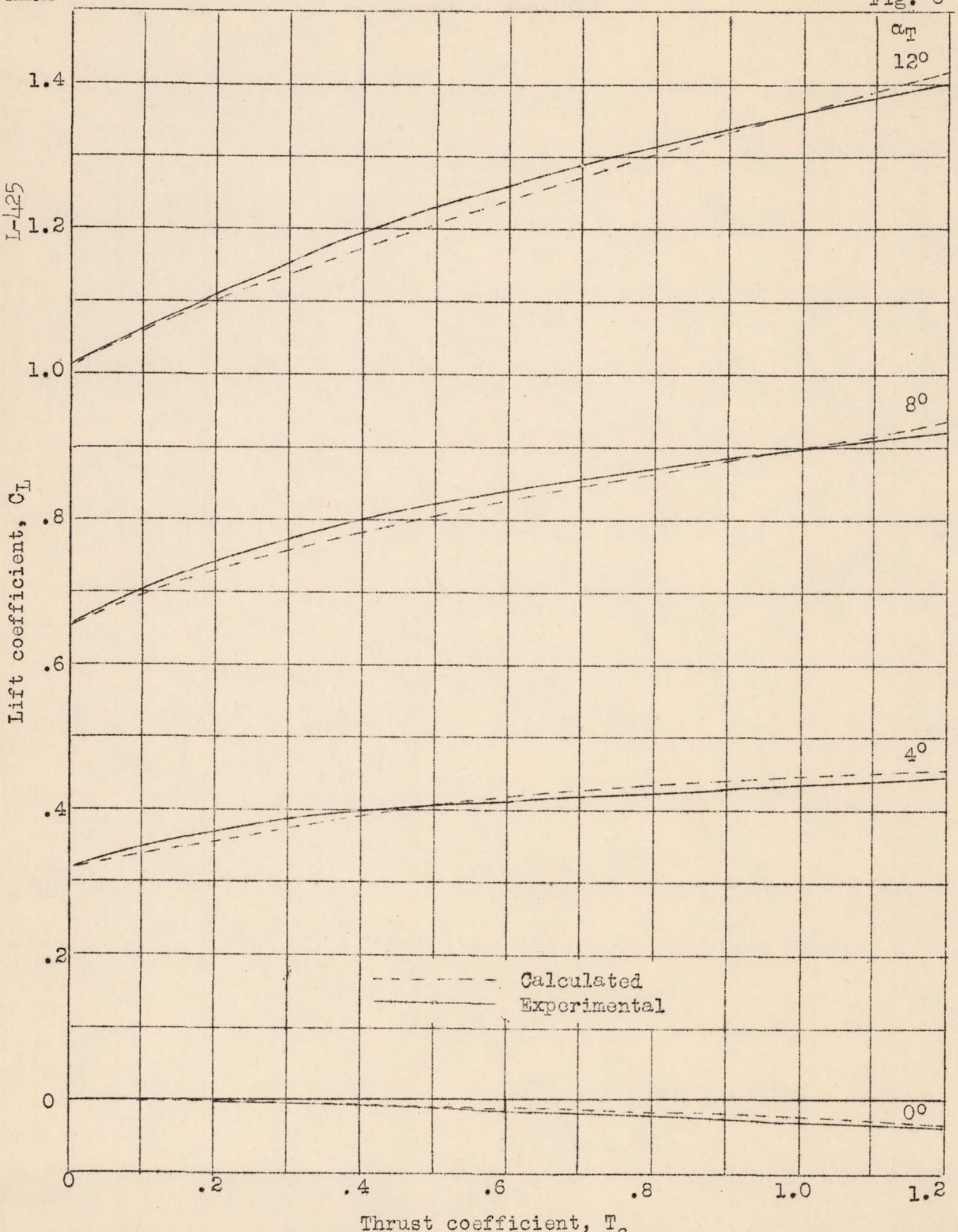

Figure 8.- Comparison between experimental and calculated lift coefficient. δ_f, 0°; nacelles off; tail off.

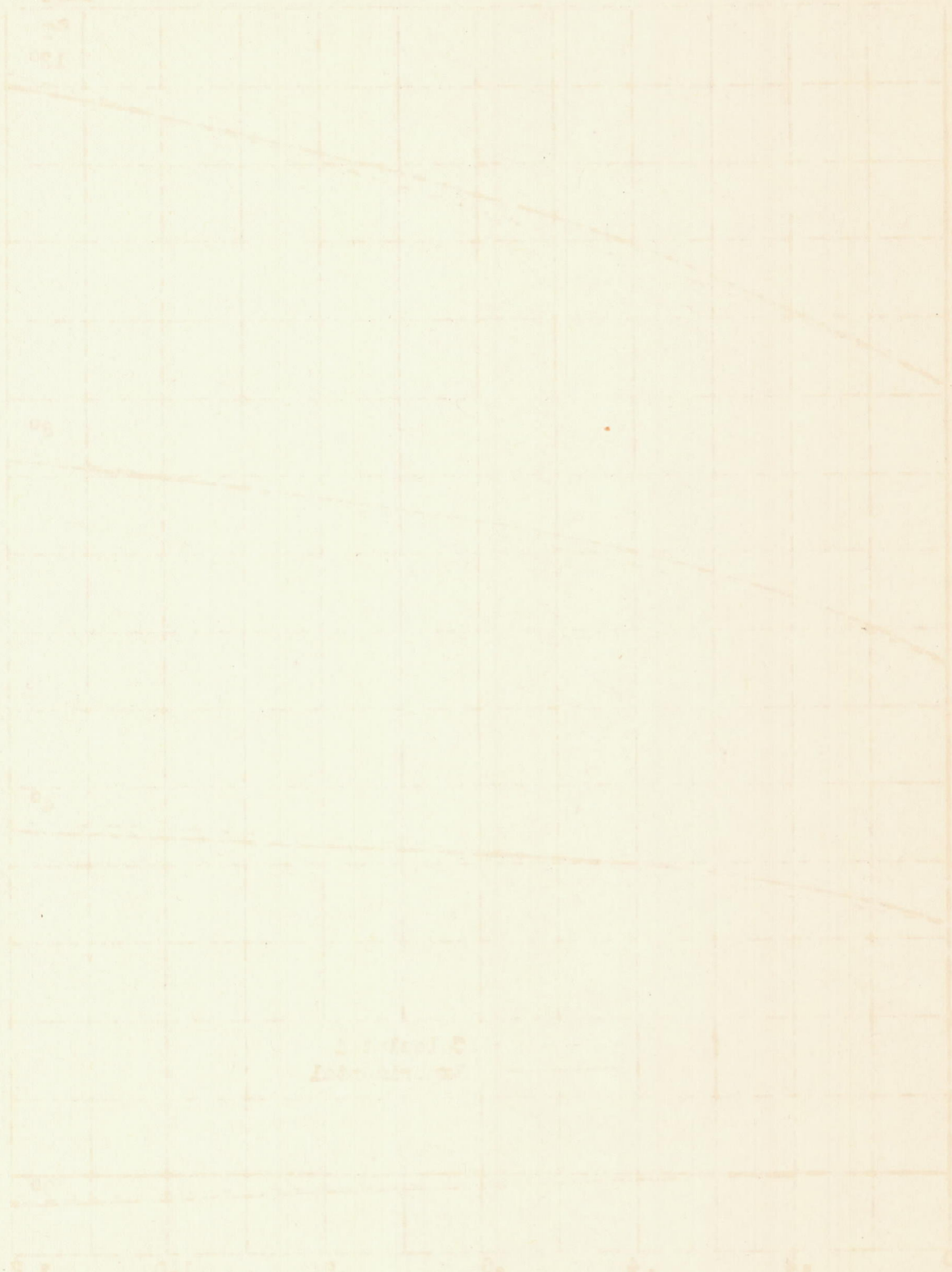

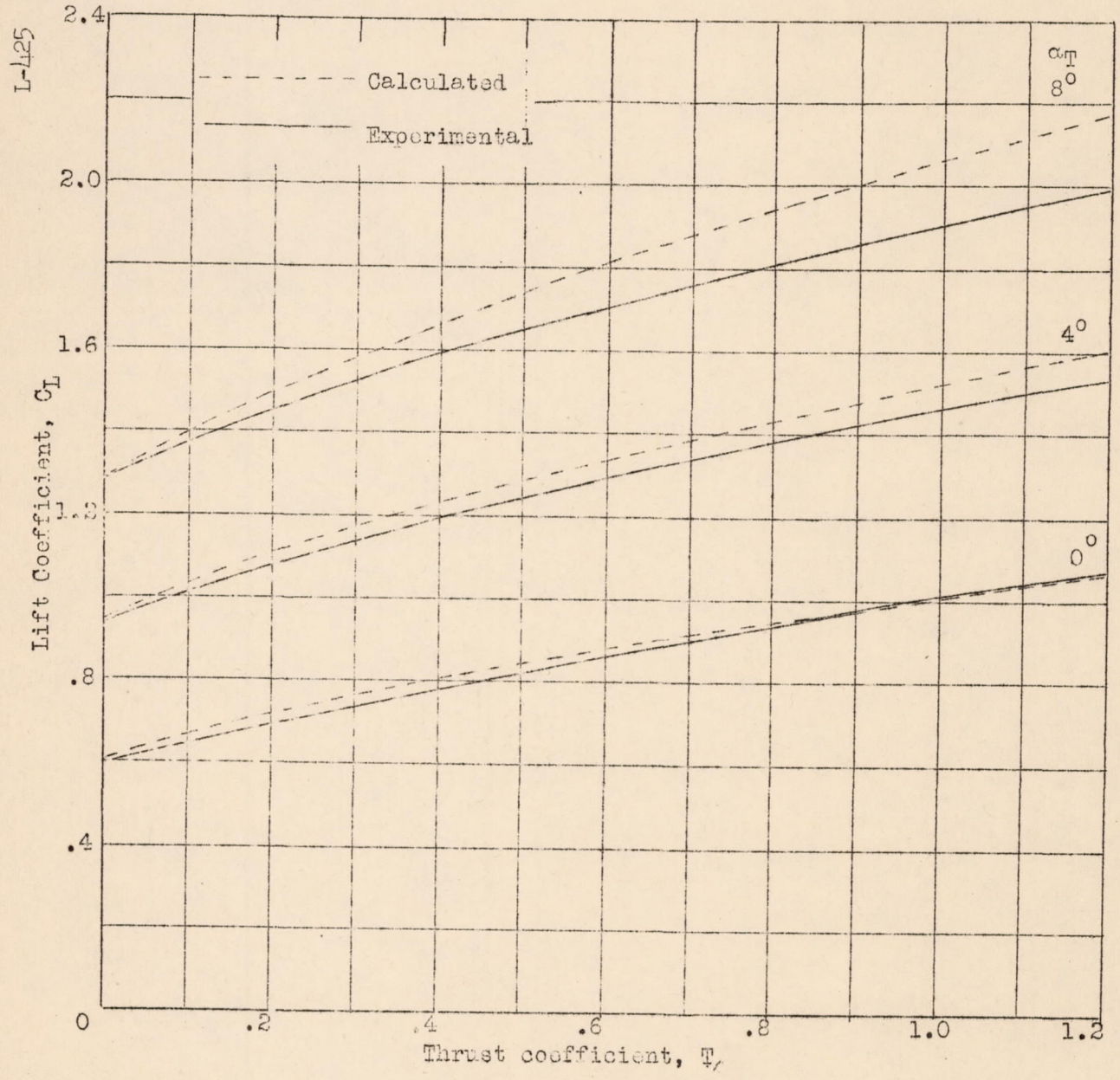

Figure 9.- Comparison between experimental and calculated lift coefficient. δ_f, 50°; nacelles off, tail off.

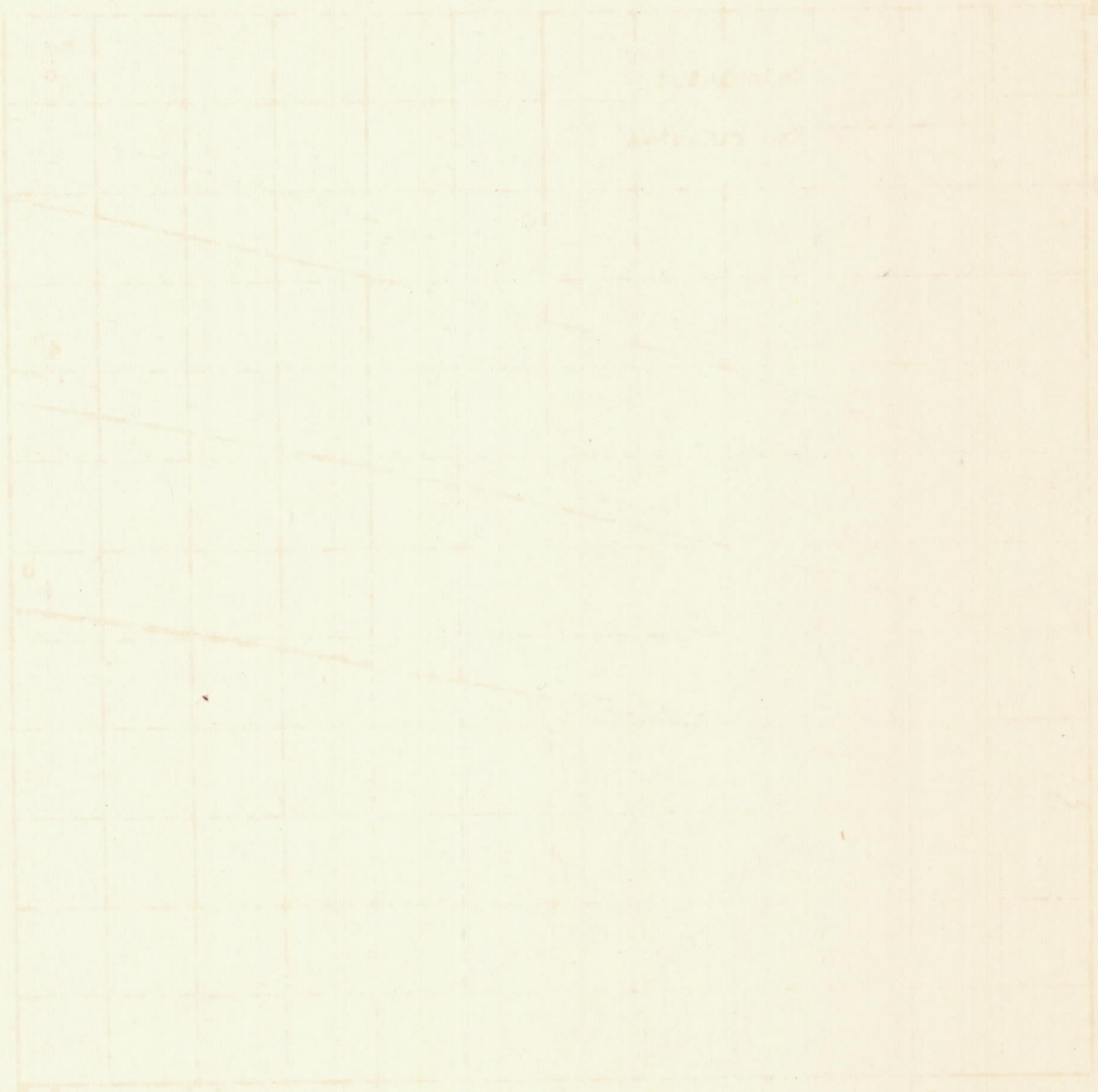

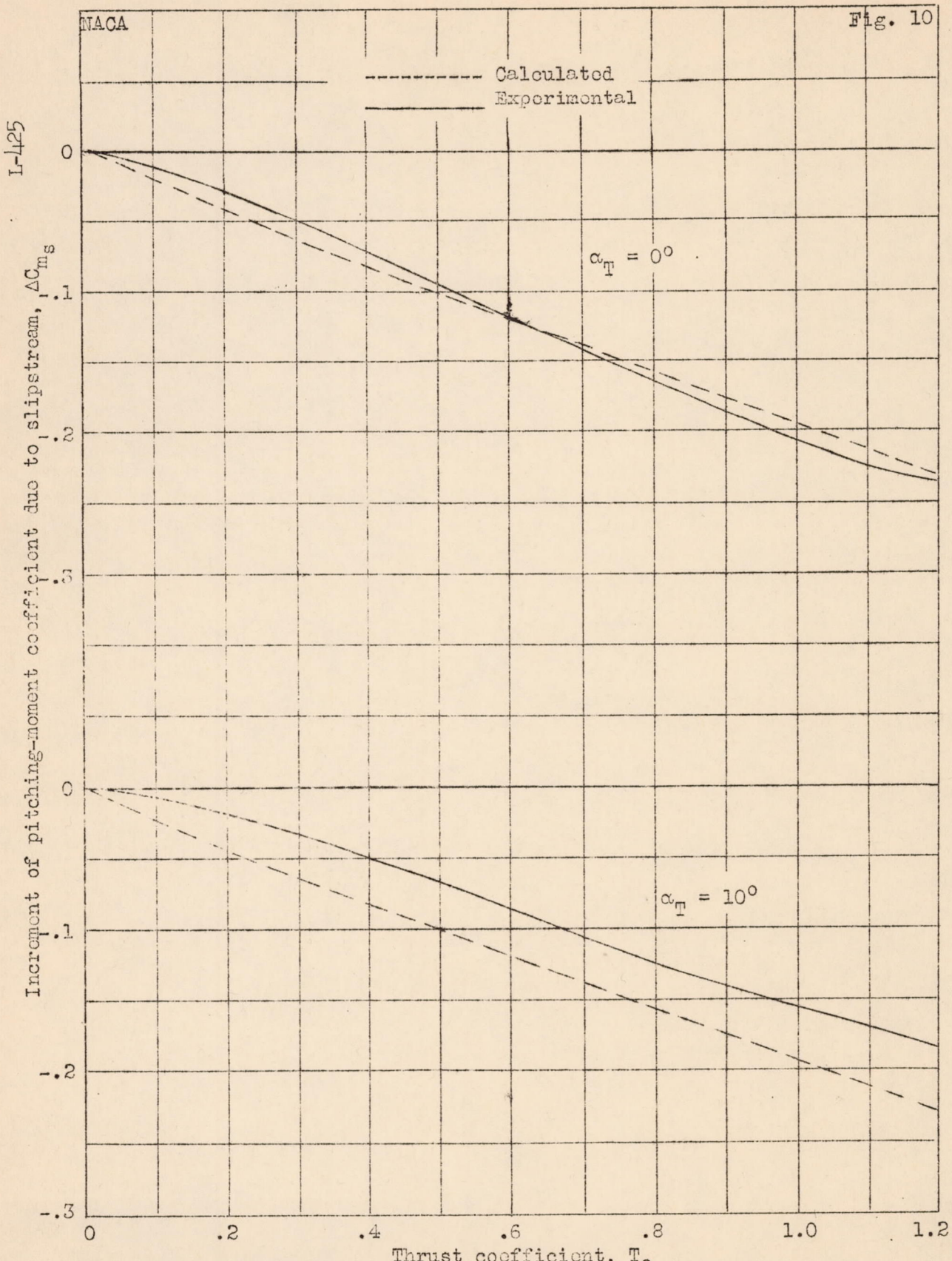

Figure 10.- Comparison between experimental and calculated increment of pitching-moment coefficient due to slipstream. δ_f, 50°, nacelles off, tail off.

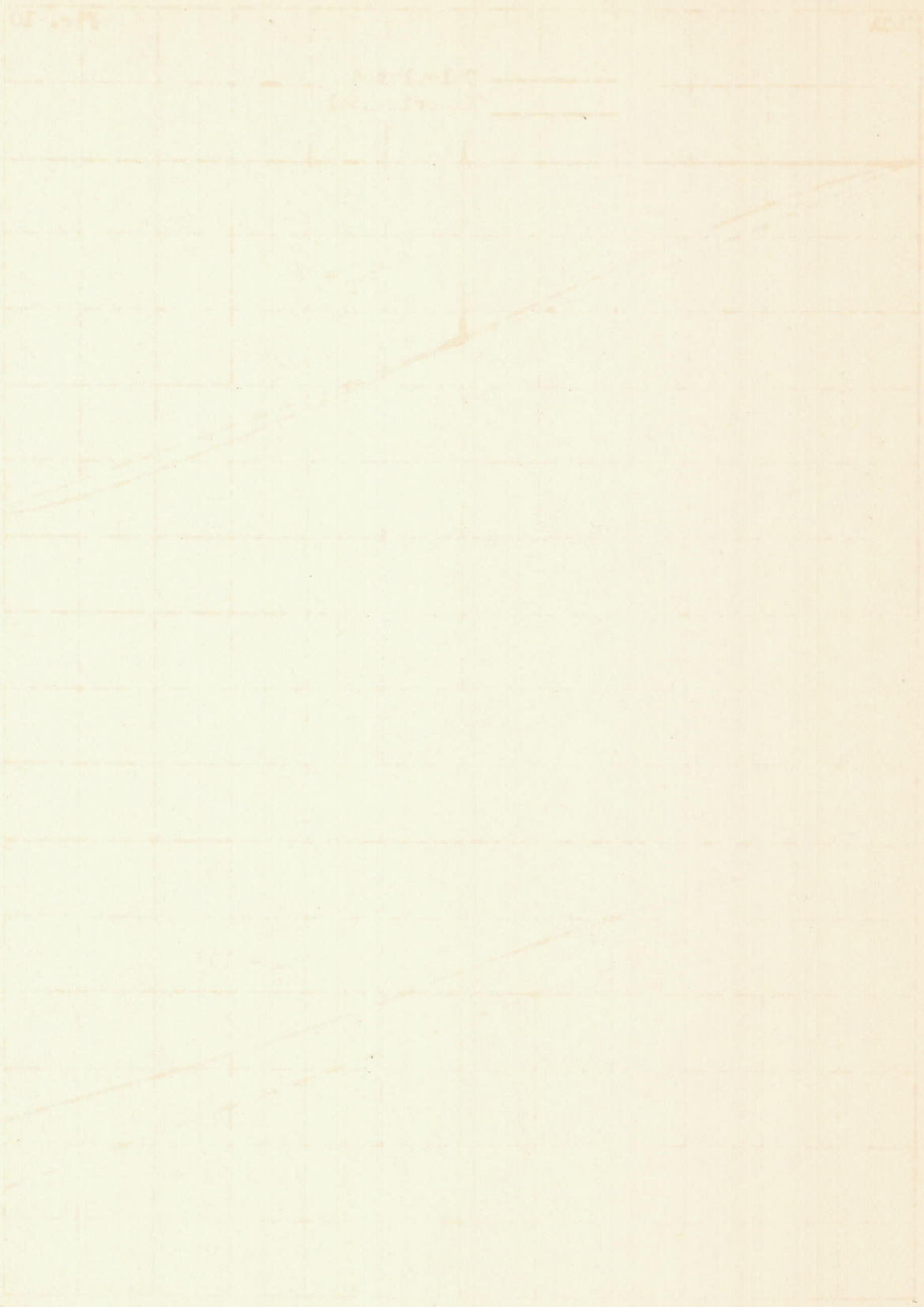

L-425

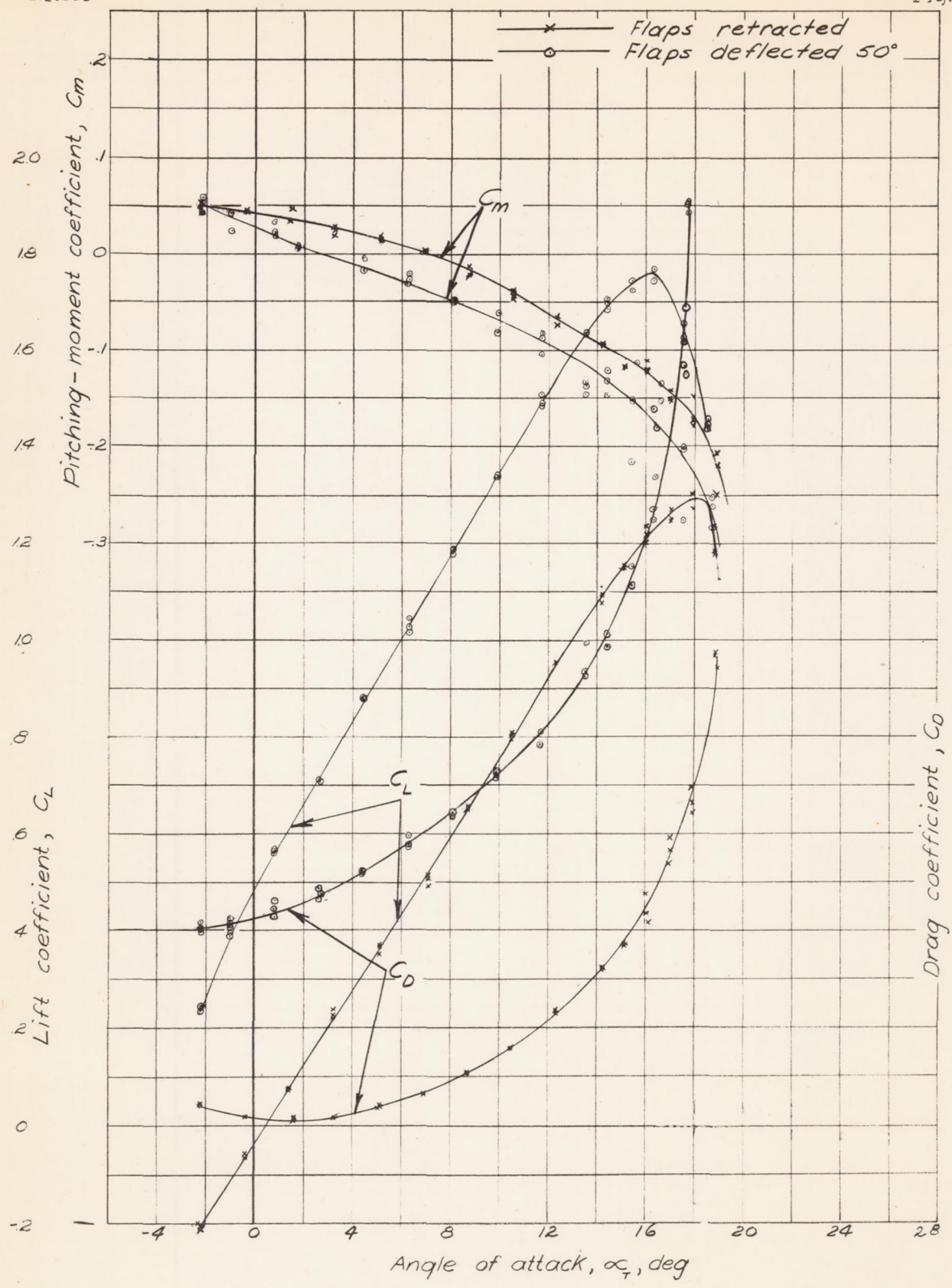

Figure 11.- Aerodynamic characteristics of model. Propellers removed; nacelles on; tail on.

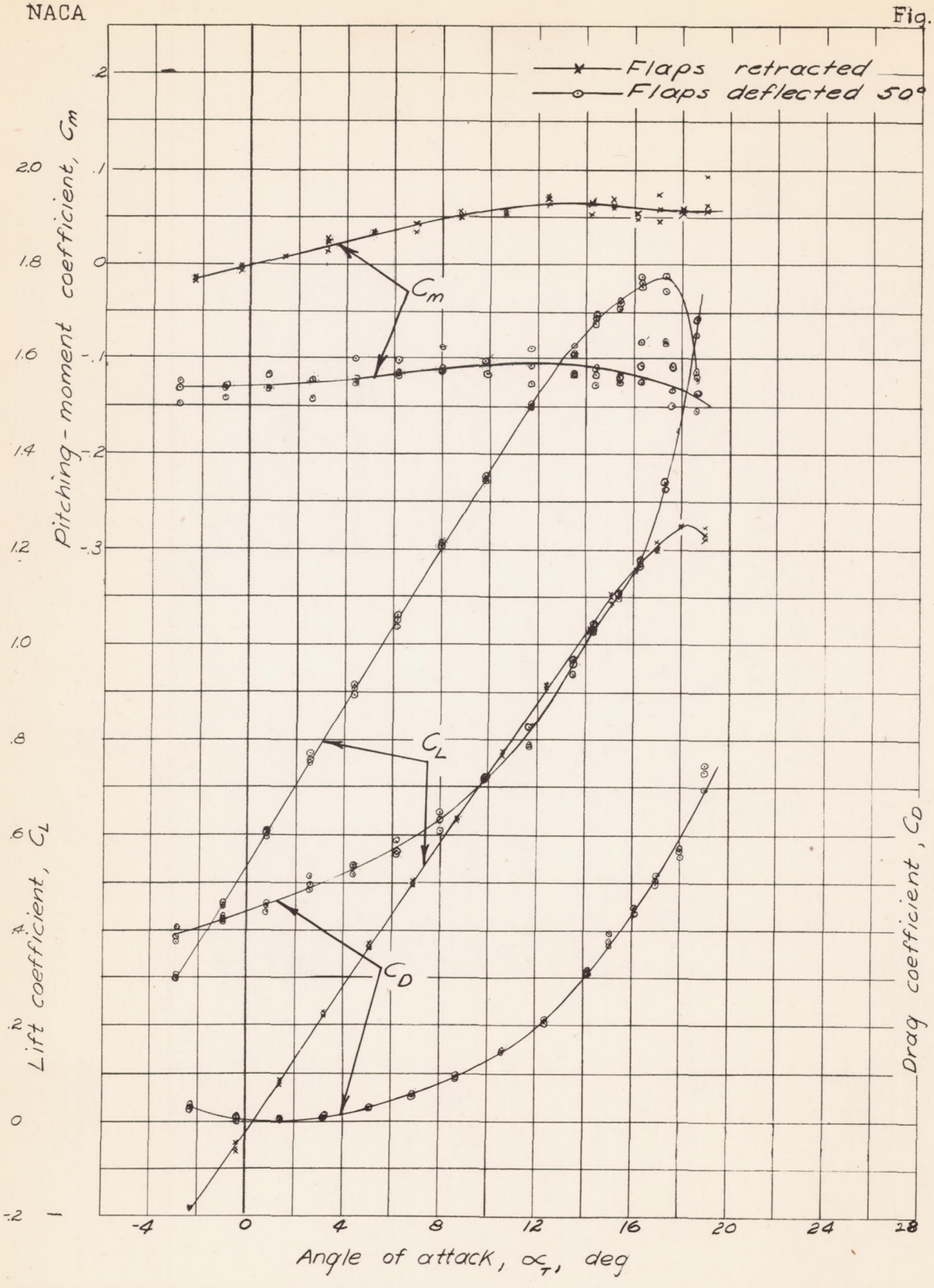

Figure 12.- Aerodynamic characteristics of model. Propellers removed; nacelles on; horizontal tail surface removed.

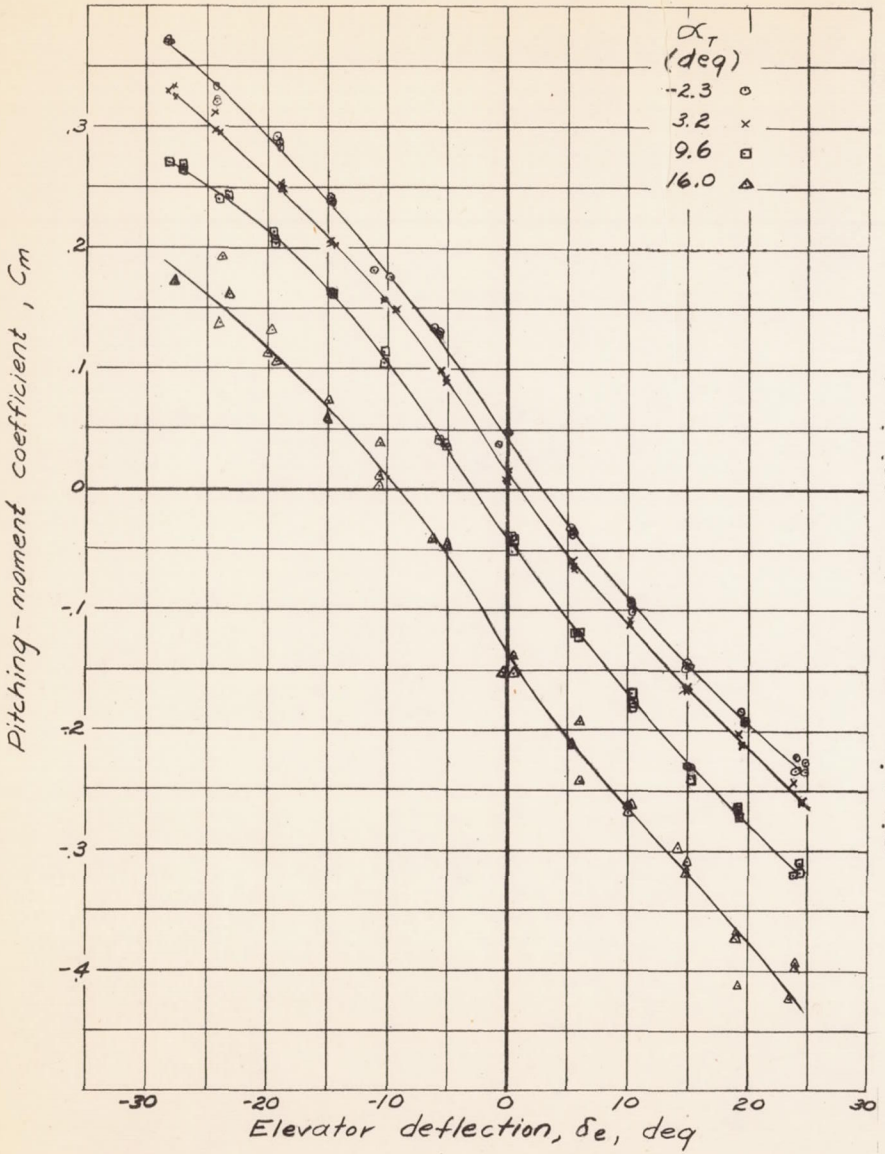

Figure 13.- Variation of C_m with δ_e at various angles of attack. Nacelles off; δ_f, 0°; propellers removed.

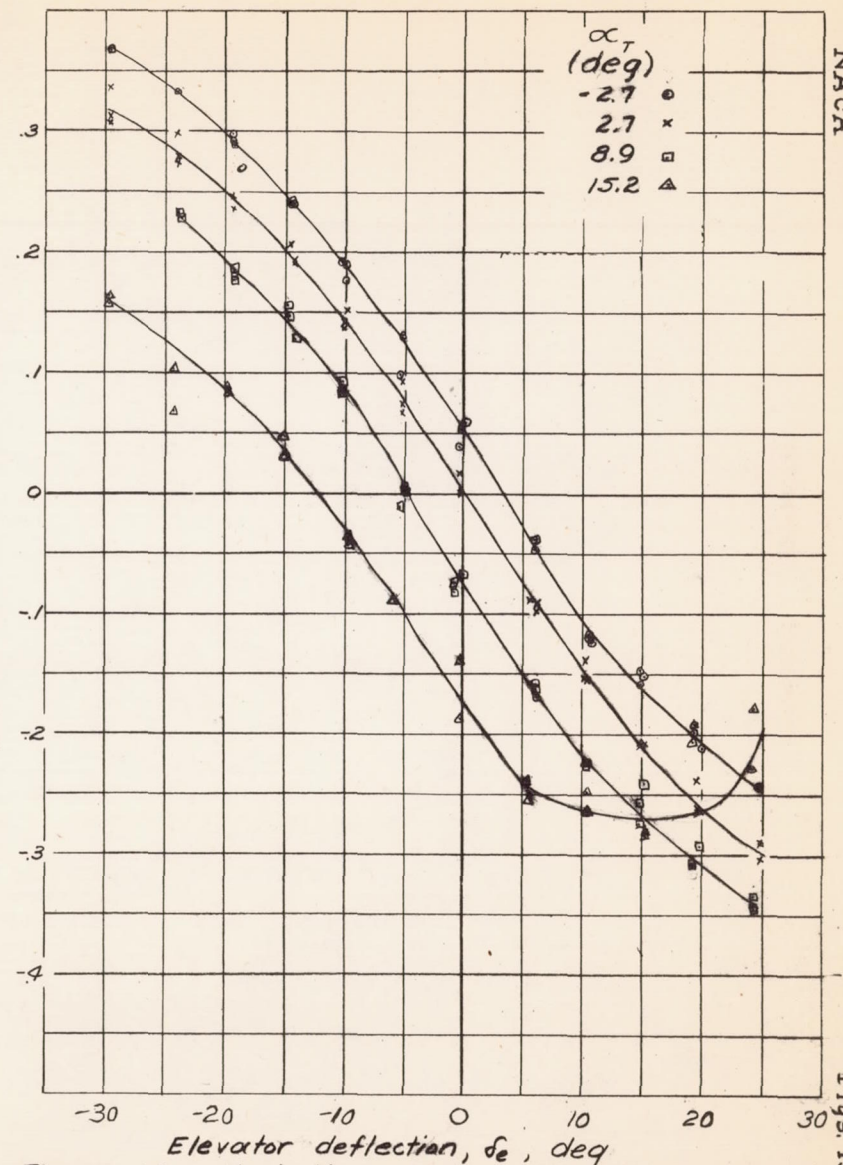

Figure 14.- Variation of C_m with δ_e at various angles of attack. Nacelles off; δ_f, 50°; propellers removed.

NACA

Figs. 13,14

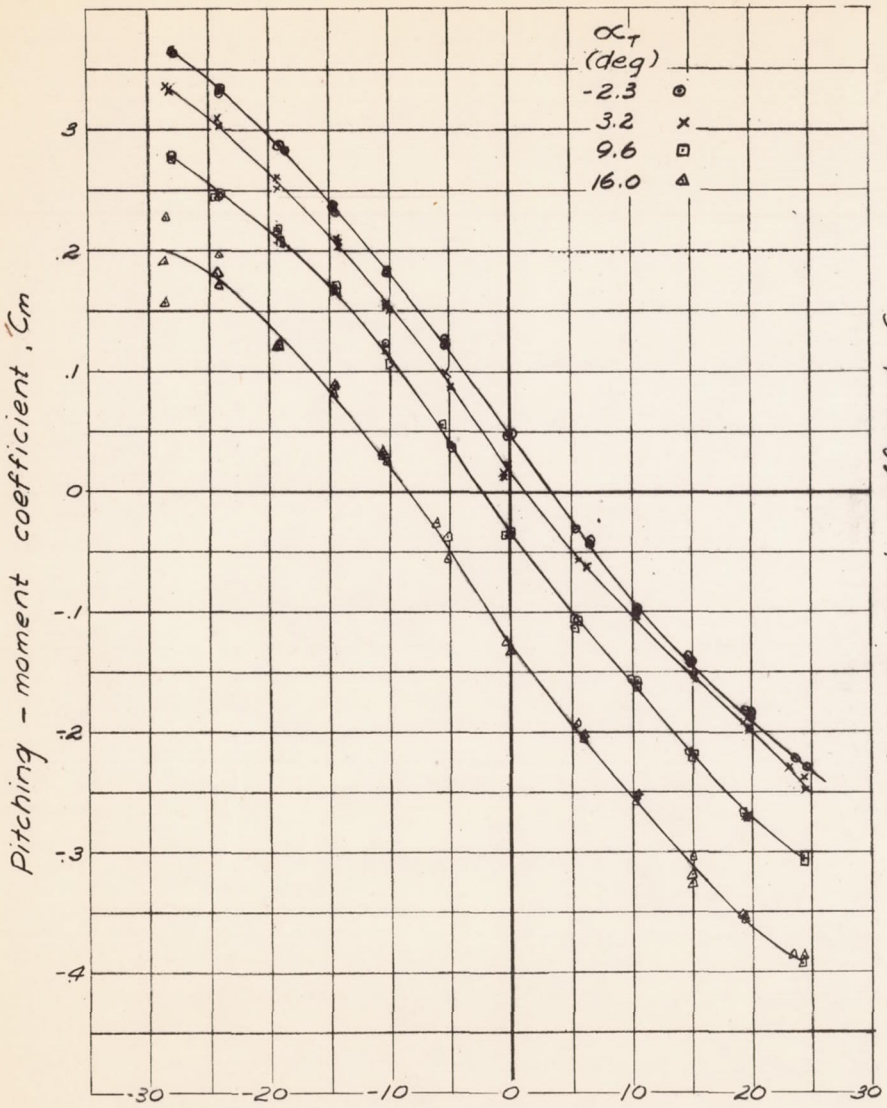

Figure 15.- Variation of C_m with δ_e at various angles of attack. Nacelles on; δ_f, 0°; propellers removed.

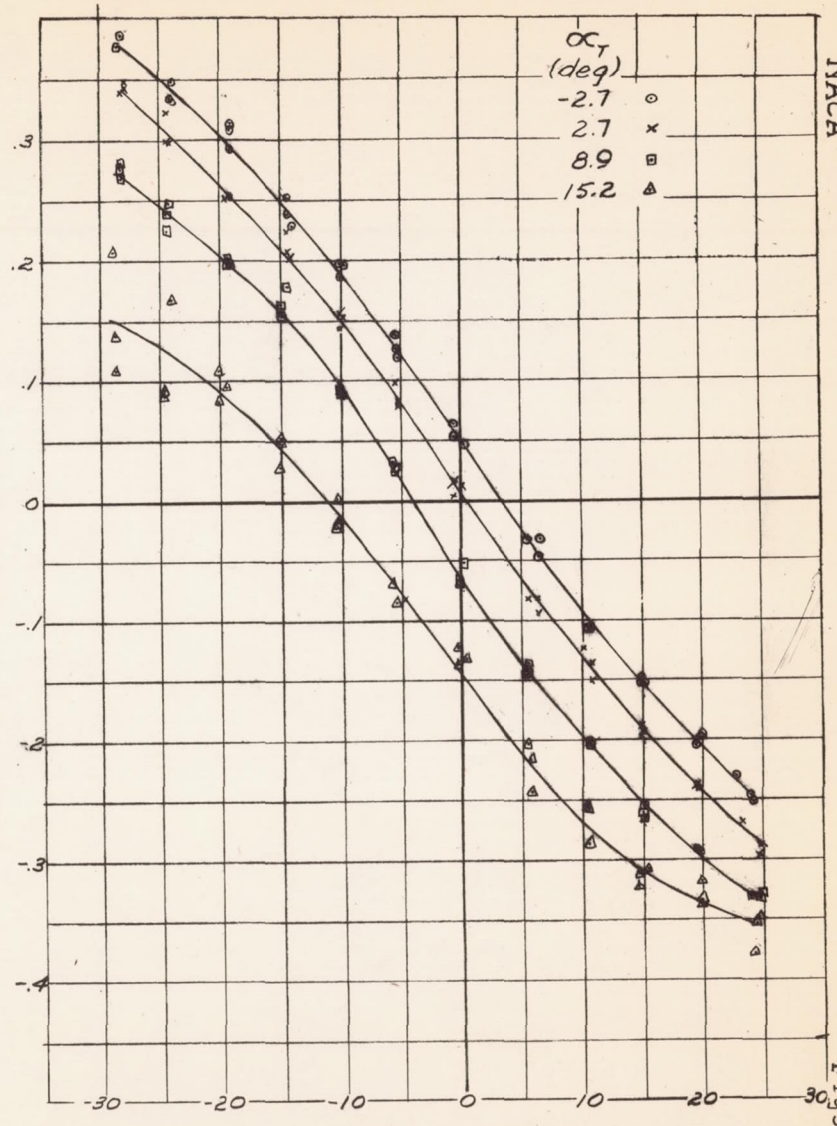

Figure 16.- Variation of C_m with δ_e at various angles of attack. Nacelles on; δ_f, 50°; propellers removed.

NACA

Figs. 15,16

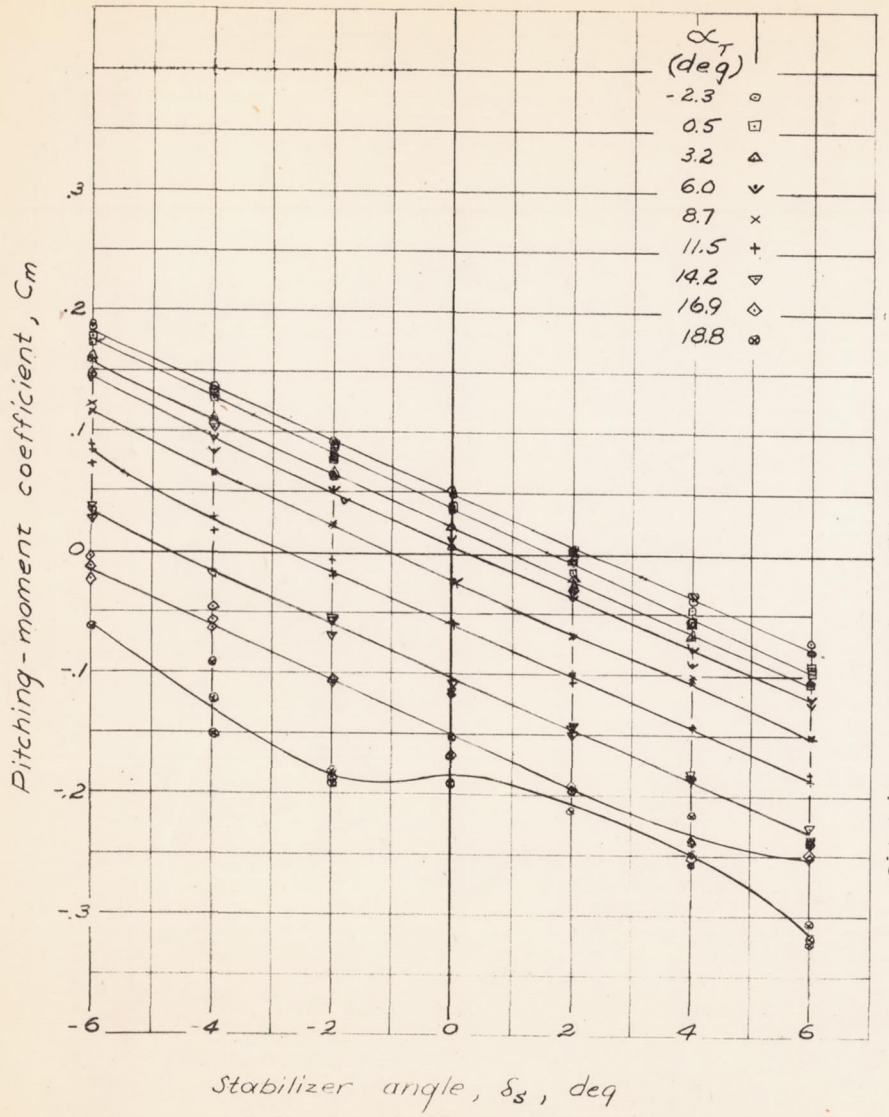

Figure 17.- Variation of C_m with δ_s at various angles of attack. Nacelles on; δ_f, 0°; propellers removed.

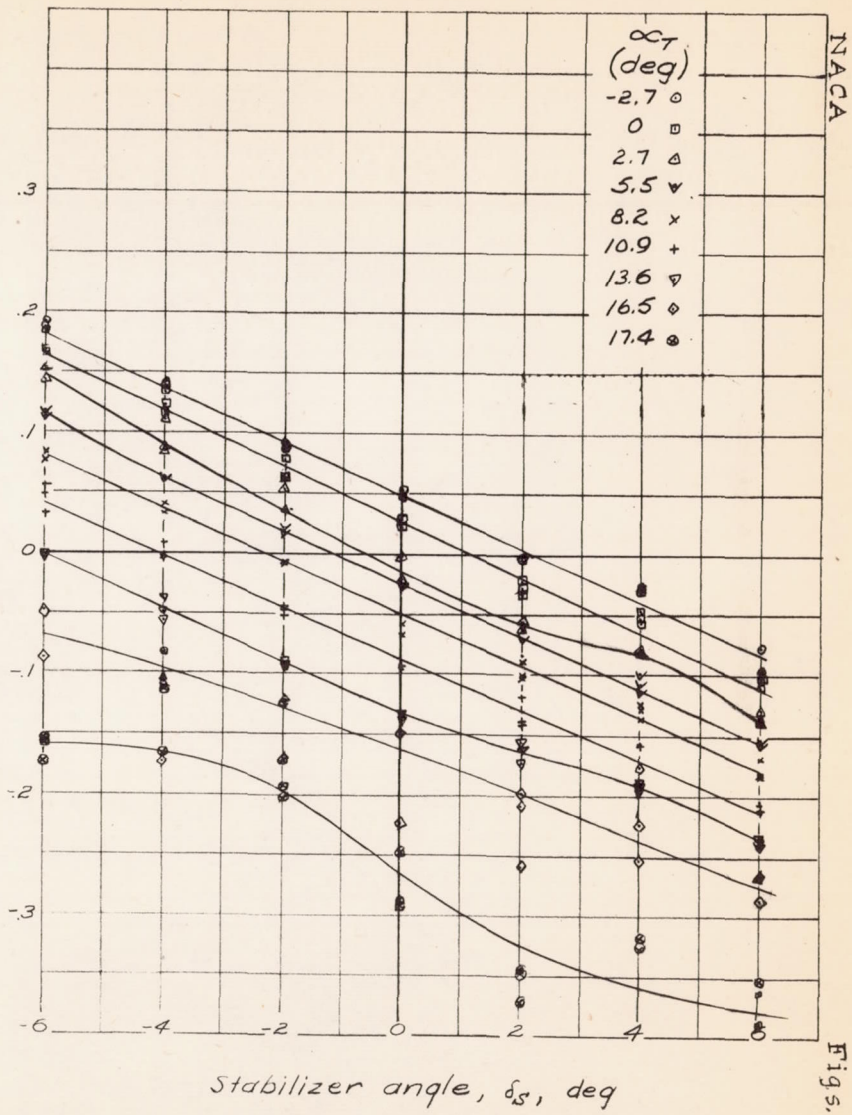

Figure 18.- Variation of C_m with δ_s at various angles of attack. Nacelles on; δ_f, 50°; propellers removed.

NACA

Figs. 17,18

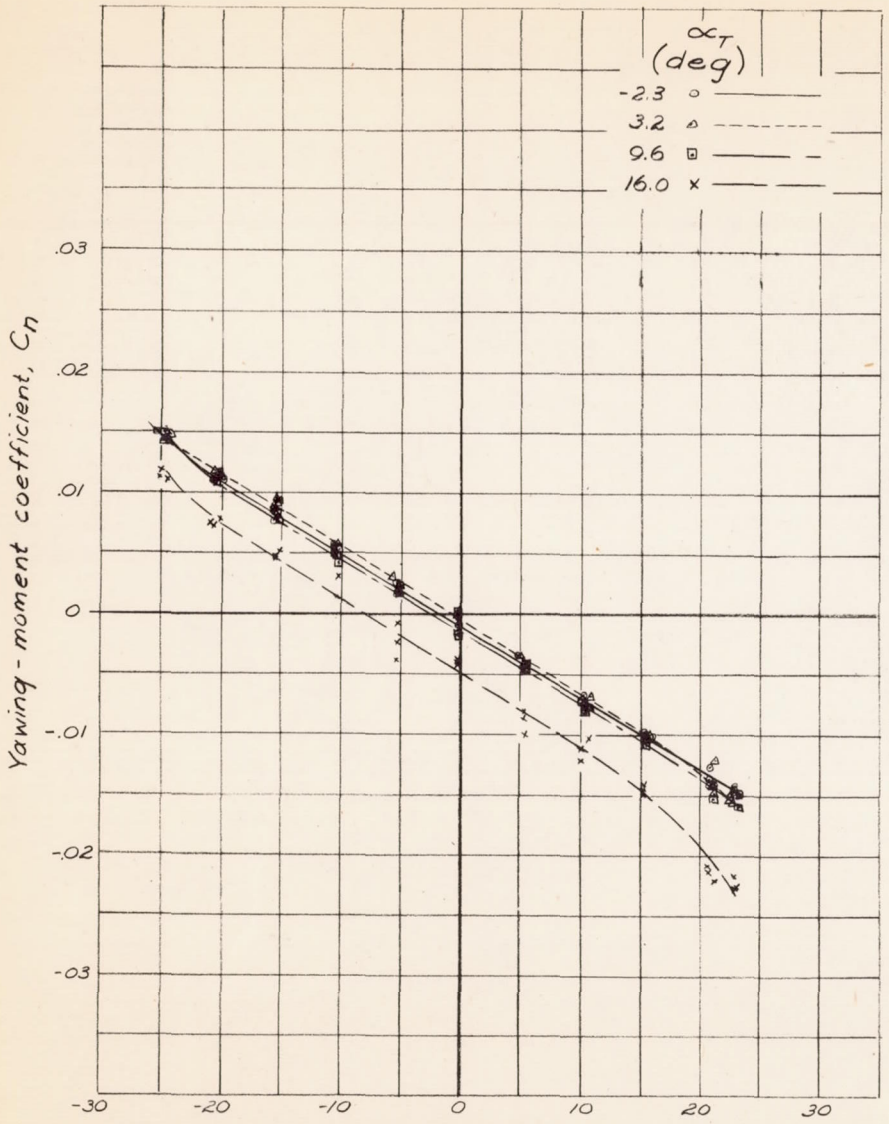

Figure 19.- Variation of C_n with δ_r at various angles of attack. Nacelles off; δ_f, 0°; horizontal tail surface removed; propellers removed.

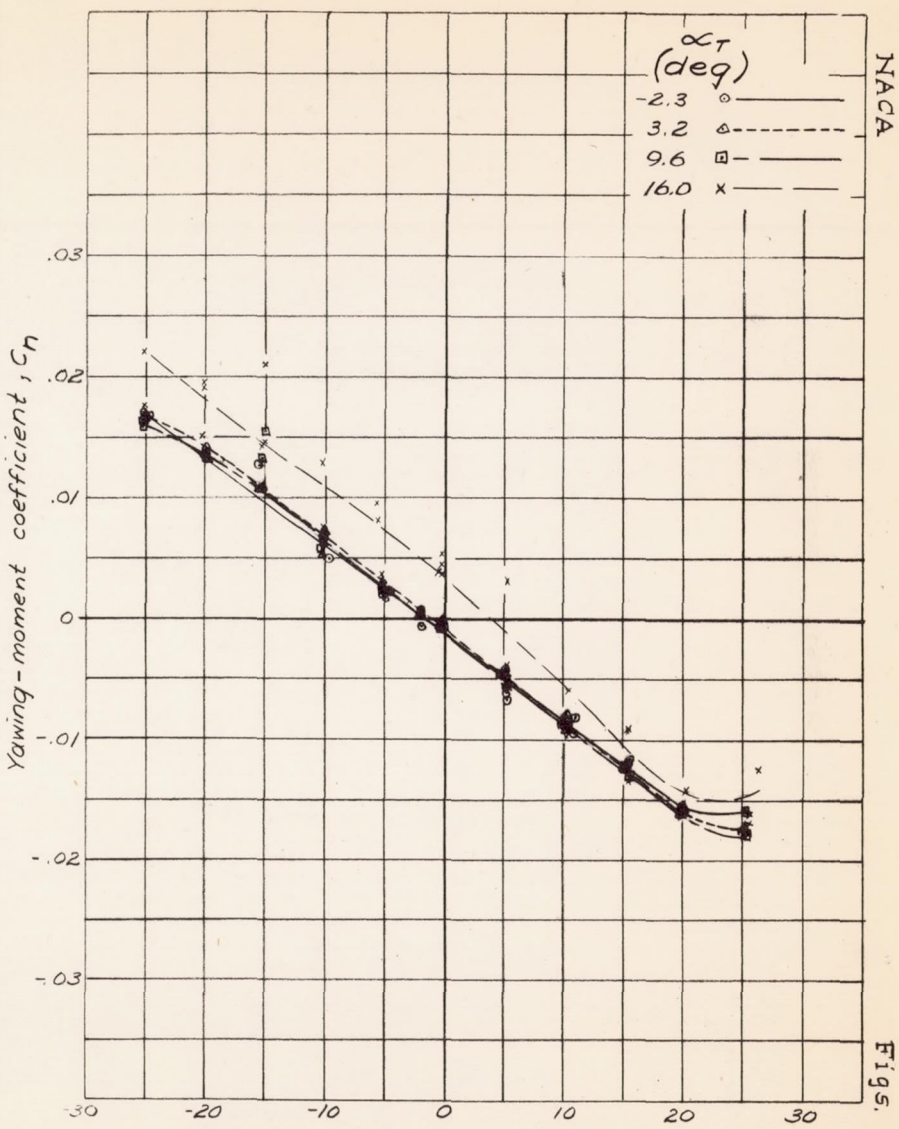

Figure 20.- Variation of C_n with δ_r at various angles of attack. Nacelles off; δ_f, 0°; horizontal tail surface attached; propellers removed.

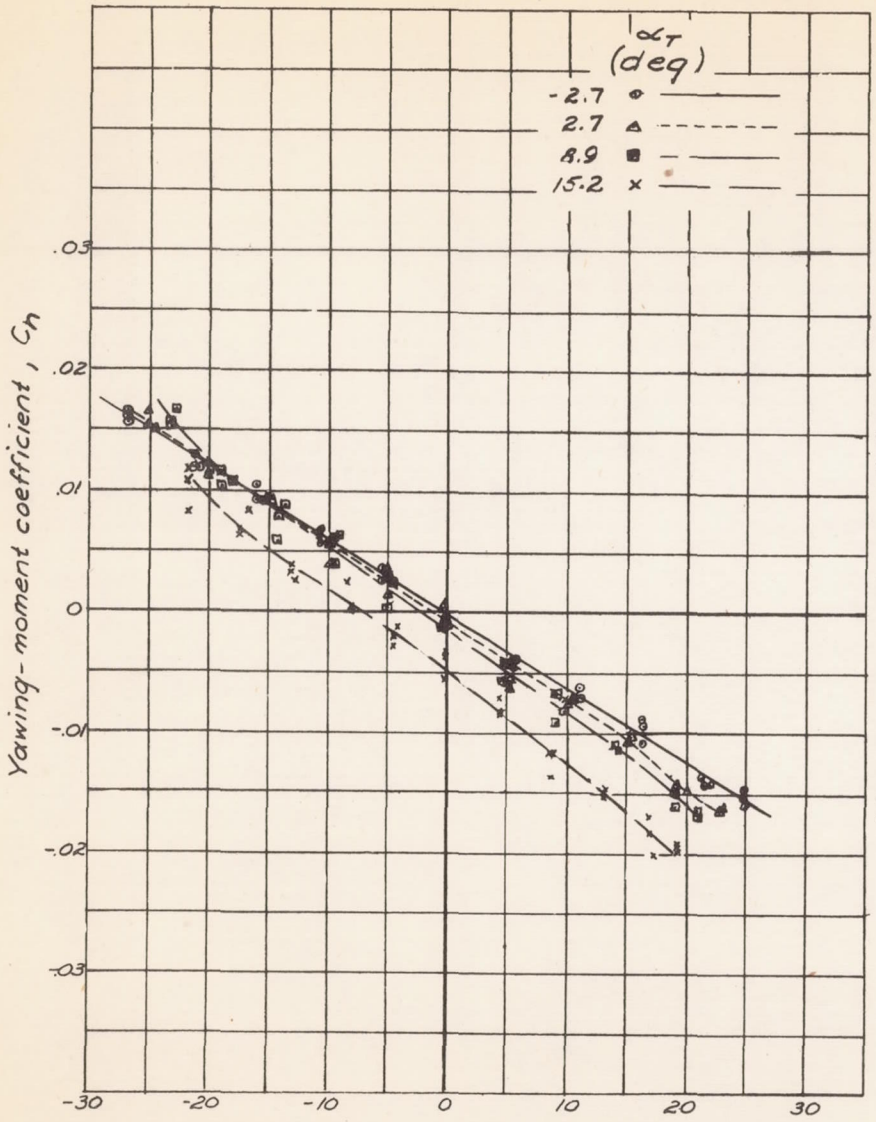

Figure 21.- Variation of C_n with δ_r at various angles of attack. Nacelles off; δ_f, 50°; horizontal tail surface removed; propellers removed.

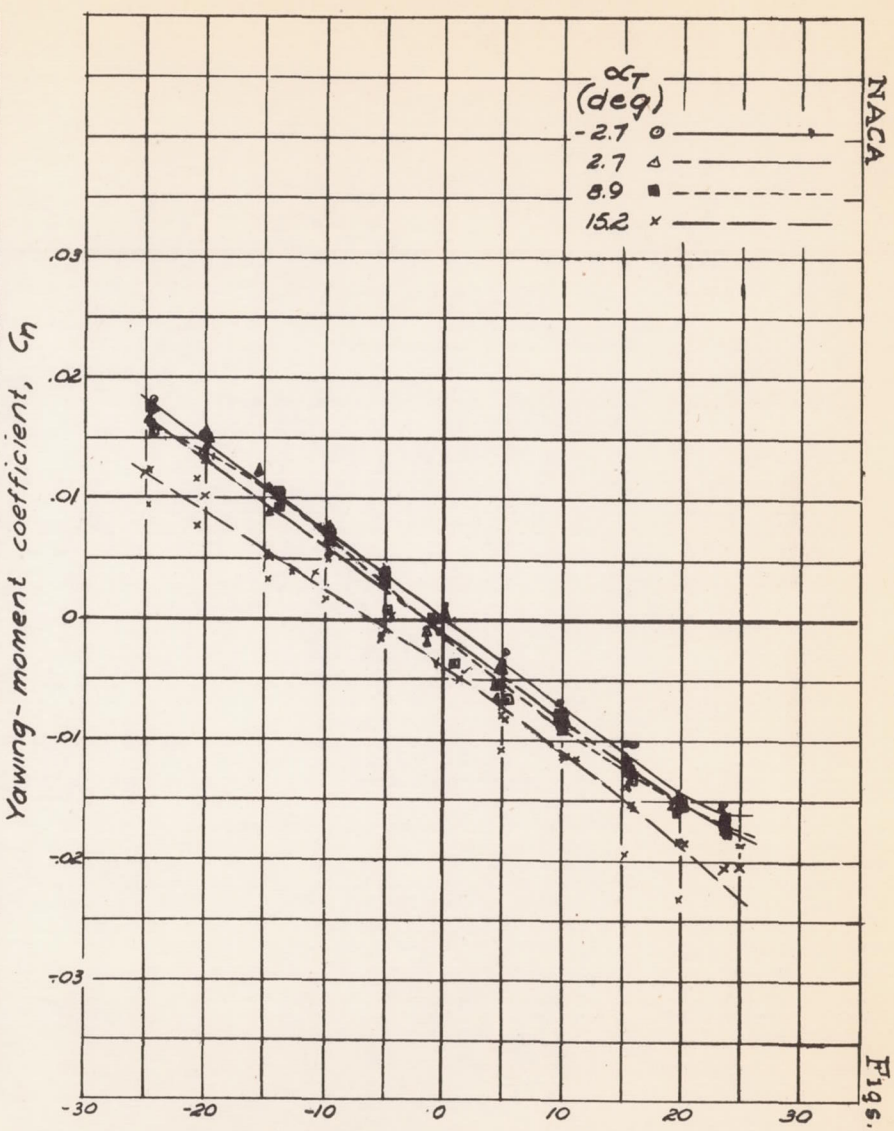

Figure 22.- Variation of C_n with δ_r at various angles of attack. Nacelles off; δ_f, 50°; horizontal tail surface attached, propellers removed.

NACA

Figs. 21, 22.

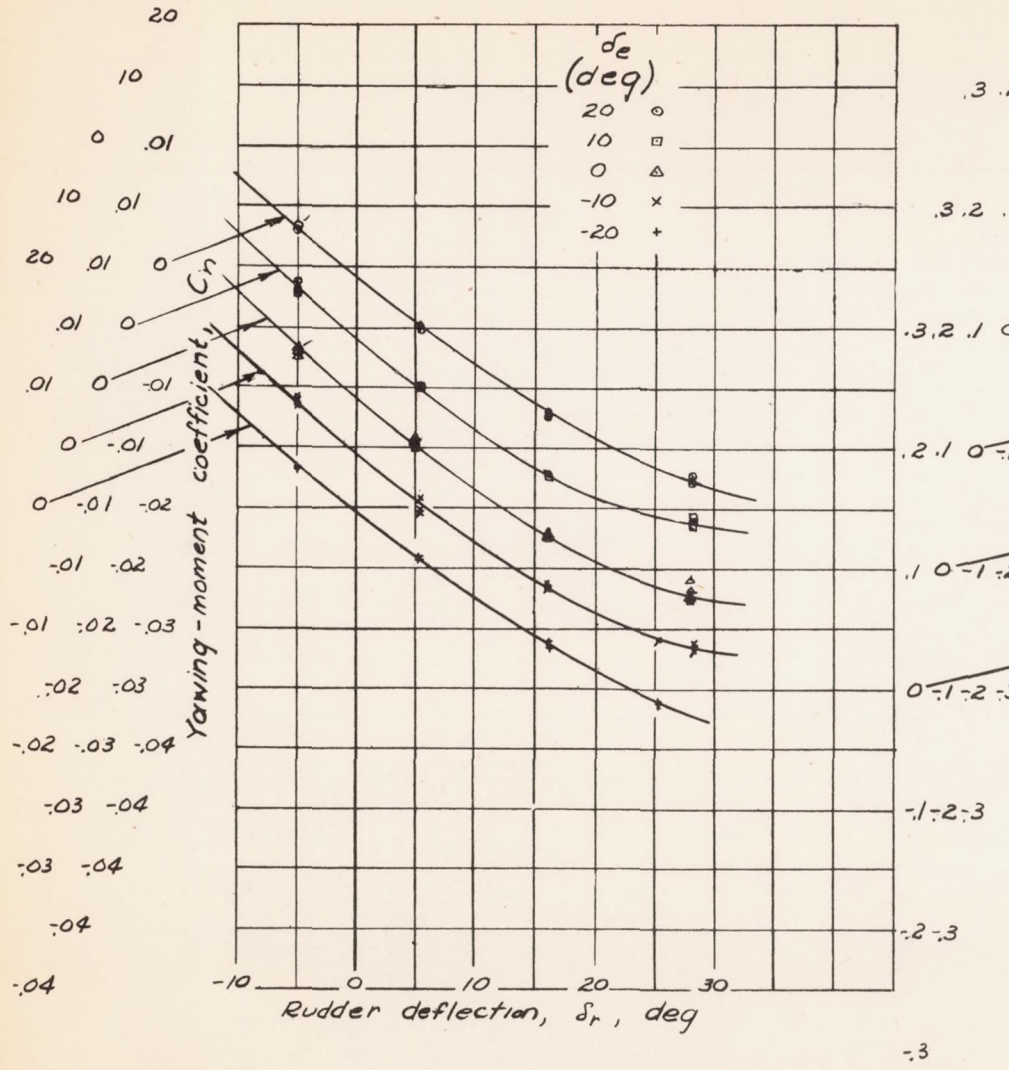

Figure 23.- Variation of C_n with δ_r for various elevator deflections. Nacelles off; δ_f, 0°; propellers removed.

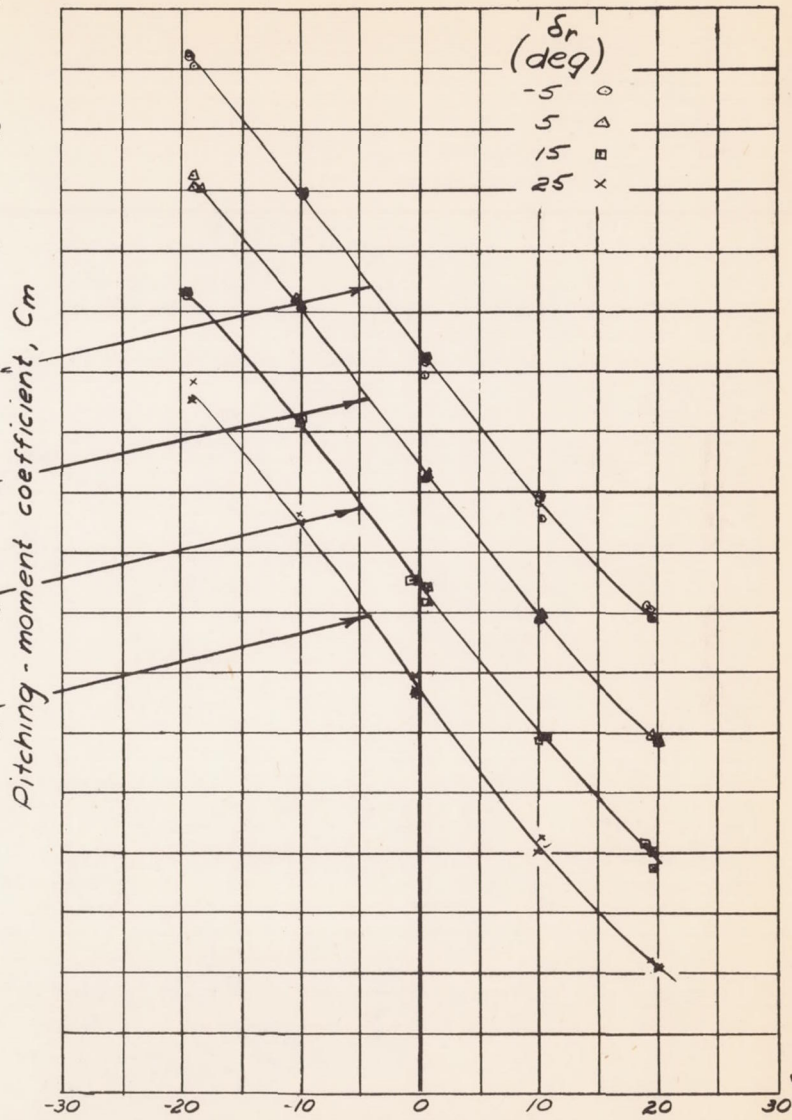

Figure 24.- Variation of C_m with δ_e for various rudder deflections. Nacelles off; δ_f, 0°; propellers removed.

NACA

Figs. 23,24

L-425

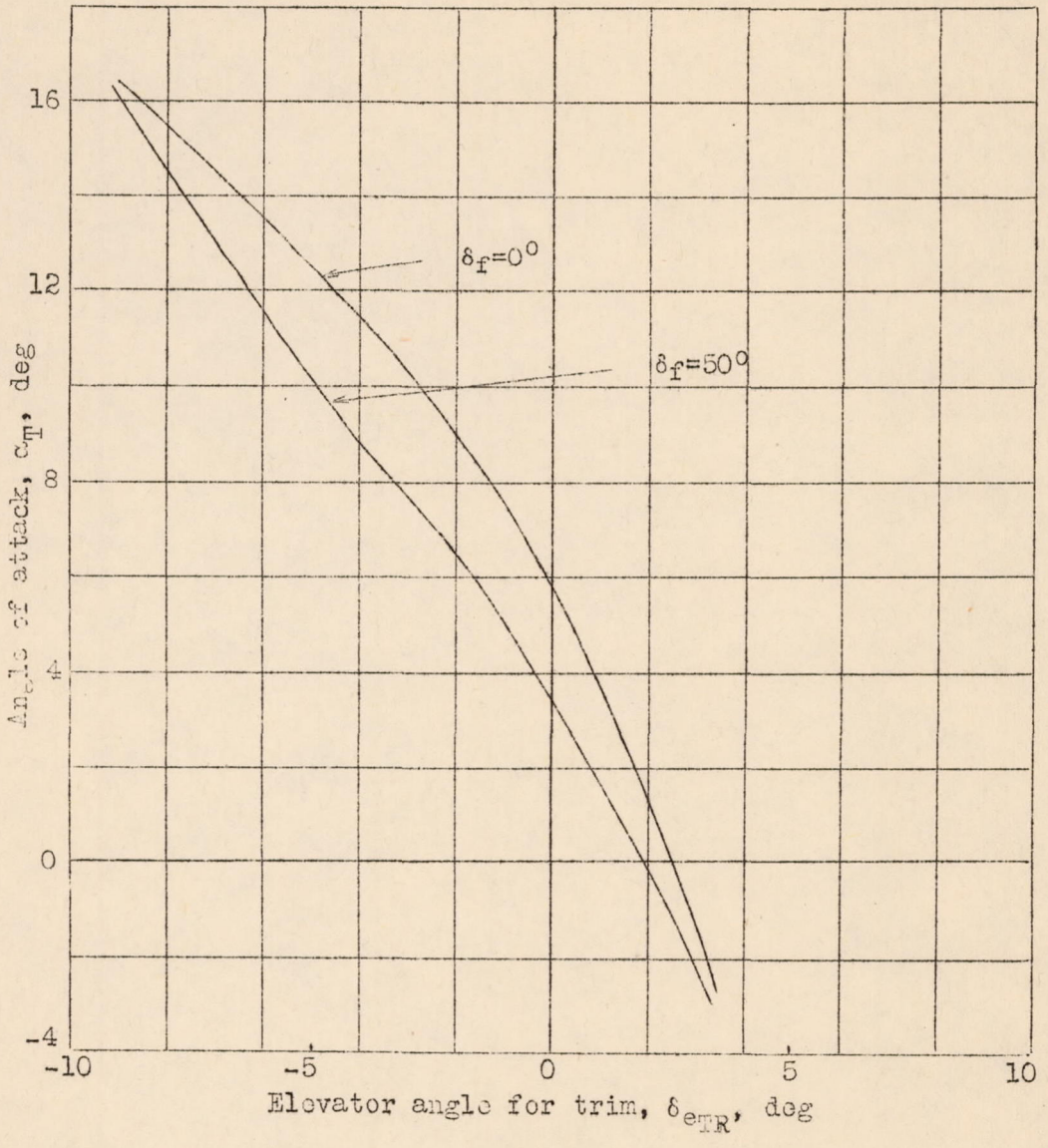

Figure 25.- Elevator angles for trim as a function of angle of attack. Propellers removed; nacelles on.

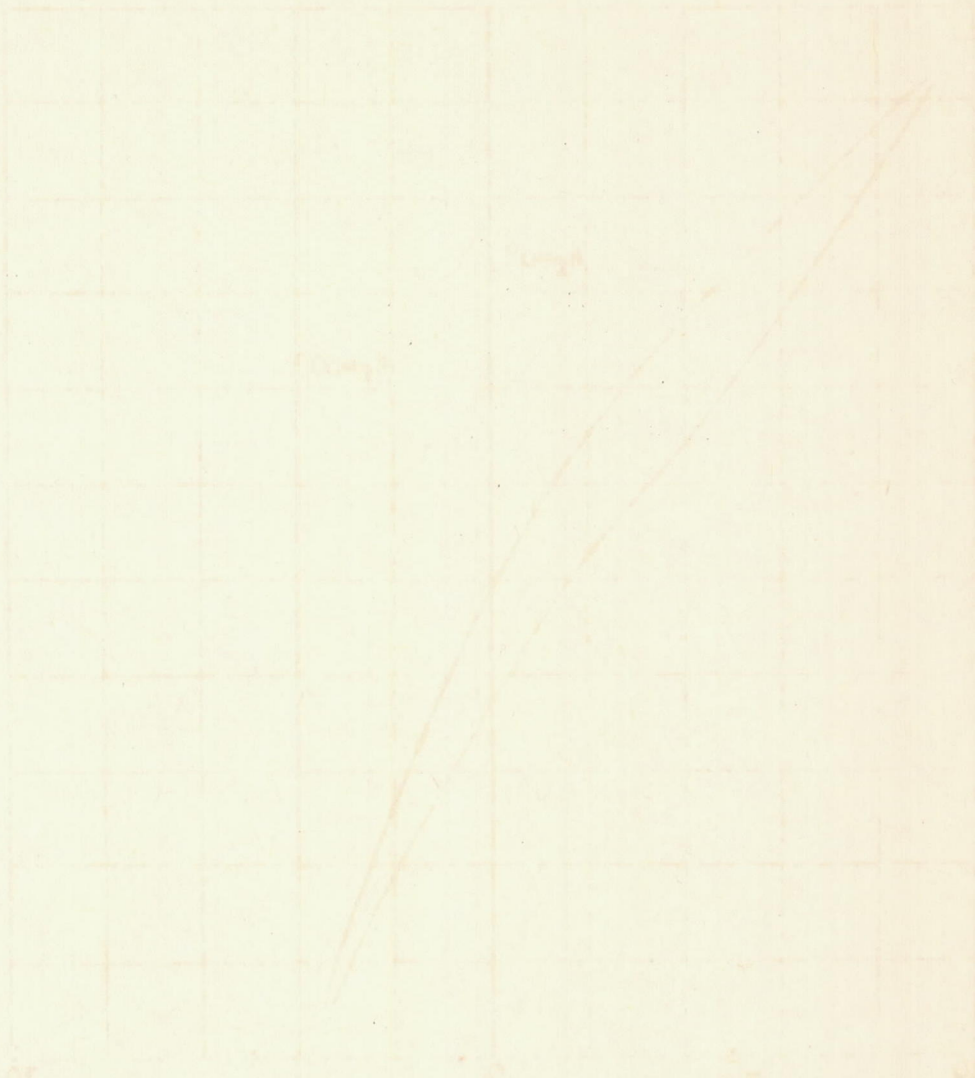

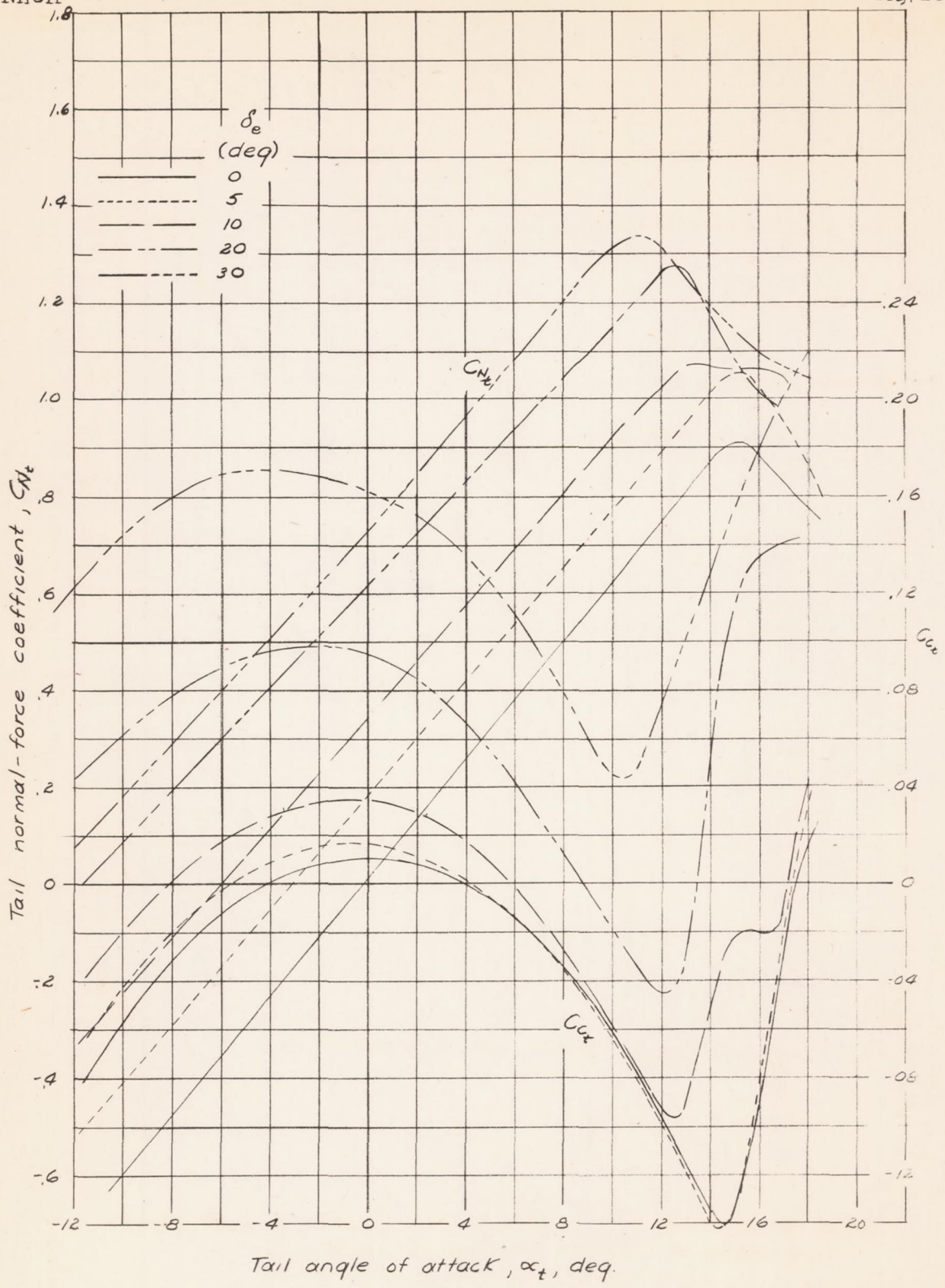

Figure 26.- Isolated horizontal tail surface characteristics. Variation of C_N and C_C with α_t at various elevator deflections. From reference 2, figure 5.

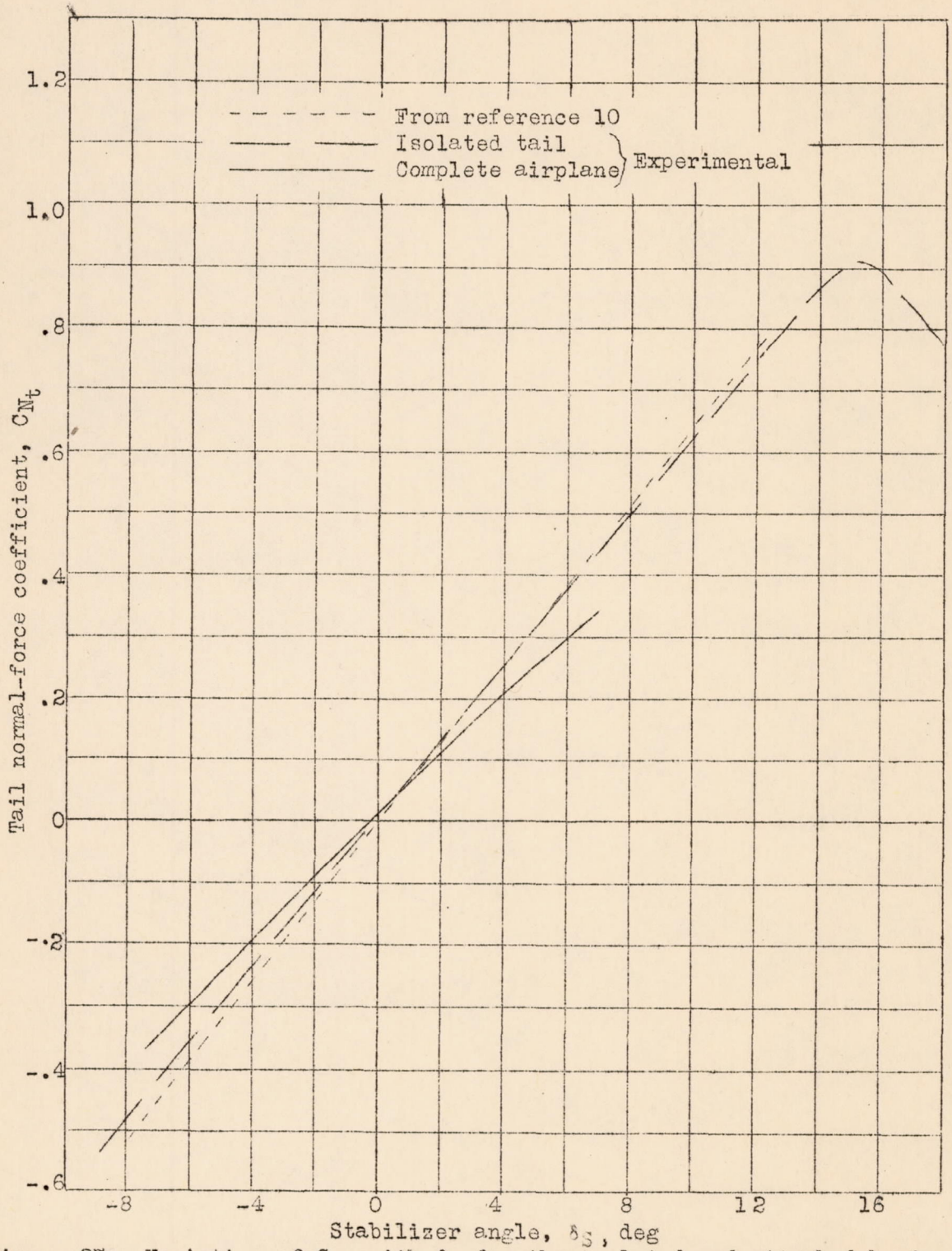

Figure 27.- Variation of C_{N_t} with δ_S for the isolated and attached horizontal tail surface together with values computed for the isolated tail. Propellers removed.

L-425

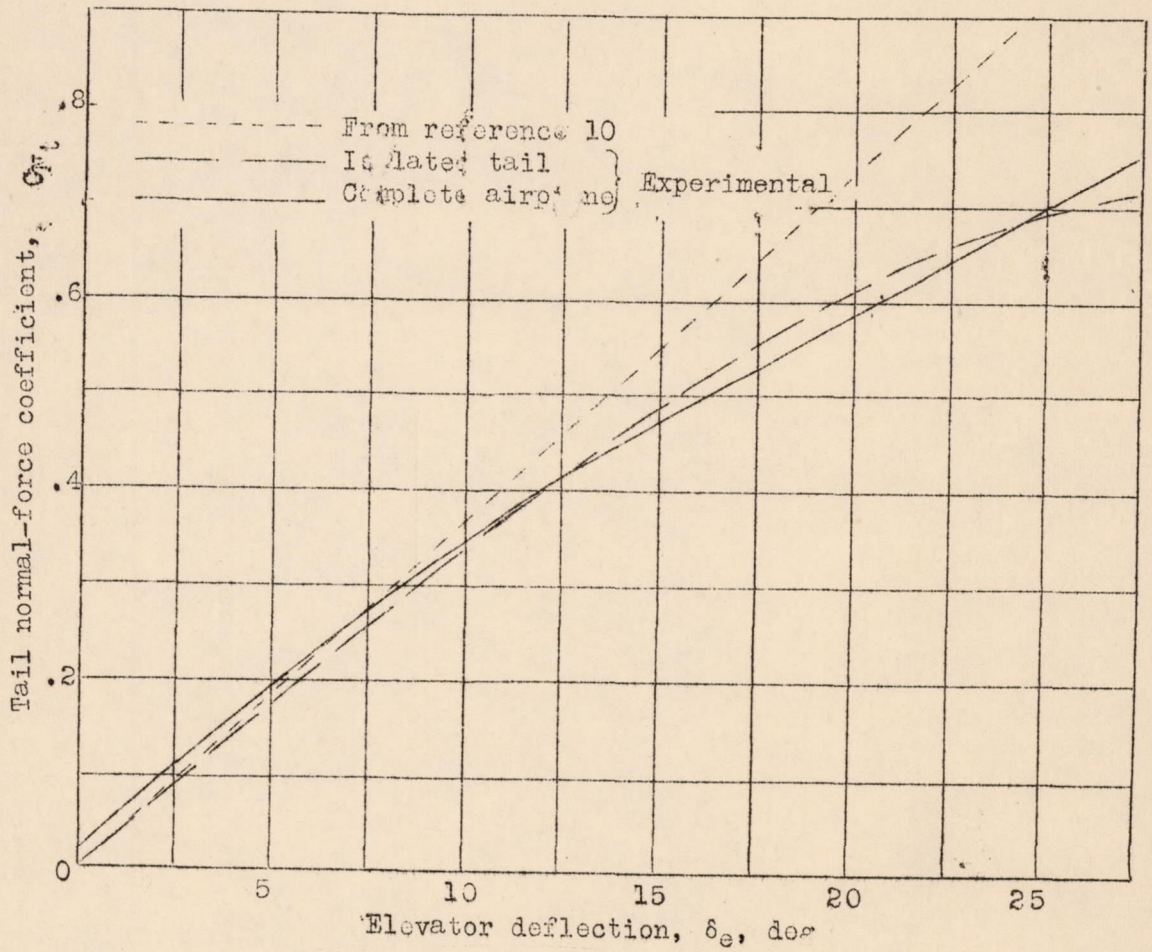

Figure 28.- Variation of C_{N_t} with δ_e for the isolated and attached horizontal tail surface together with values computed for the isolated tail. Propellers removed.

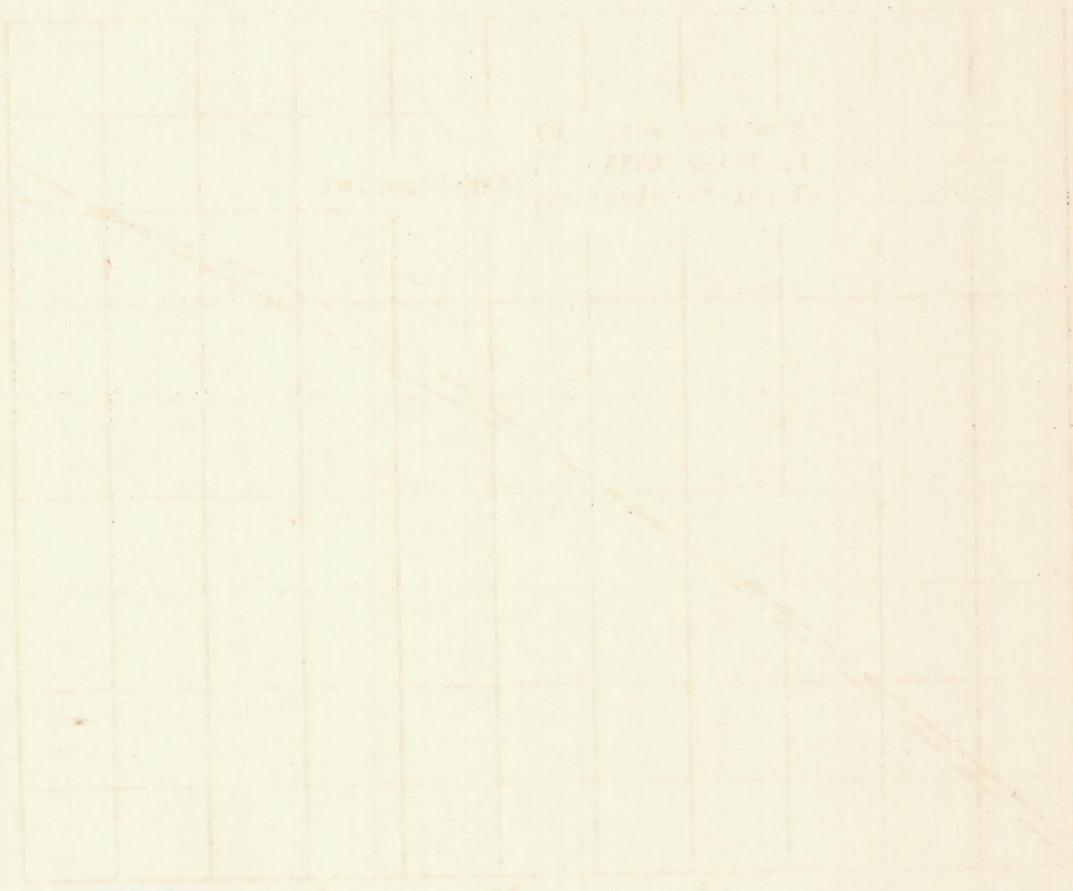

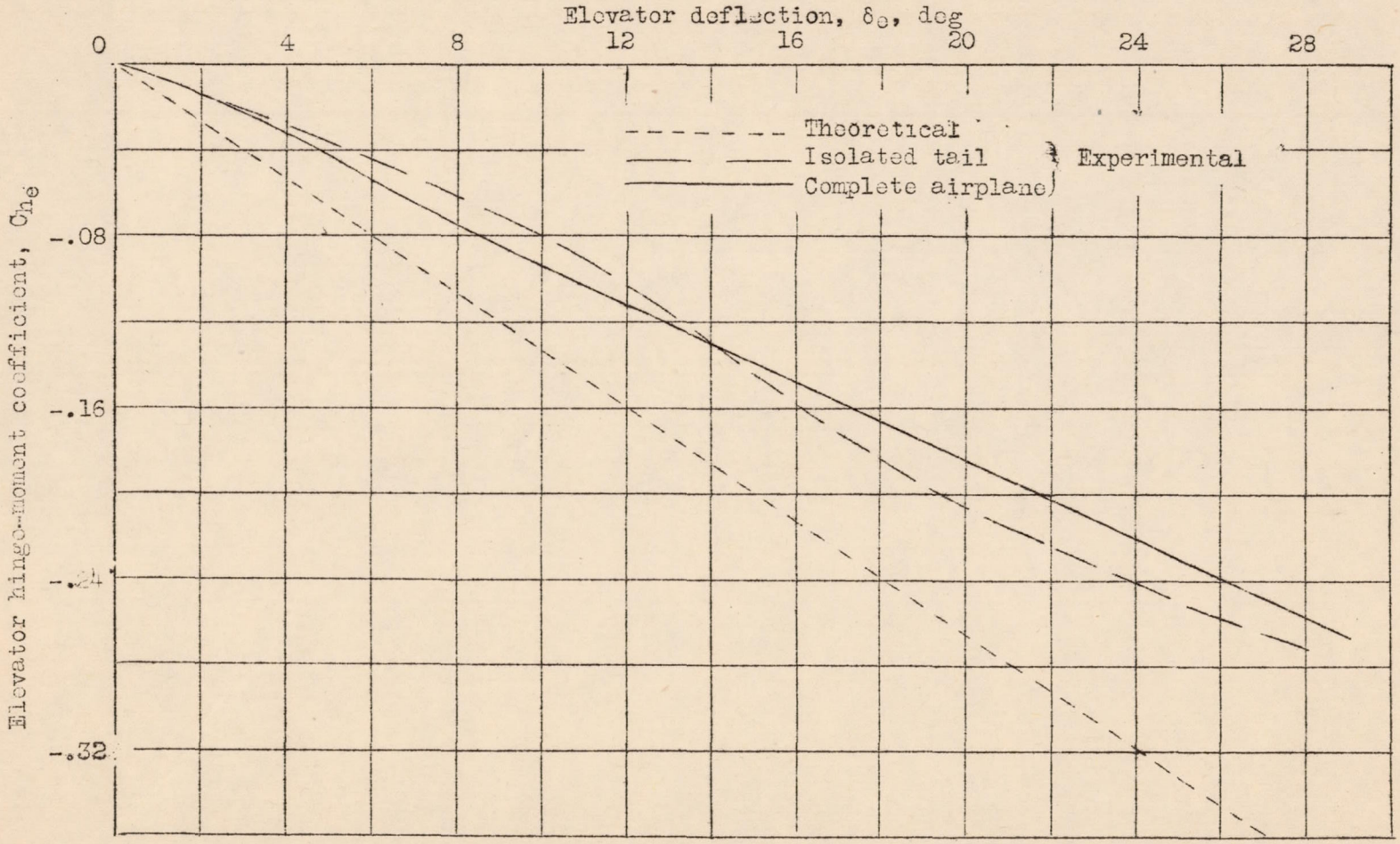

Figure 29.- Variation of C_{h_e} with δ_e for the isolated and attached horizontal tail surface together with values computed for the isolated tail. Propellers removed.

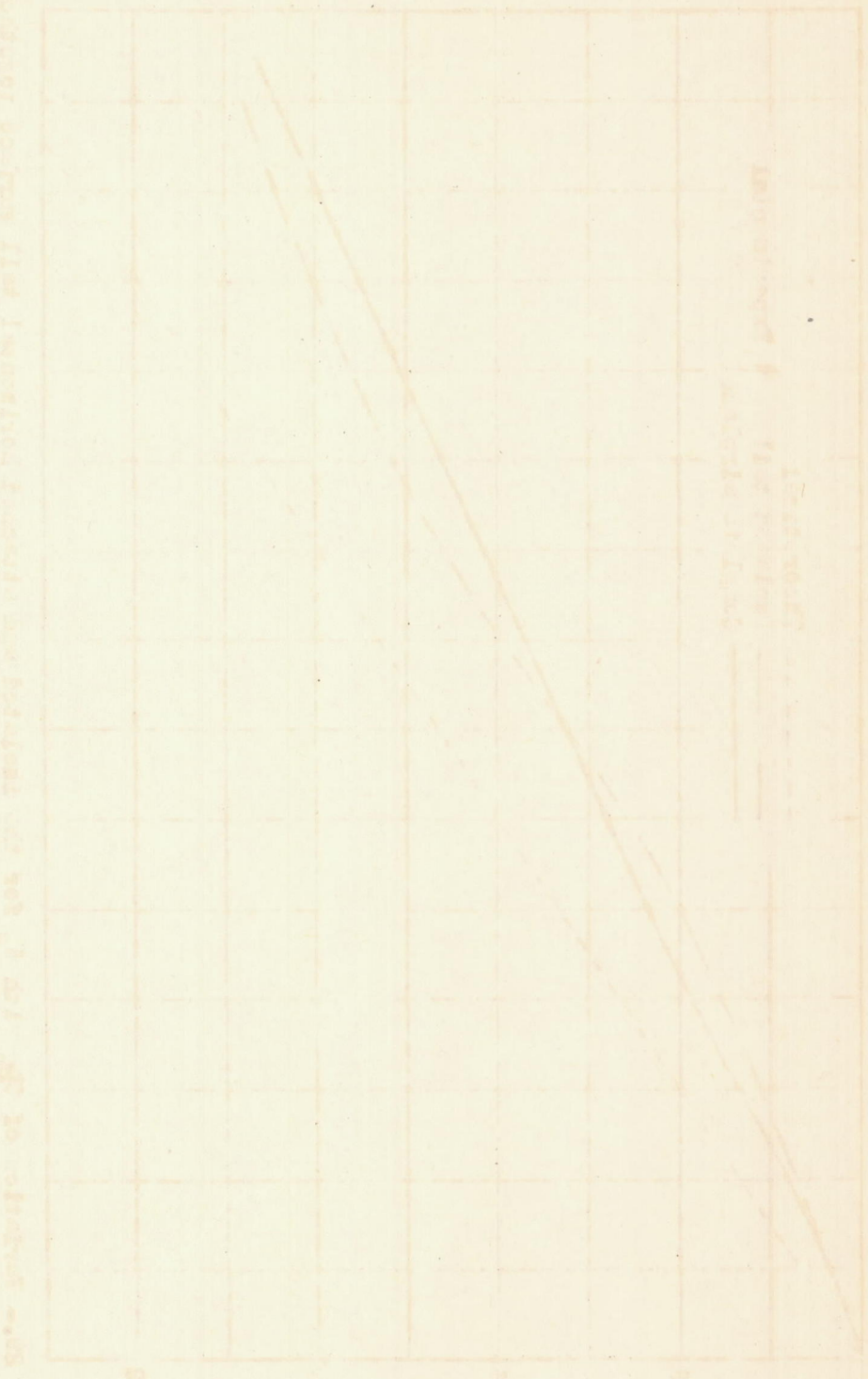

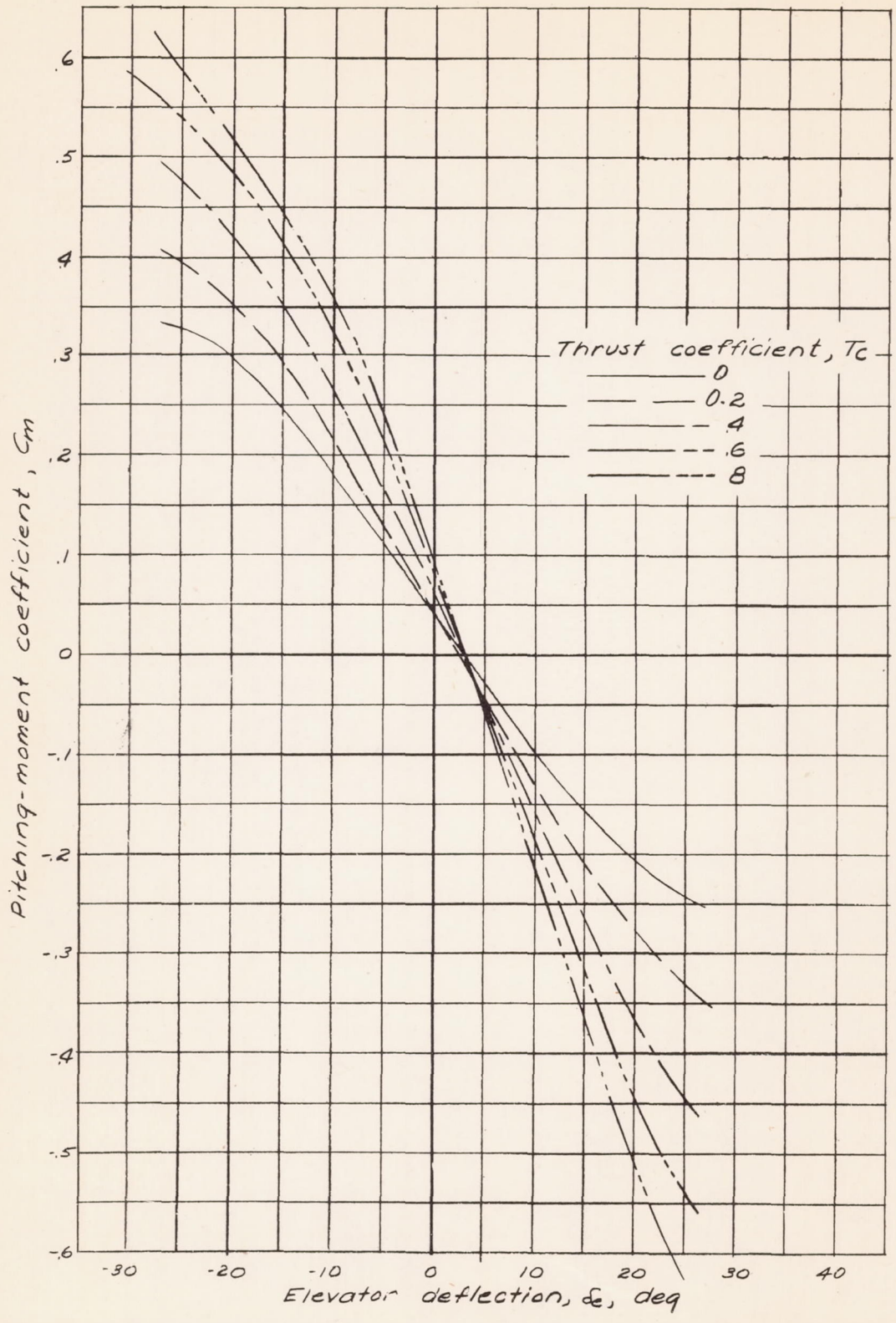

Figure 30.- Variation of C_m with δ_e for various thrust coefficients. α_T, -4.1°; δ_f, 0°; nacelles off.

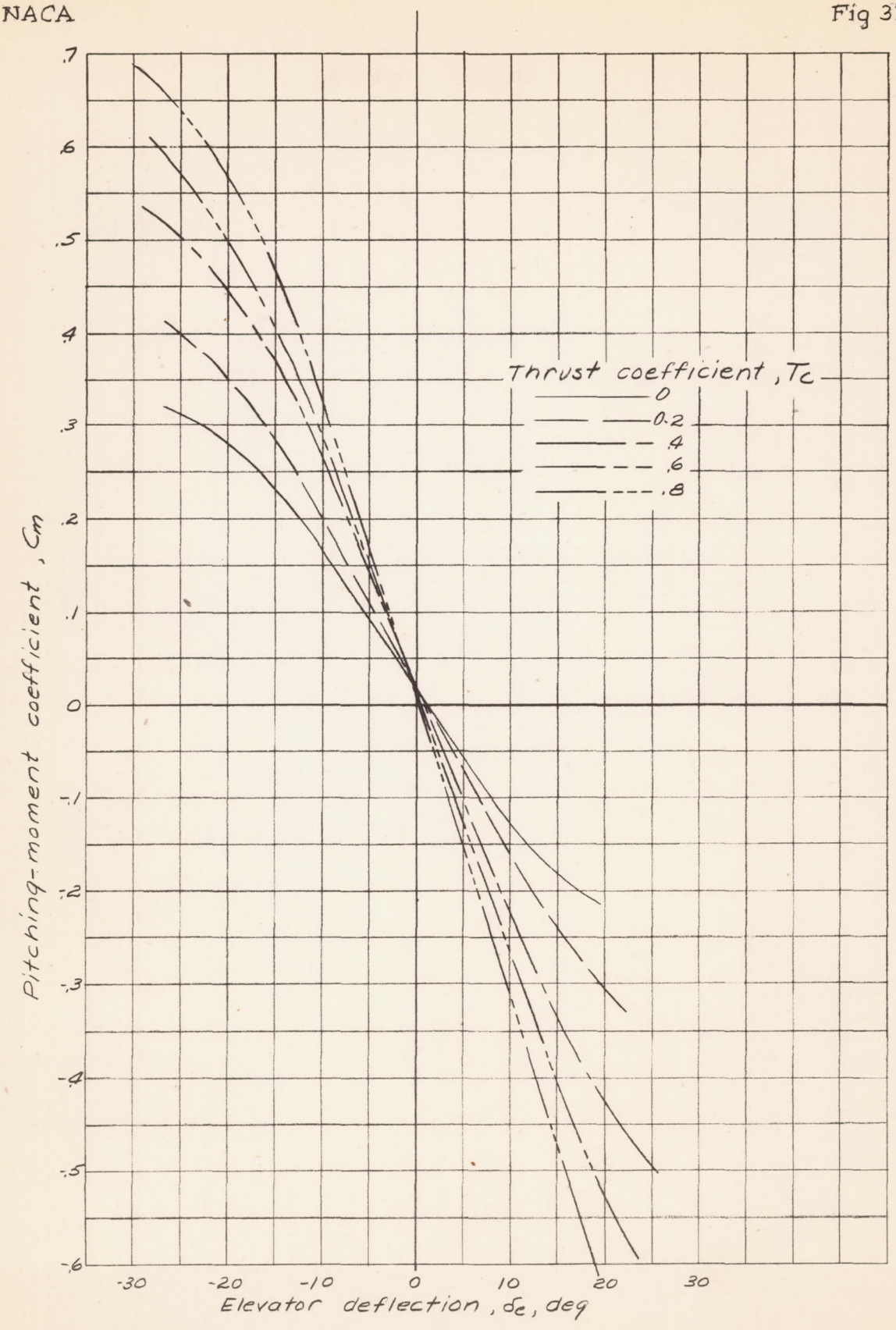

Figure 31.- Variation of C_m with δ_e for various thrust coefficients. α_T, 1.4°; δ_f, 0°; nacelles off.

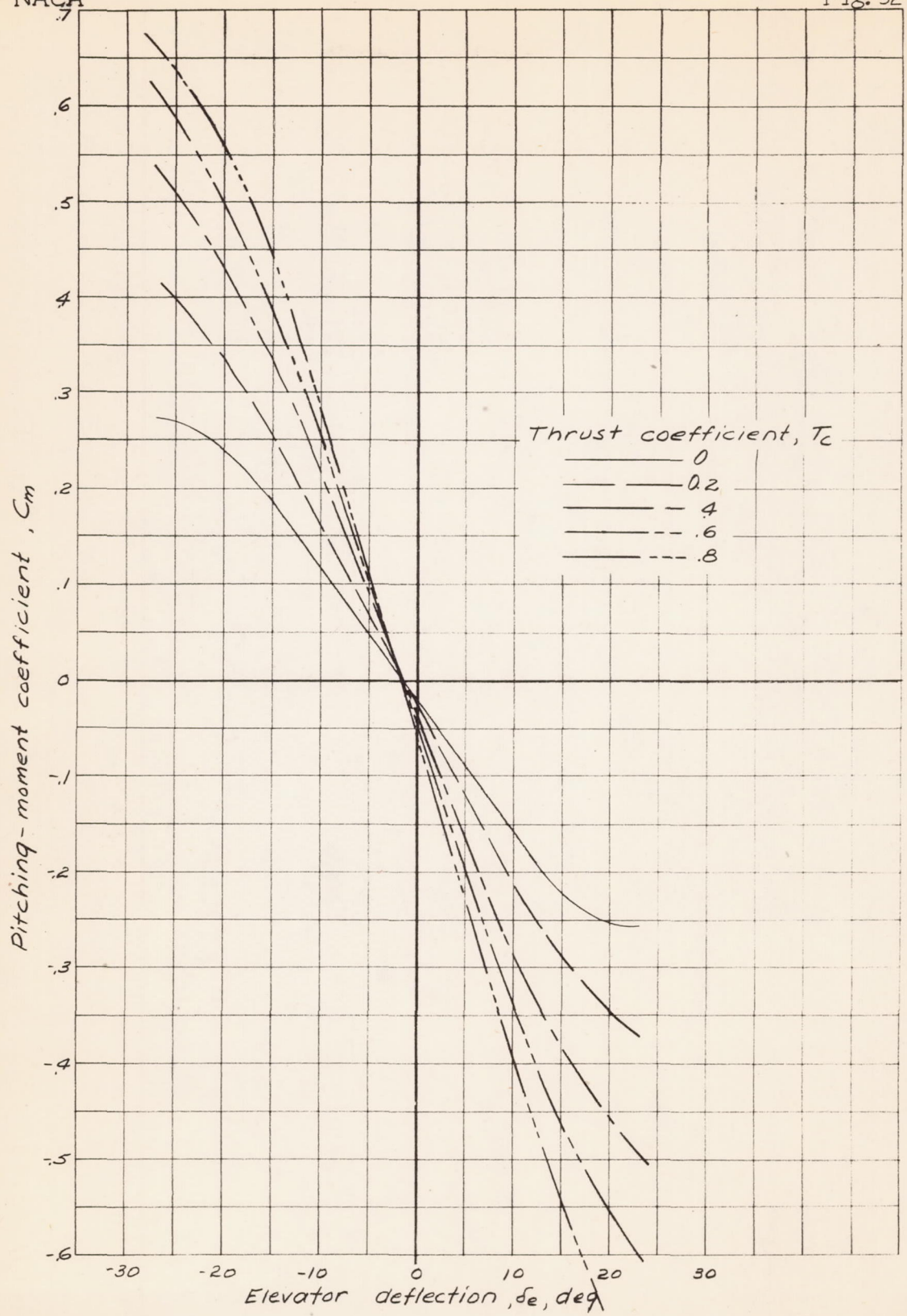

Figure 32.- Variation of C_m with δ_e for various thrust coefficients. α_T, 7.7°; δ_f, 0°; nacelles off.

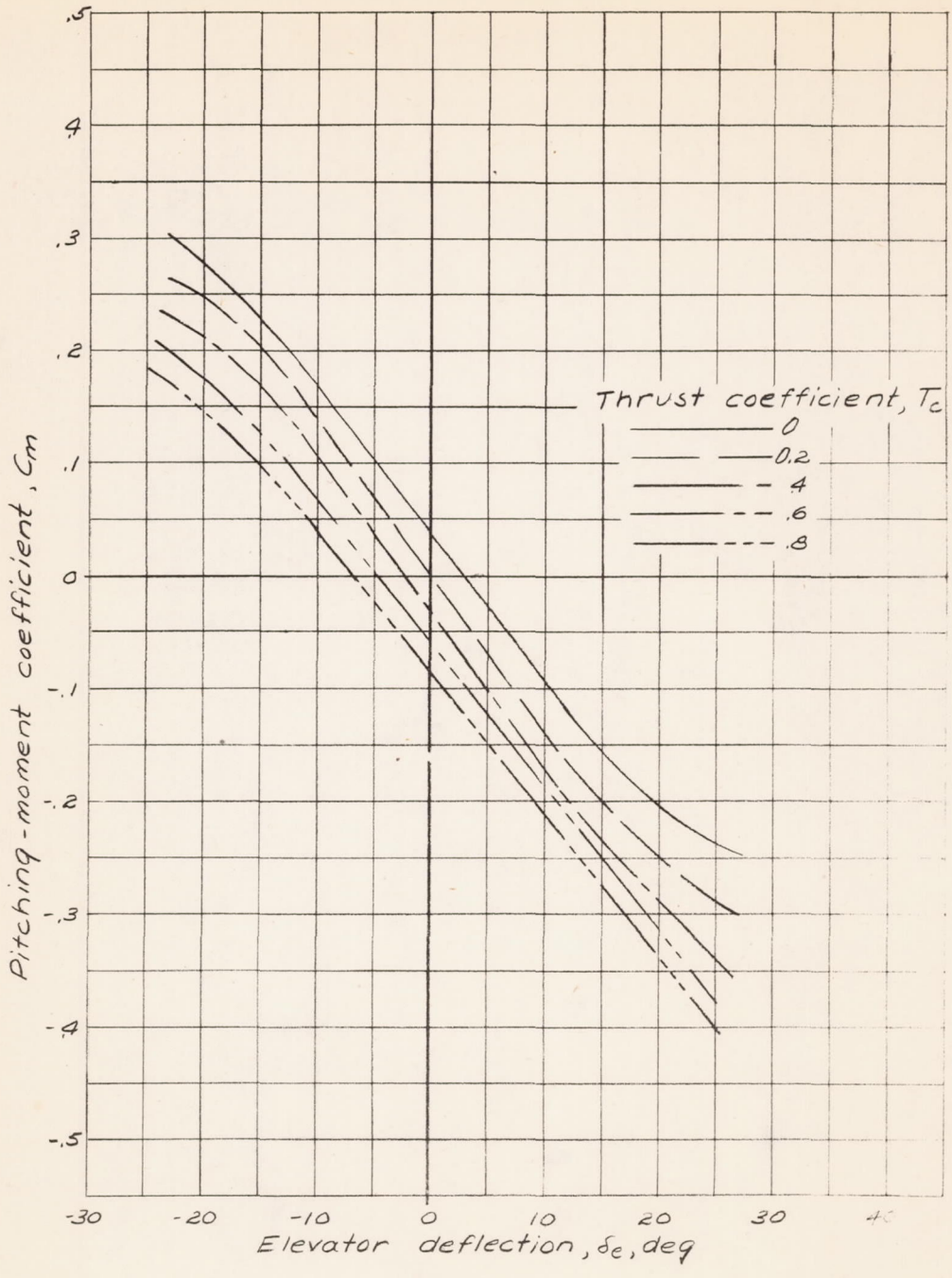

Figure 33.- Variation of C_m with δ_e at various thrust coefficients. α_T, -4.7°; δ_f, 50°; nacelles off.

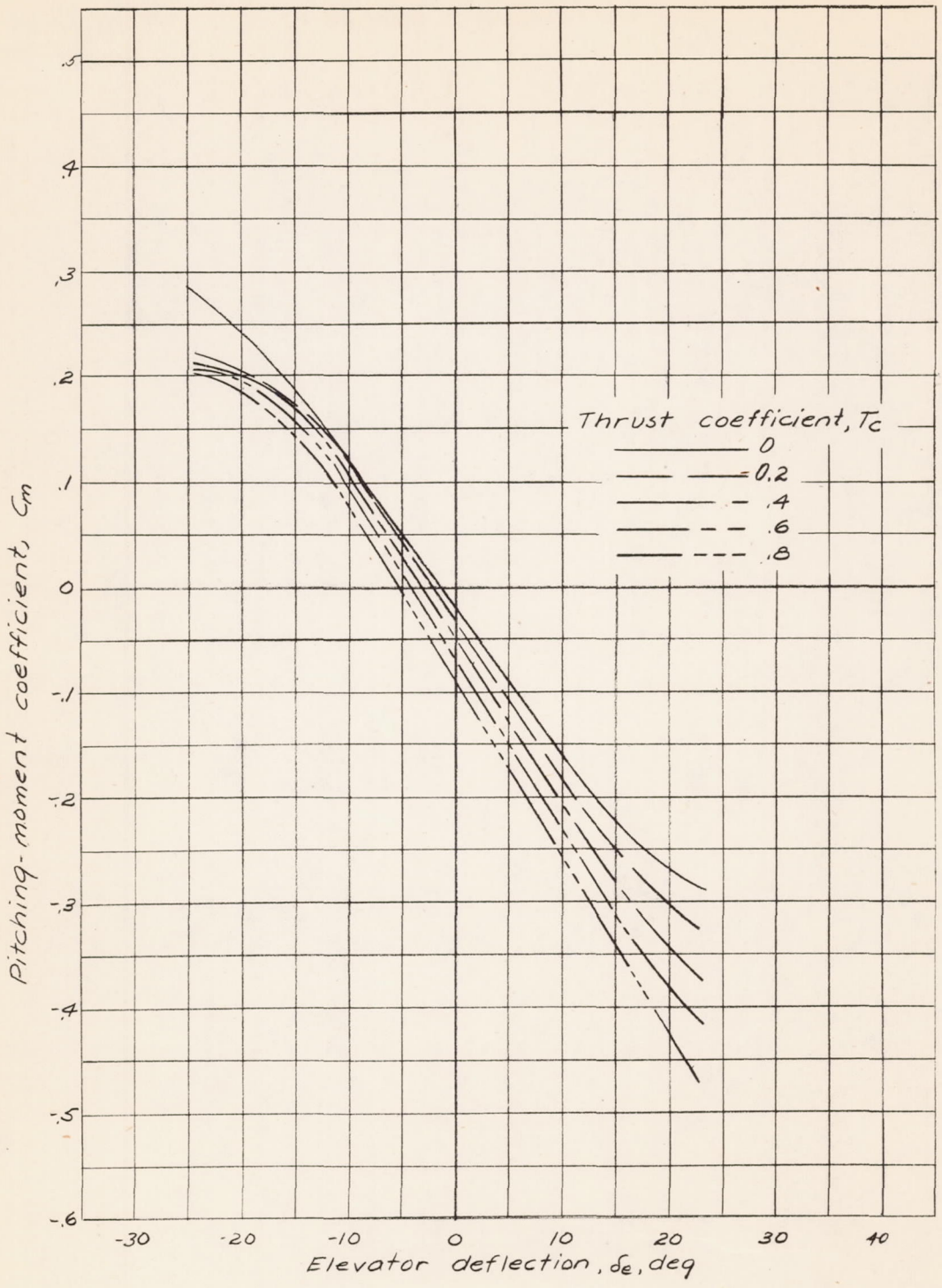

Figure 34.- Variation of C_m with δ_e at various thrust coefficients. α_T, 0.5°; δ_f, 50°; nacelles off.

L-425

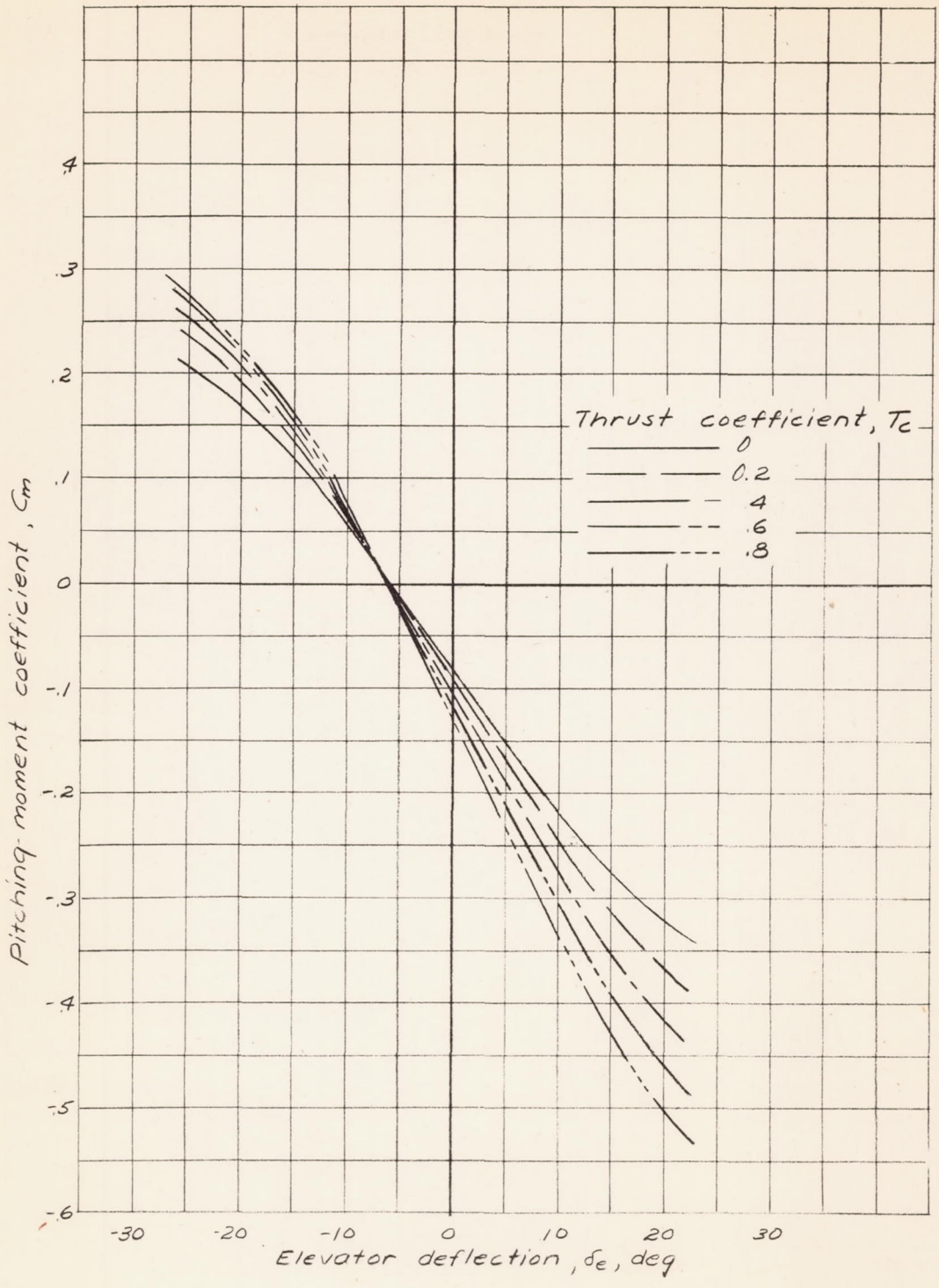

Figure 35.- Variation of C_m with δ_e at various thrust coefficients. α_T, 6.7°; δ_f, 50°; nacelles off.

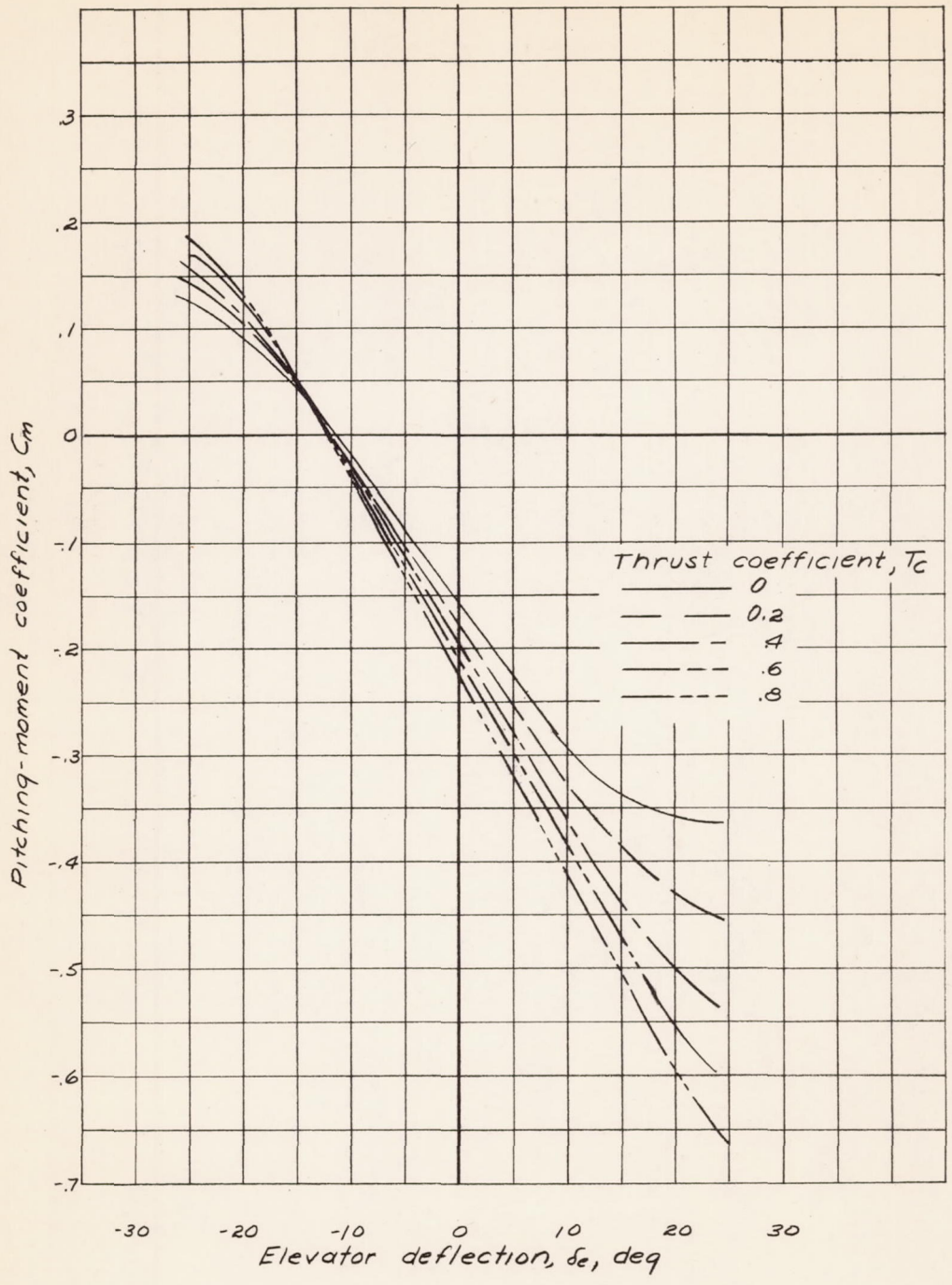

Figure 36.- Variation of C_m with δ_e at various thrust coefficients. α_T, 13.0°; δ_f, 50°; nacelles off.

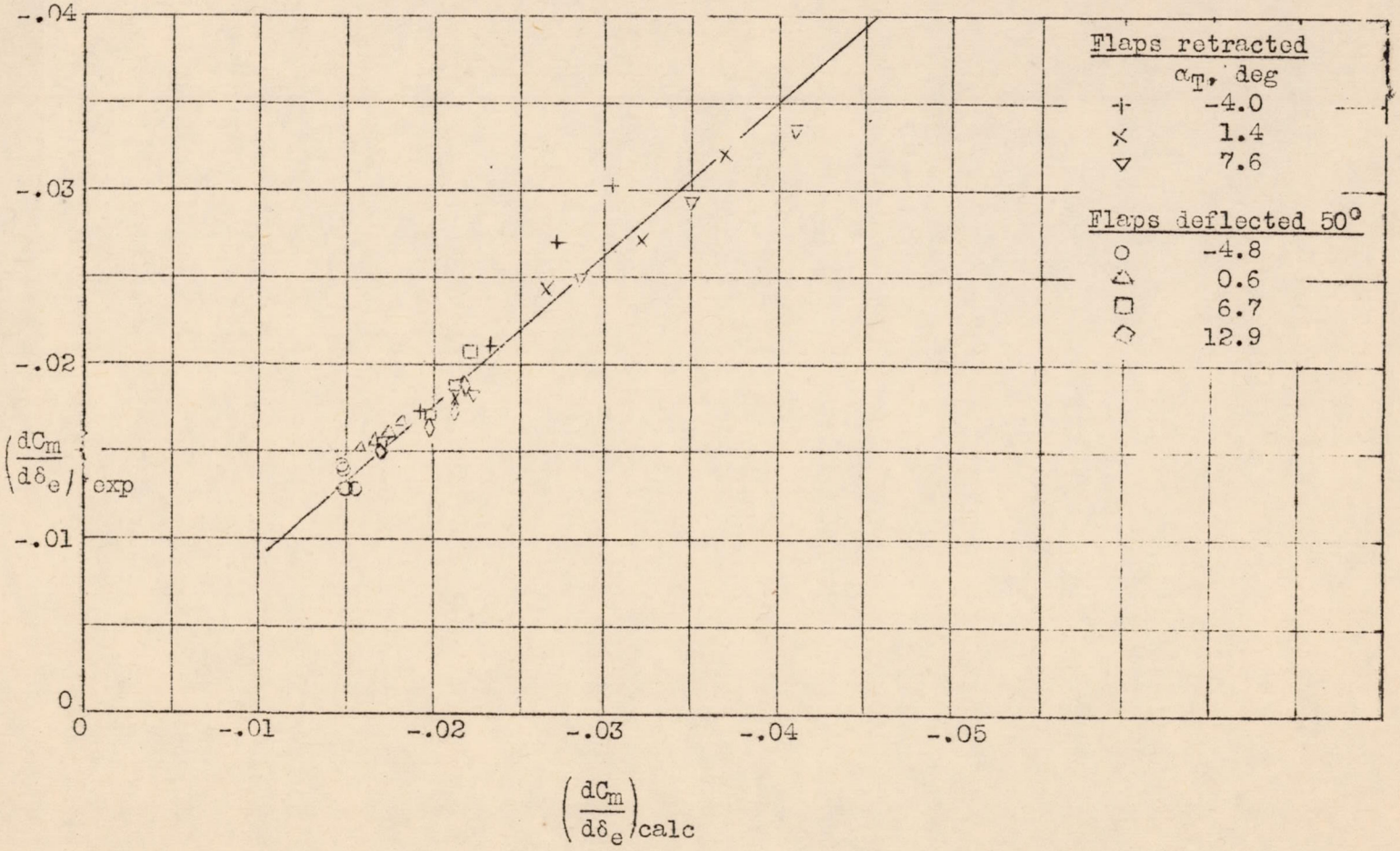

Figure 37.- Comparison between experimental and calculated elevator effectiveness.

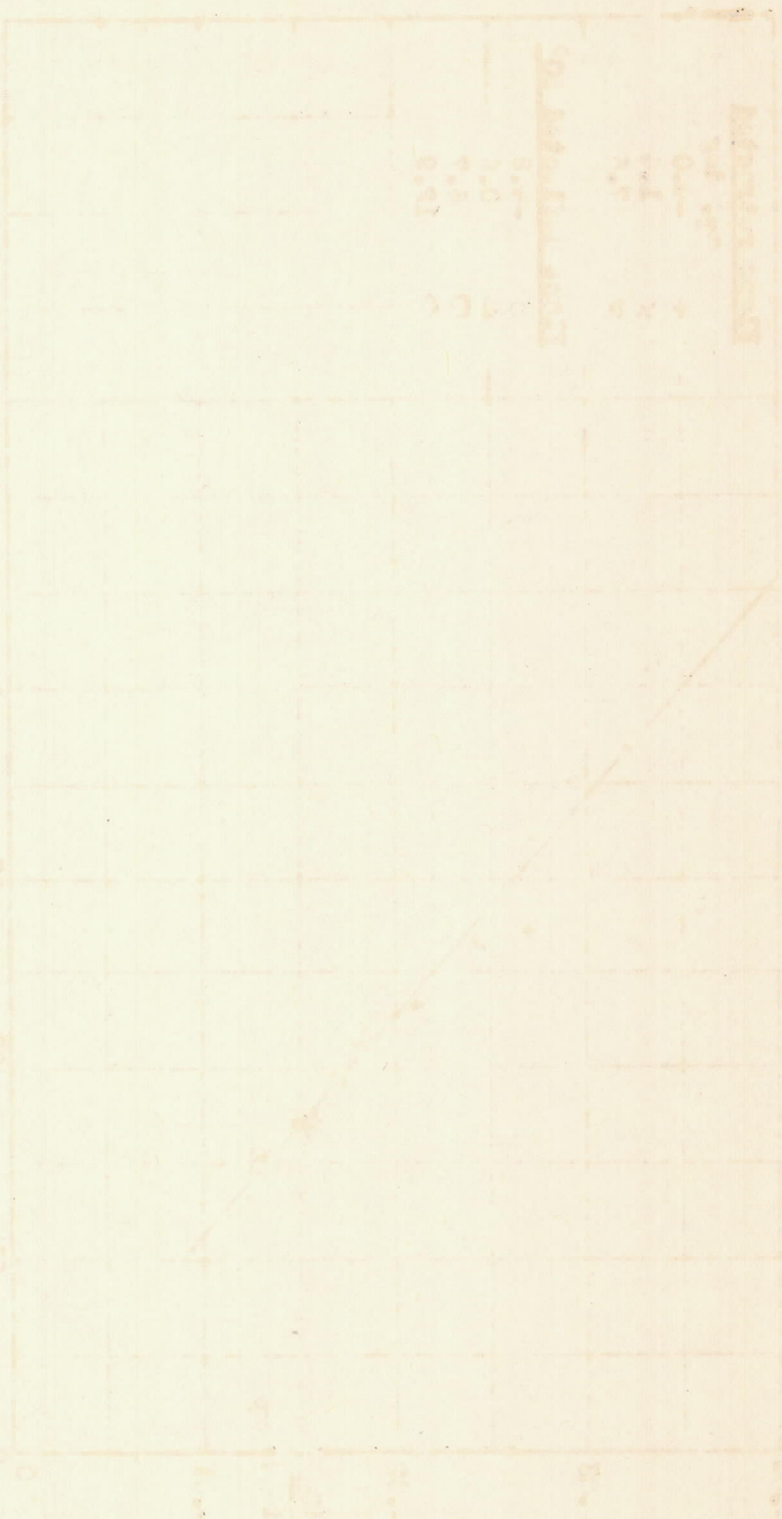

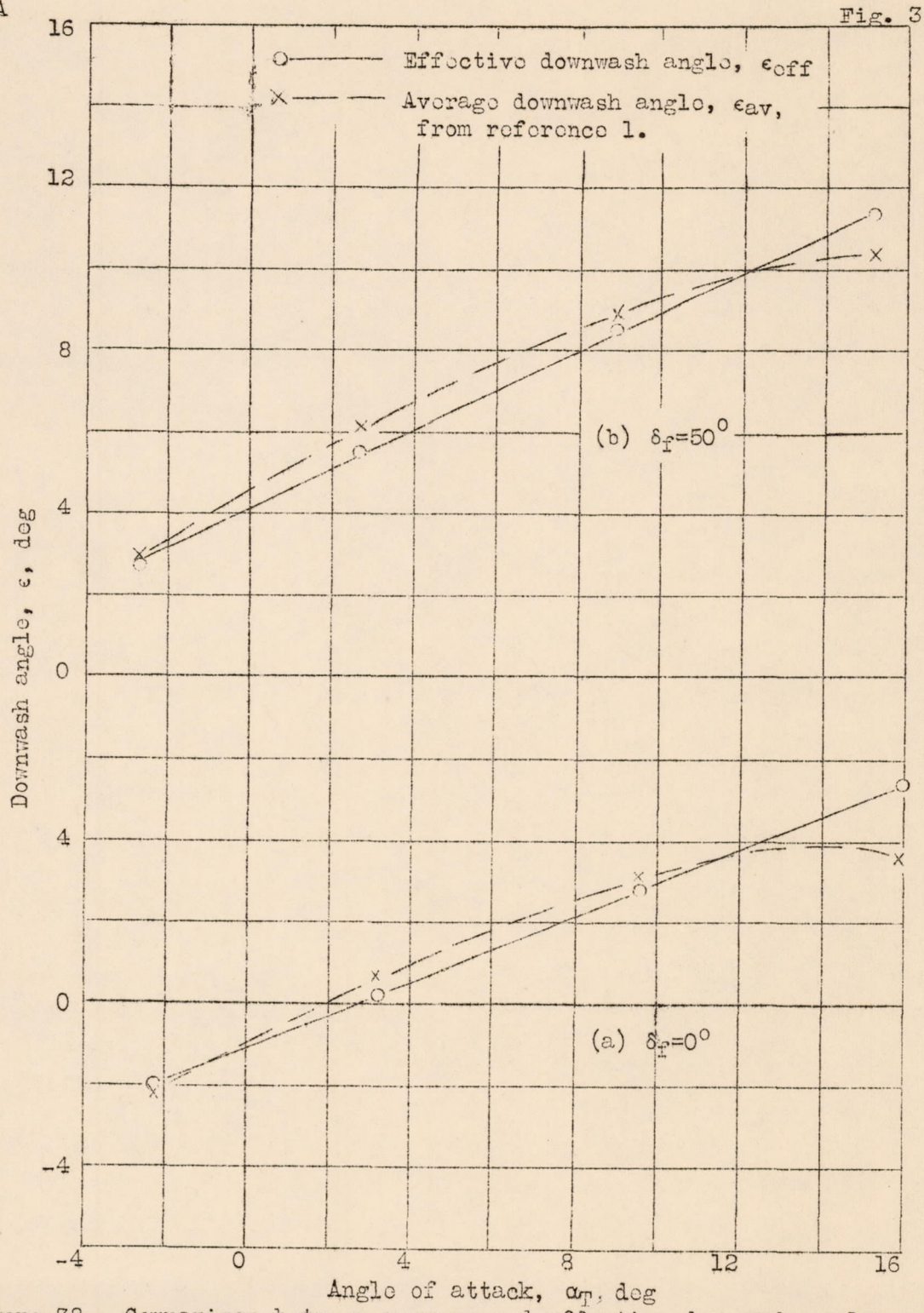

Figure 38.- Comparison between average and effective downwash angles at tail. Propellers removed; nacelles on.

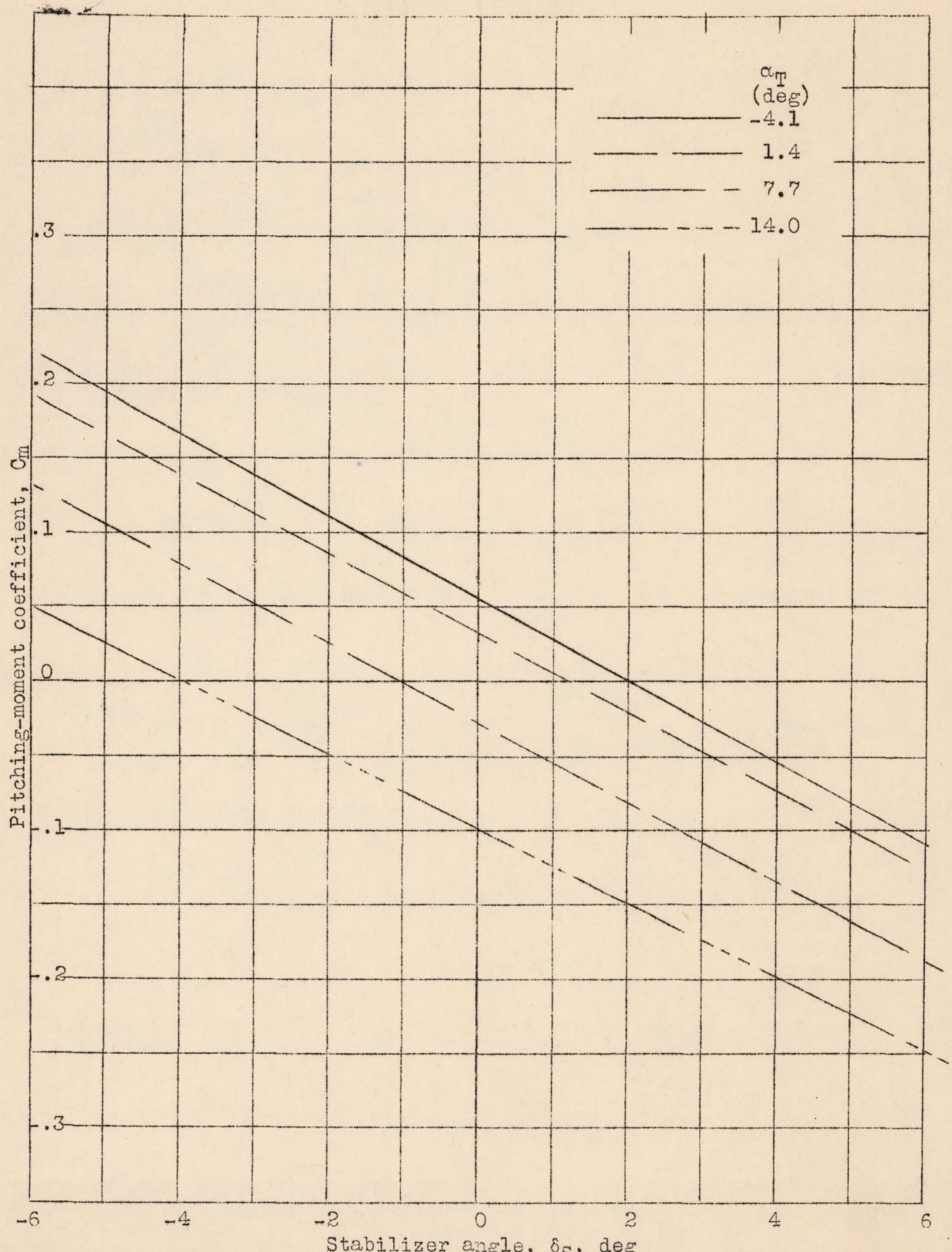

Figure 39.- Variation of C_m with δ_S at various angles of attack. T_c, 0.161; δ_f, 0°; nacelles off.

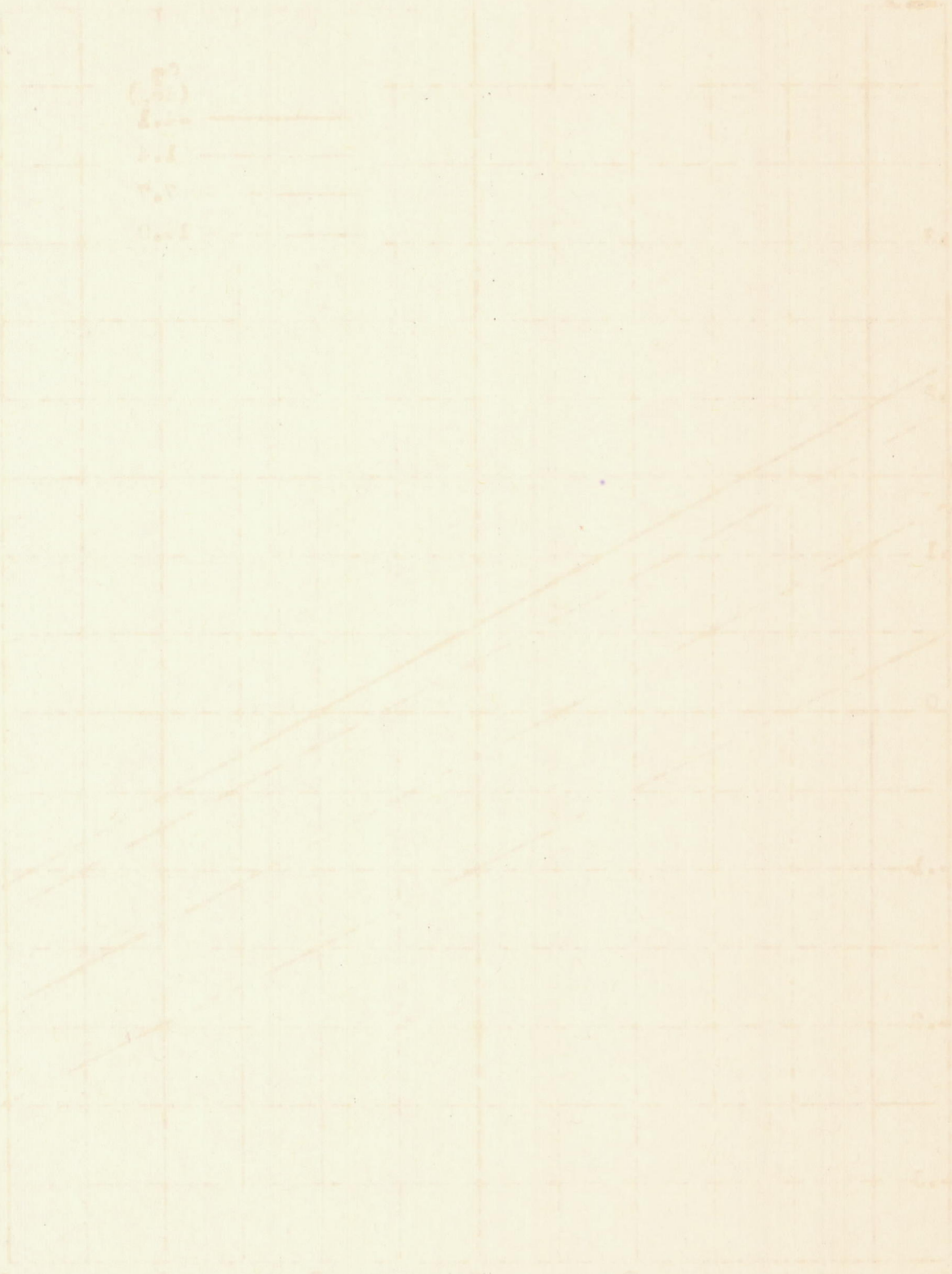

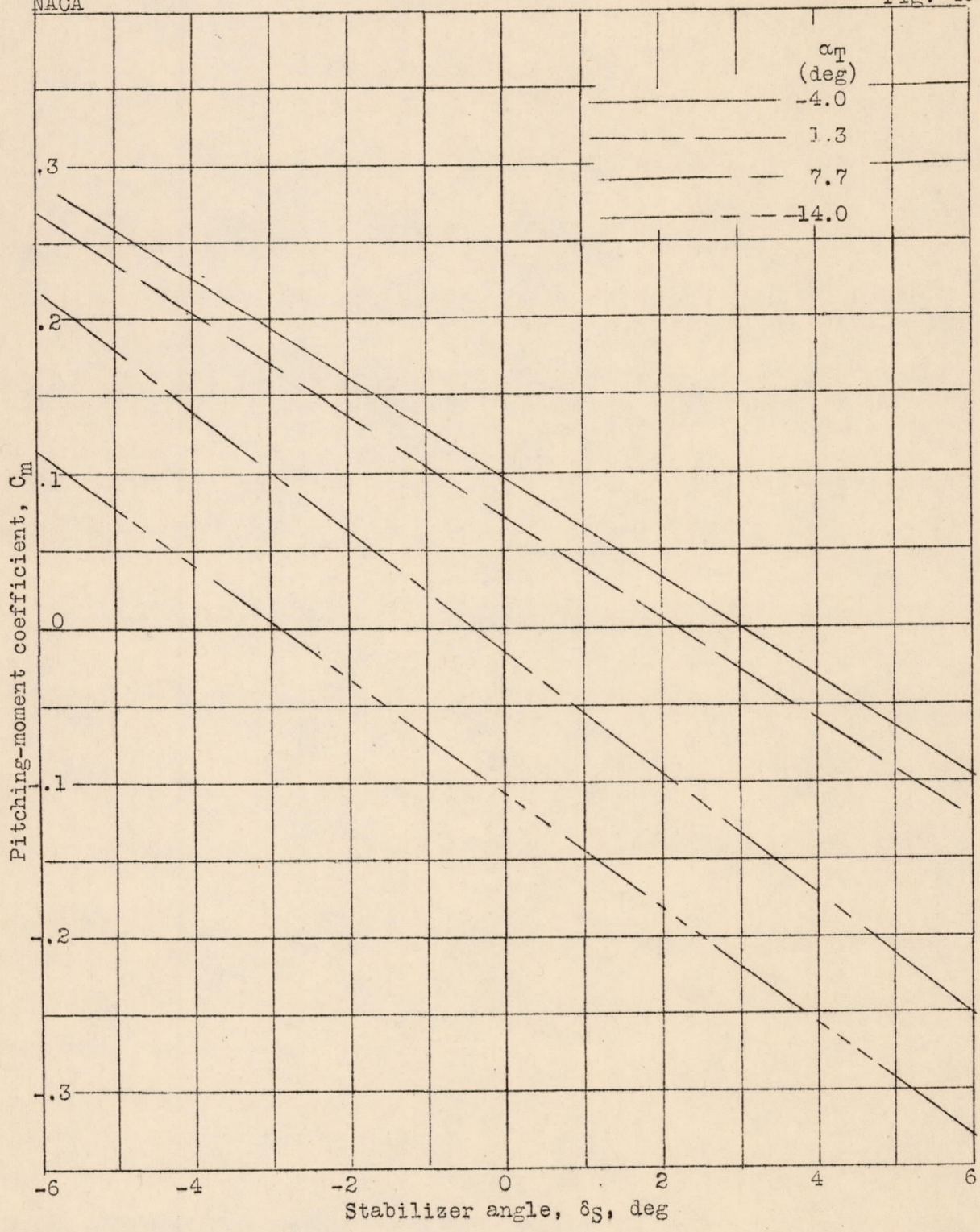

Figure 40.- Variation of C_m with δ_S at various angles of attack. T_c, 0.619; δ_f, 0°; nacelles off.

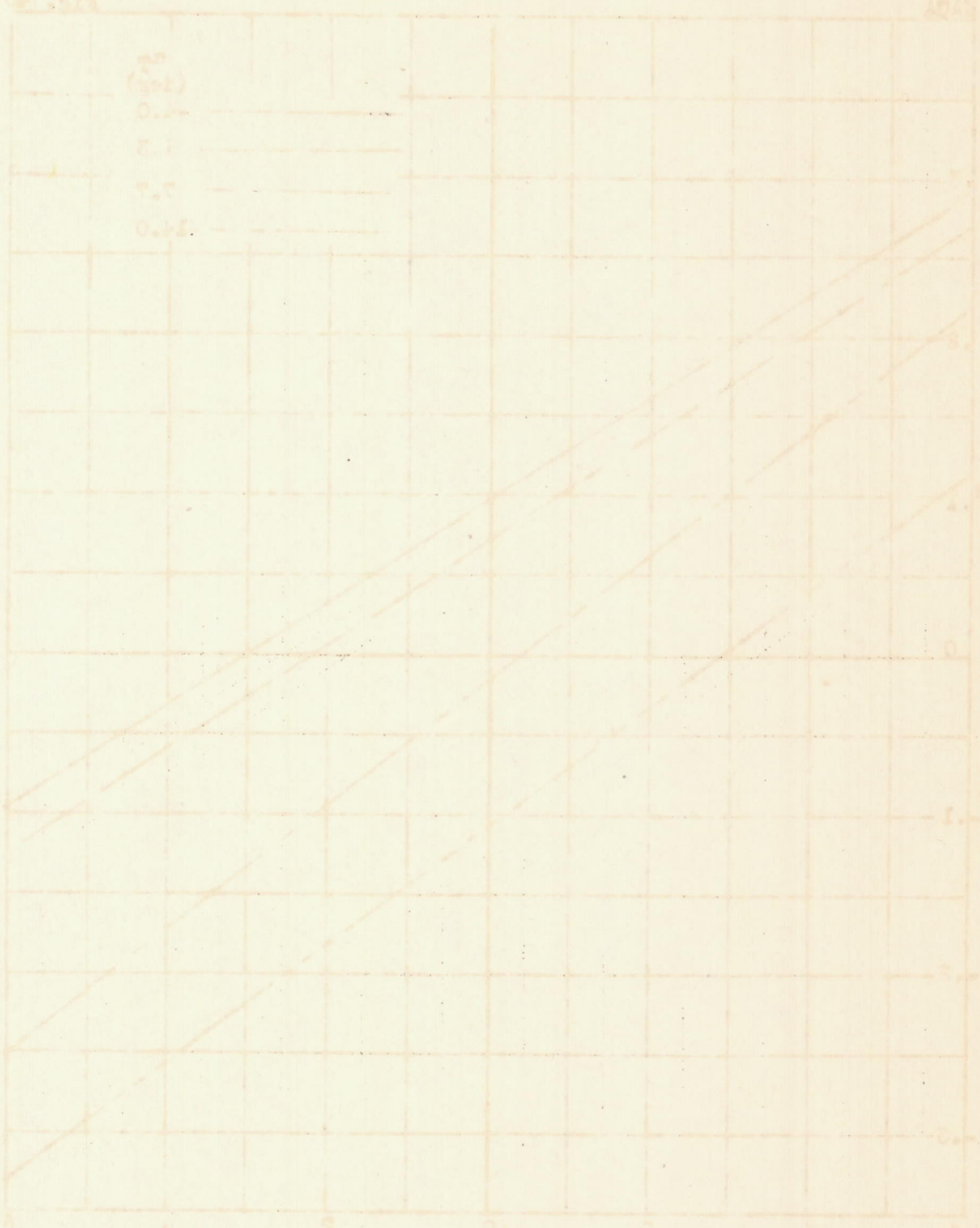

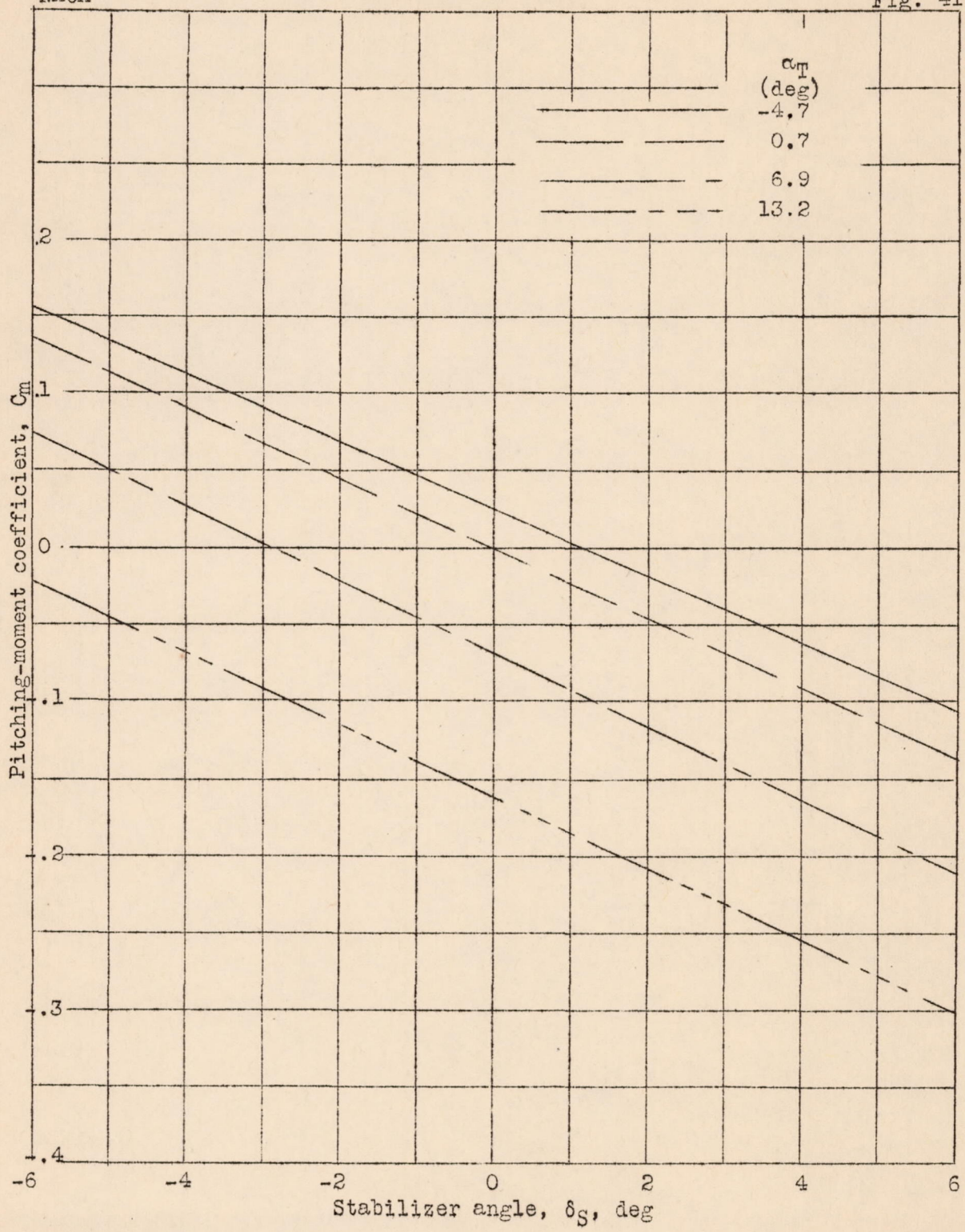

Figure 41.- Variation of C_m with δ_S at various angles of attack. T_c, 0.161; δ_f, 50°; nacelles off.

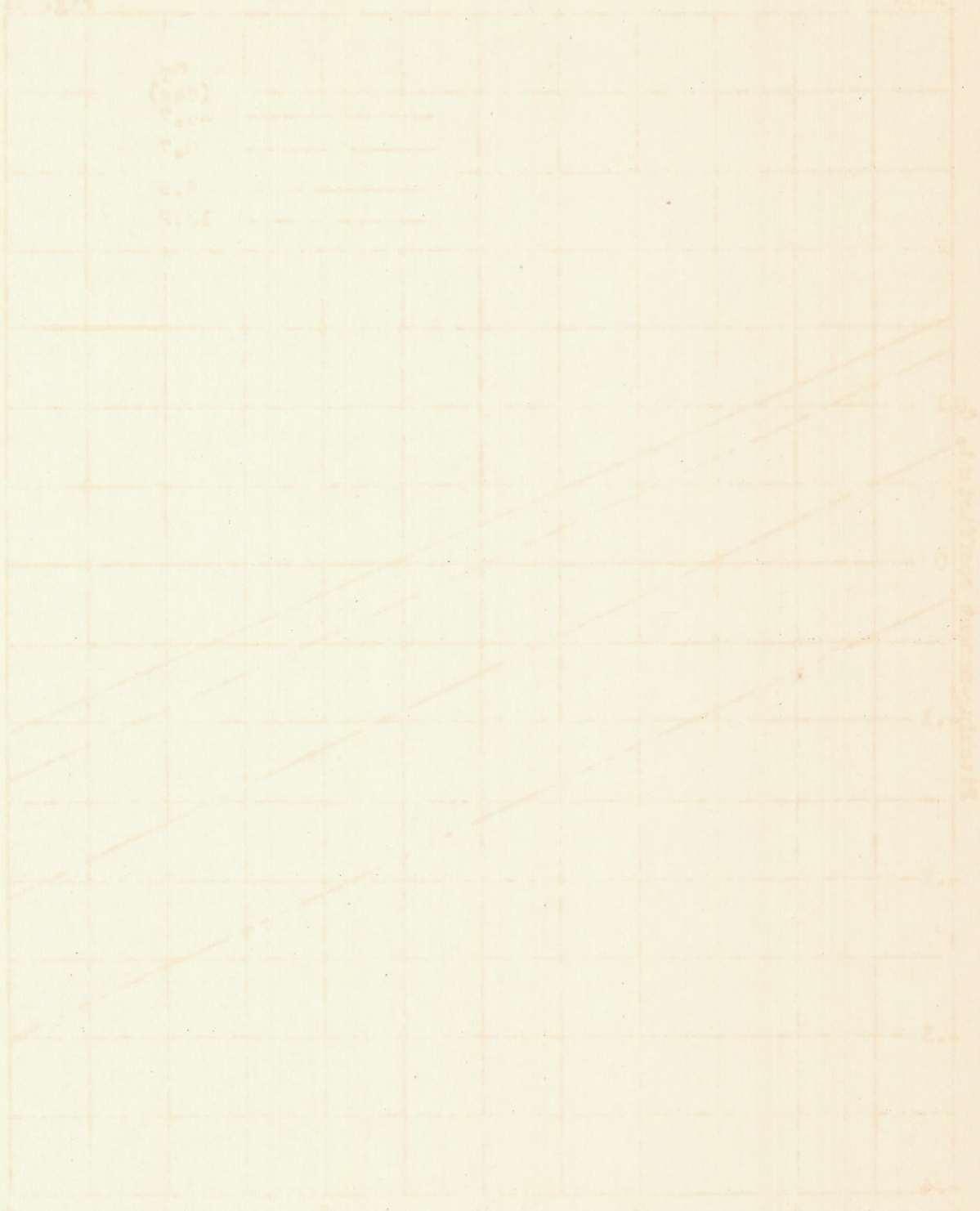

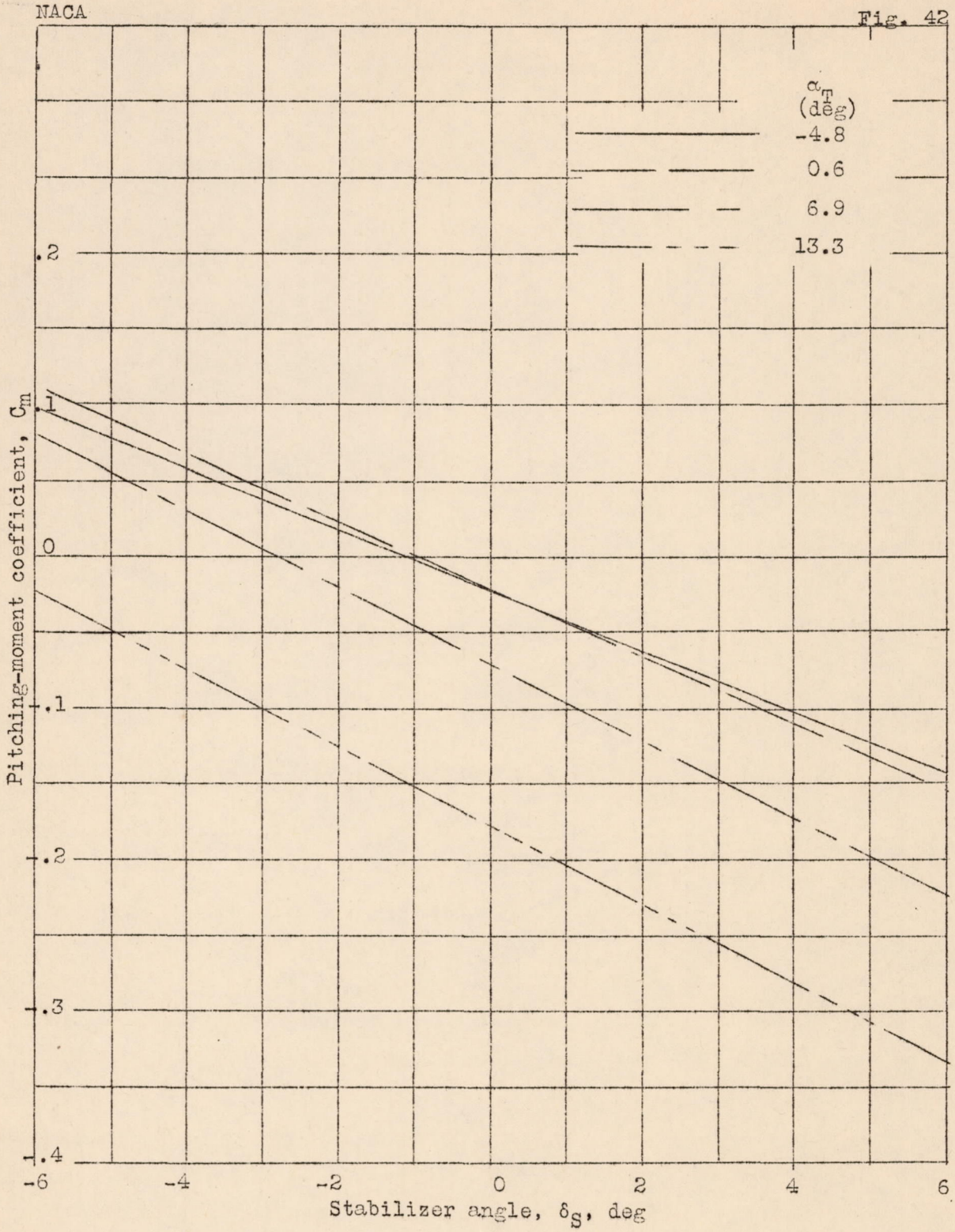

Figure 42.- Variation of C_m with δ_S at various angles of attack. T_c, 0.619; δ_f, 50°; nacelles off.

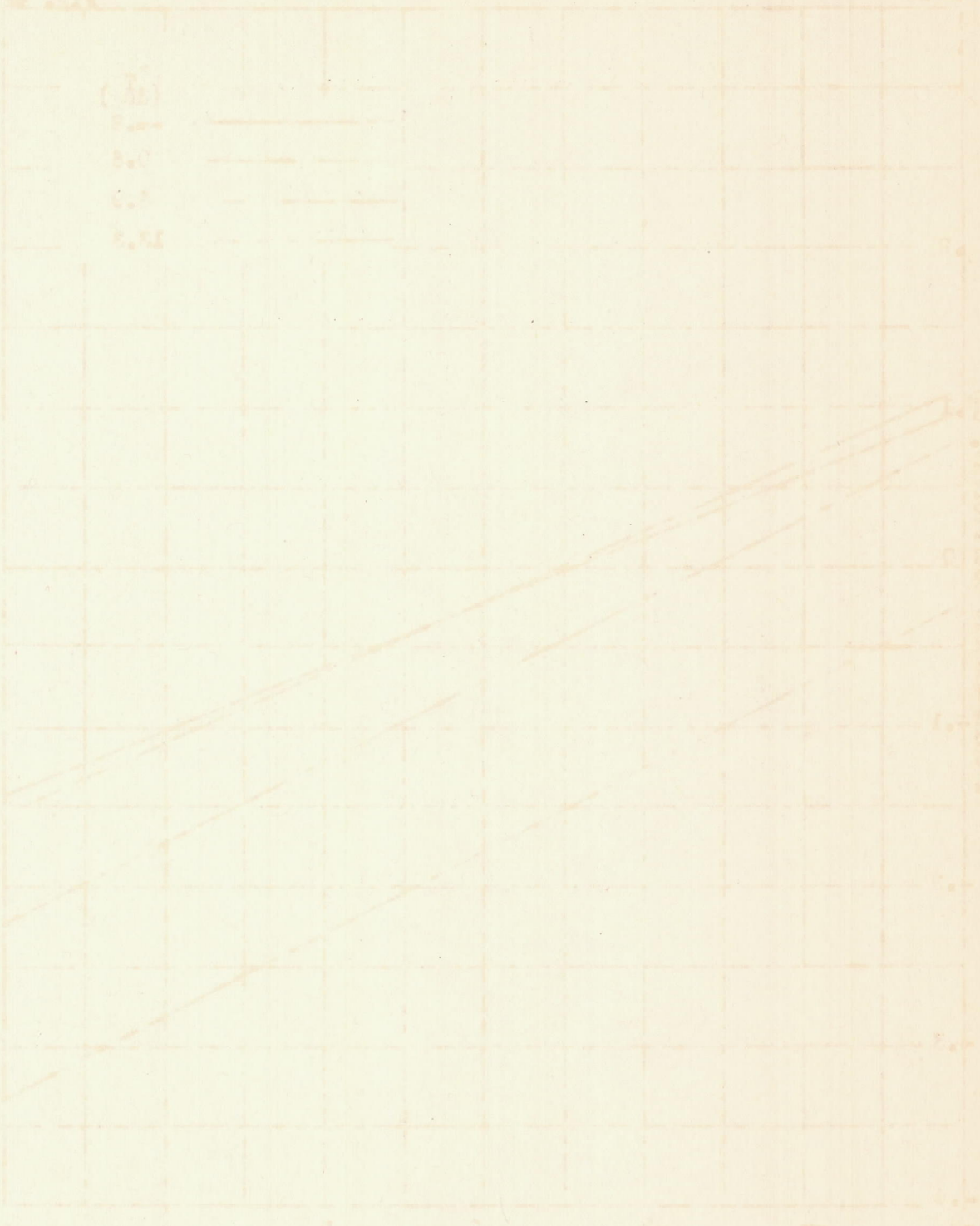

L-425

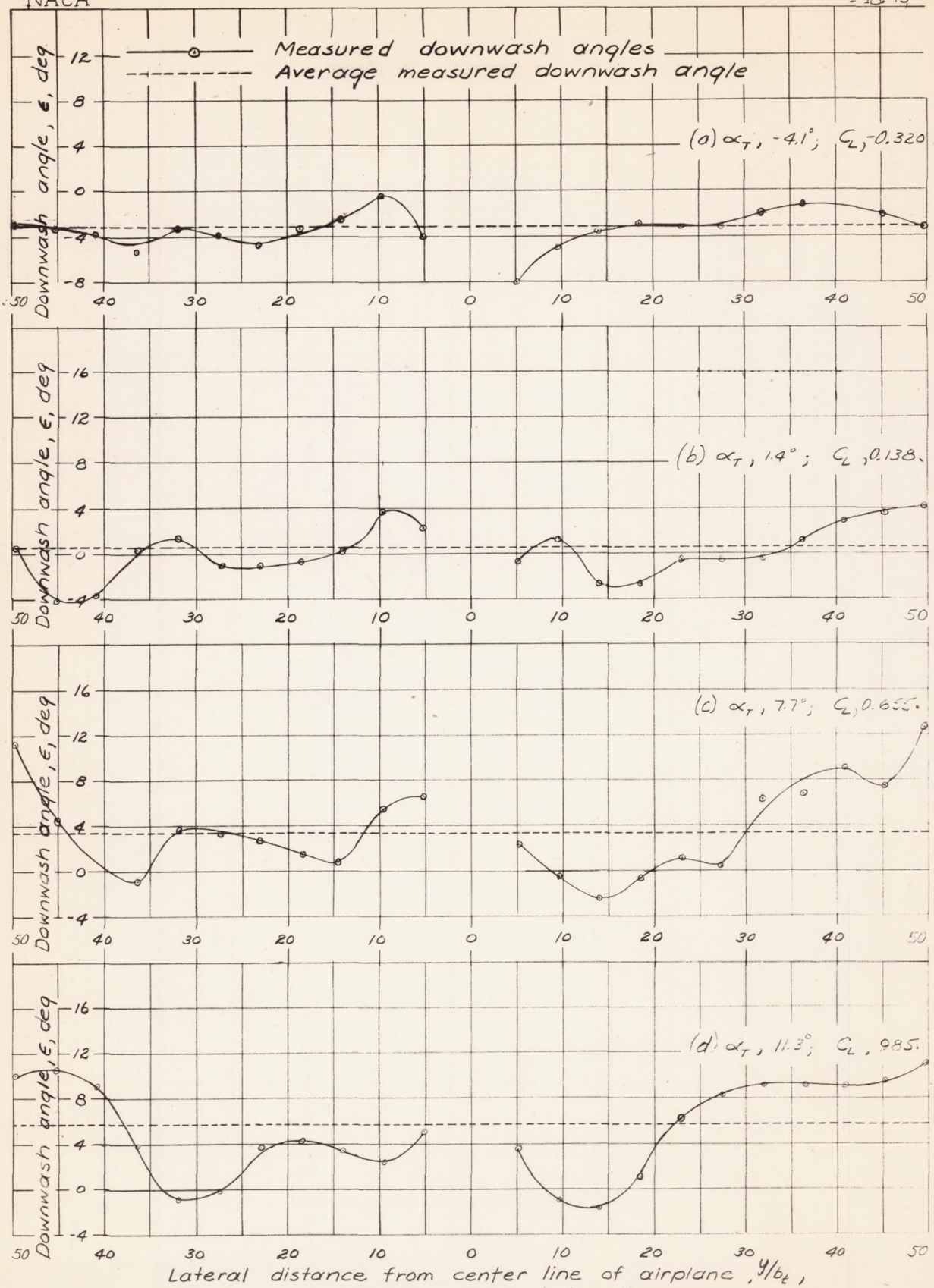

Figure 43.- Distribution of downwash across span of horizontal tail surface. T_c, 0.161; δ_f, 0°; nacelles off. Values of ε from ref. 1.

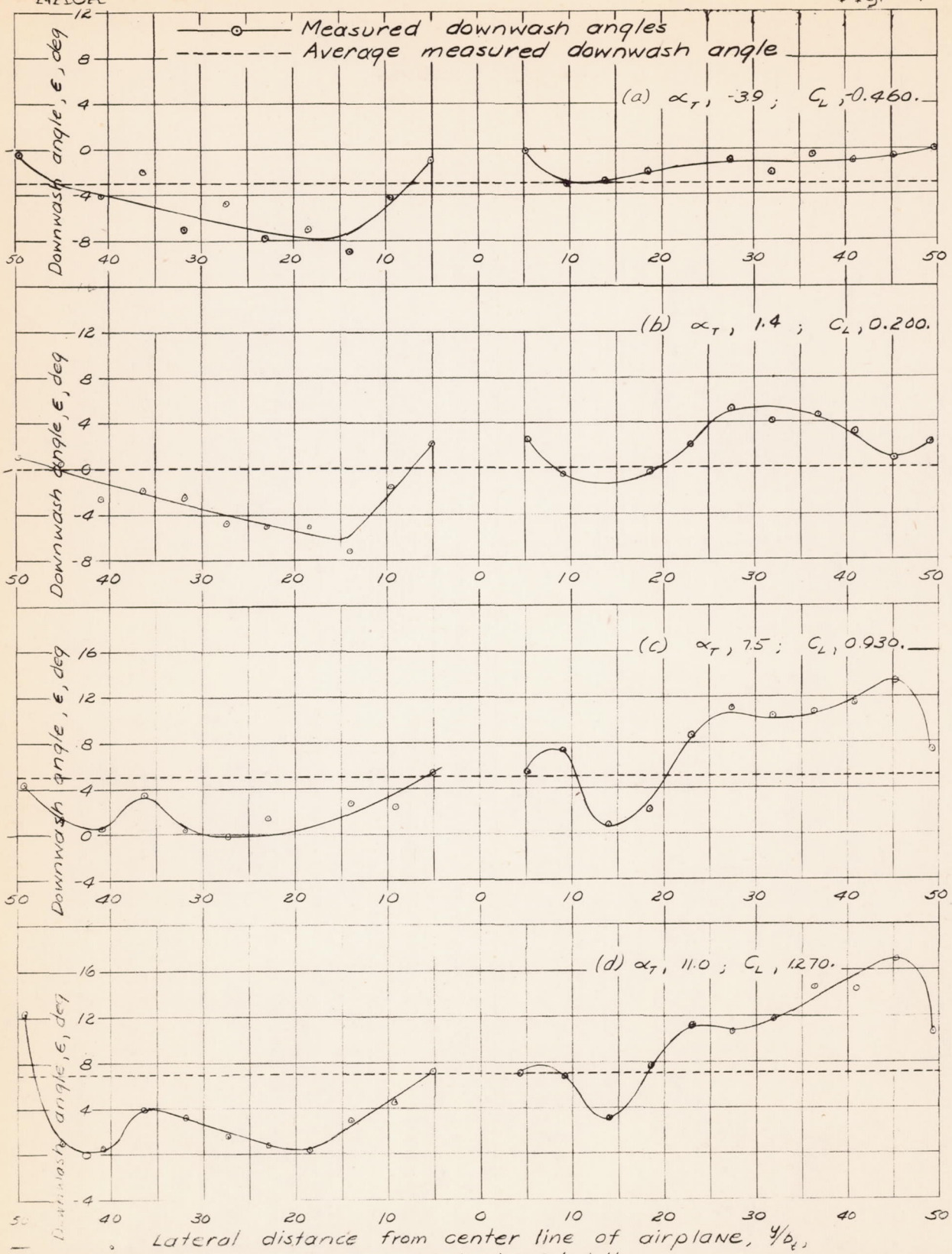

Figure 44.- Distribution of downwash across span of horizontal tail surface. T_c, 1.30; $\delta_f = 0°$; nacelles off. Values of ϵ from reference 1.

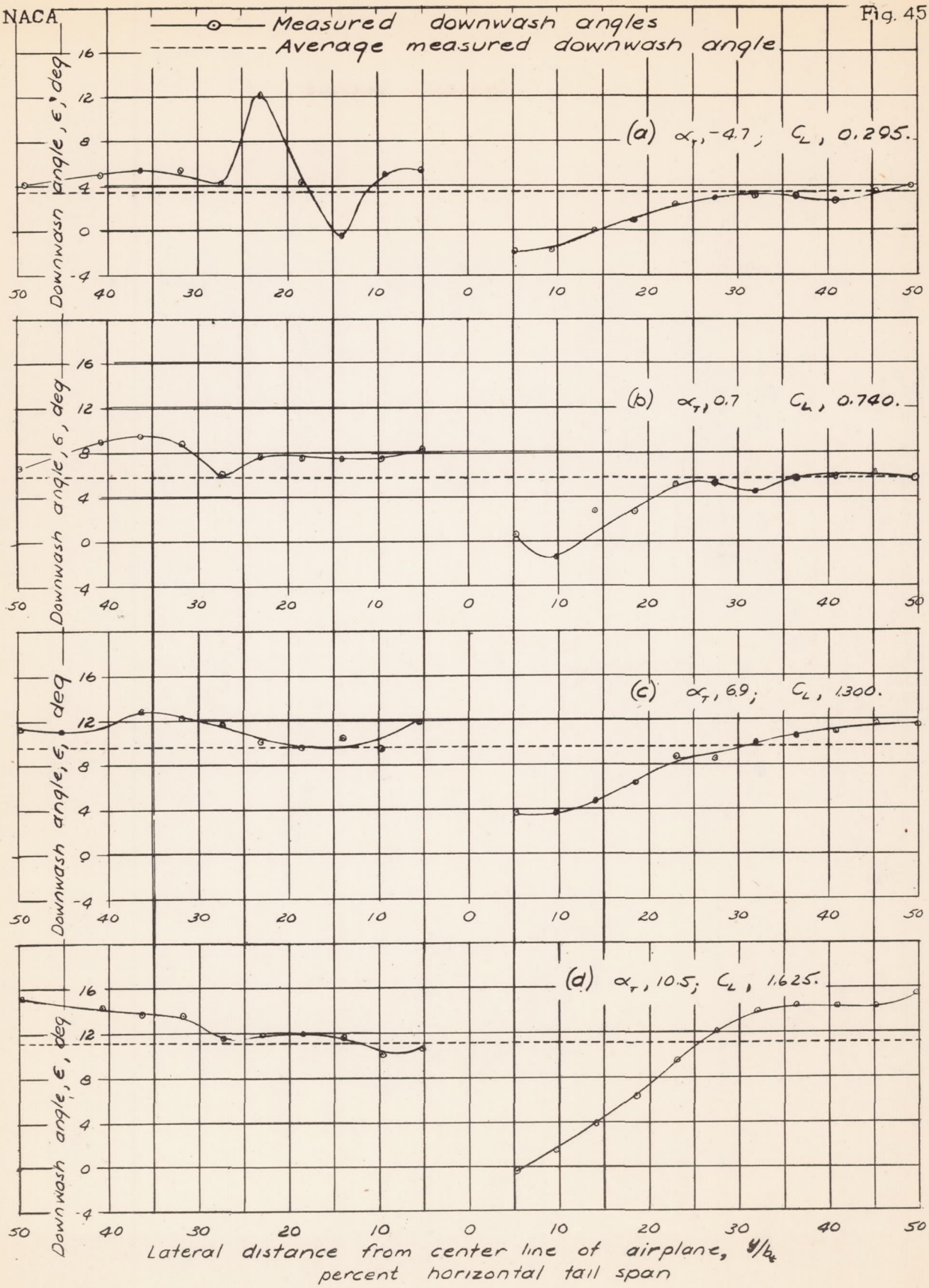

Figure 45.- Distribution of downwash across span of horizontal tail surface. T_c, 0.161; δ_f, 50°; nacelles off. Values of ϵ from reference 1.

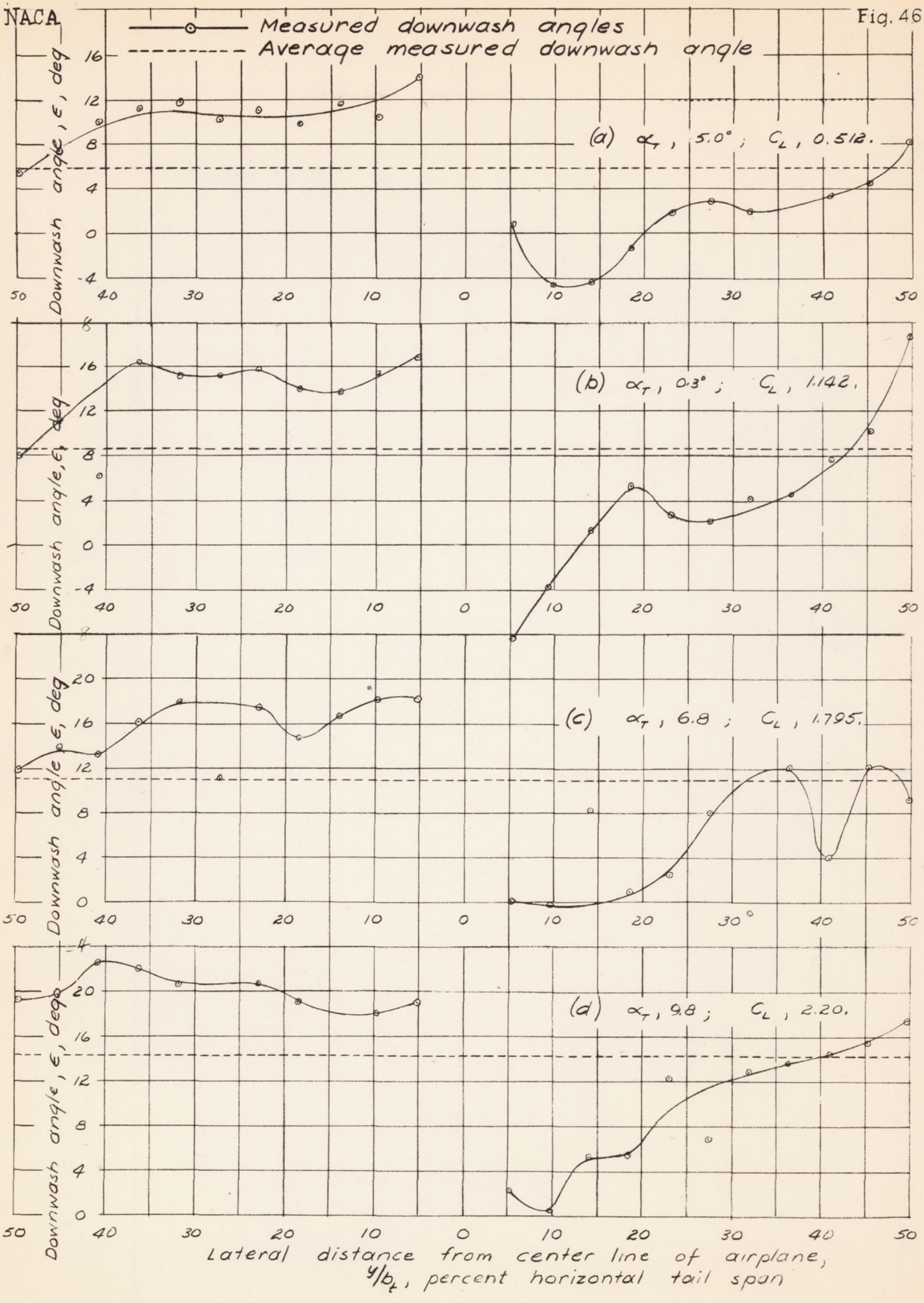

Figure 46.- Distribution of downwash across span of horizontal tail surface. T_c, 1.30; δ_f, 50°; nacelles off. Values of ϵ from reference 1.

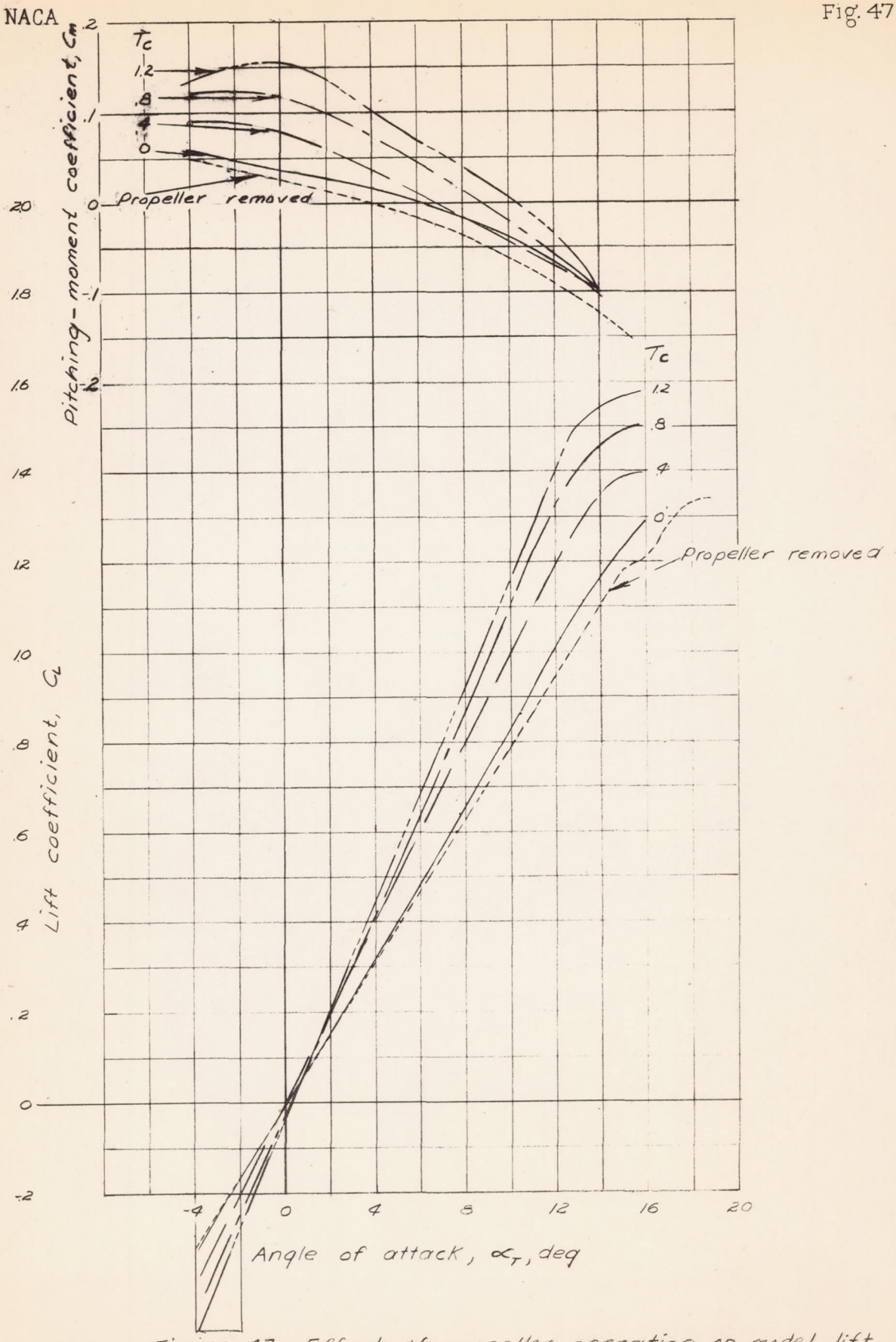

Figure 47 - Effect of propeller operation on model lift and pitching-moment coefficients. δ_f, 0°; horizontal tail on; nacelles off.

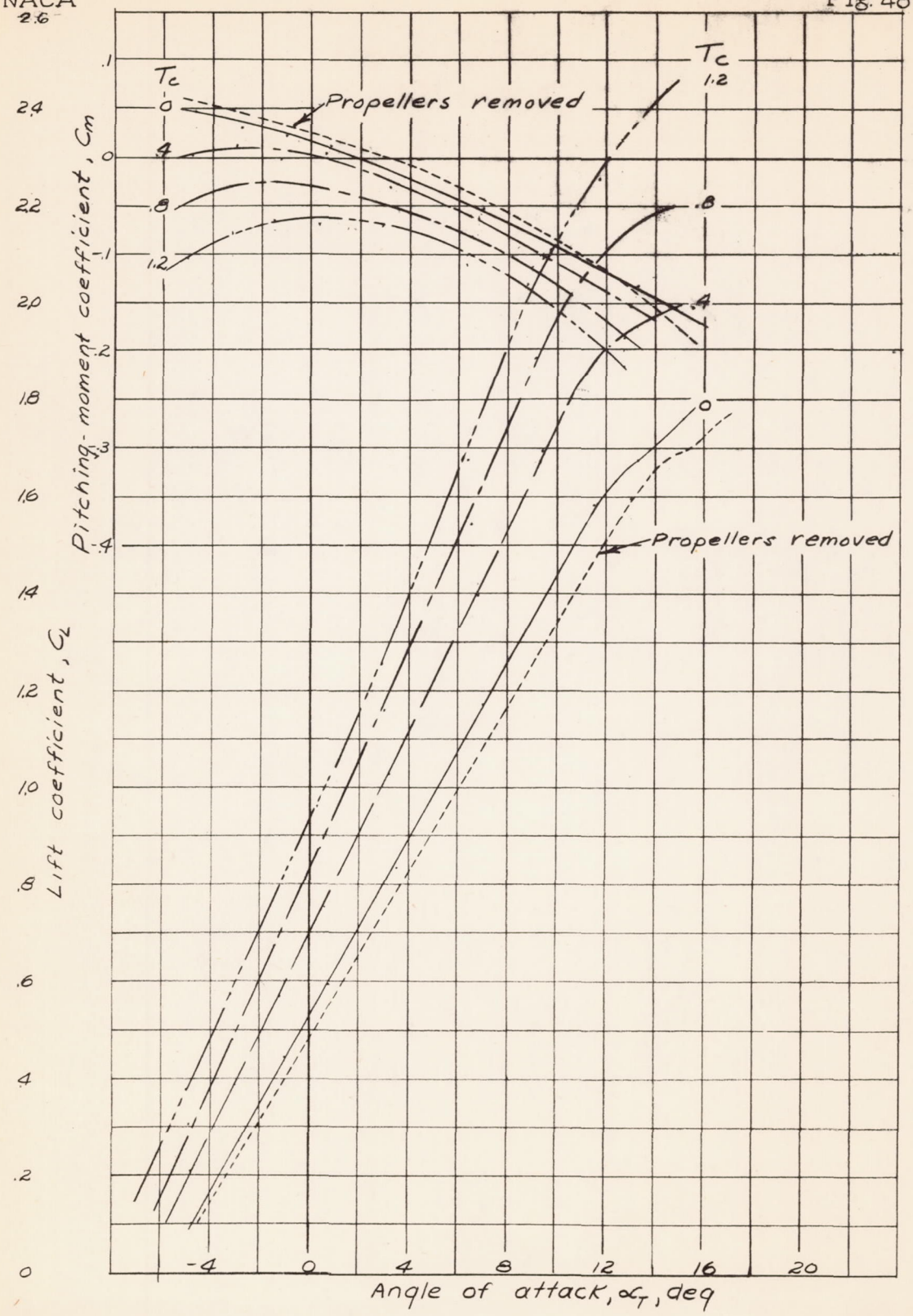

Figure 48.- Effect of propeller operation on model lift and pitching-moment coefficients. δ_f, 50°; horizontal tail on; nacelles off.

L-425

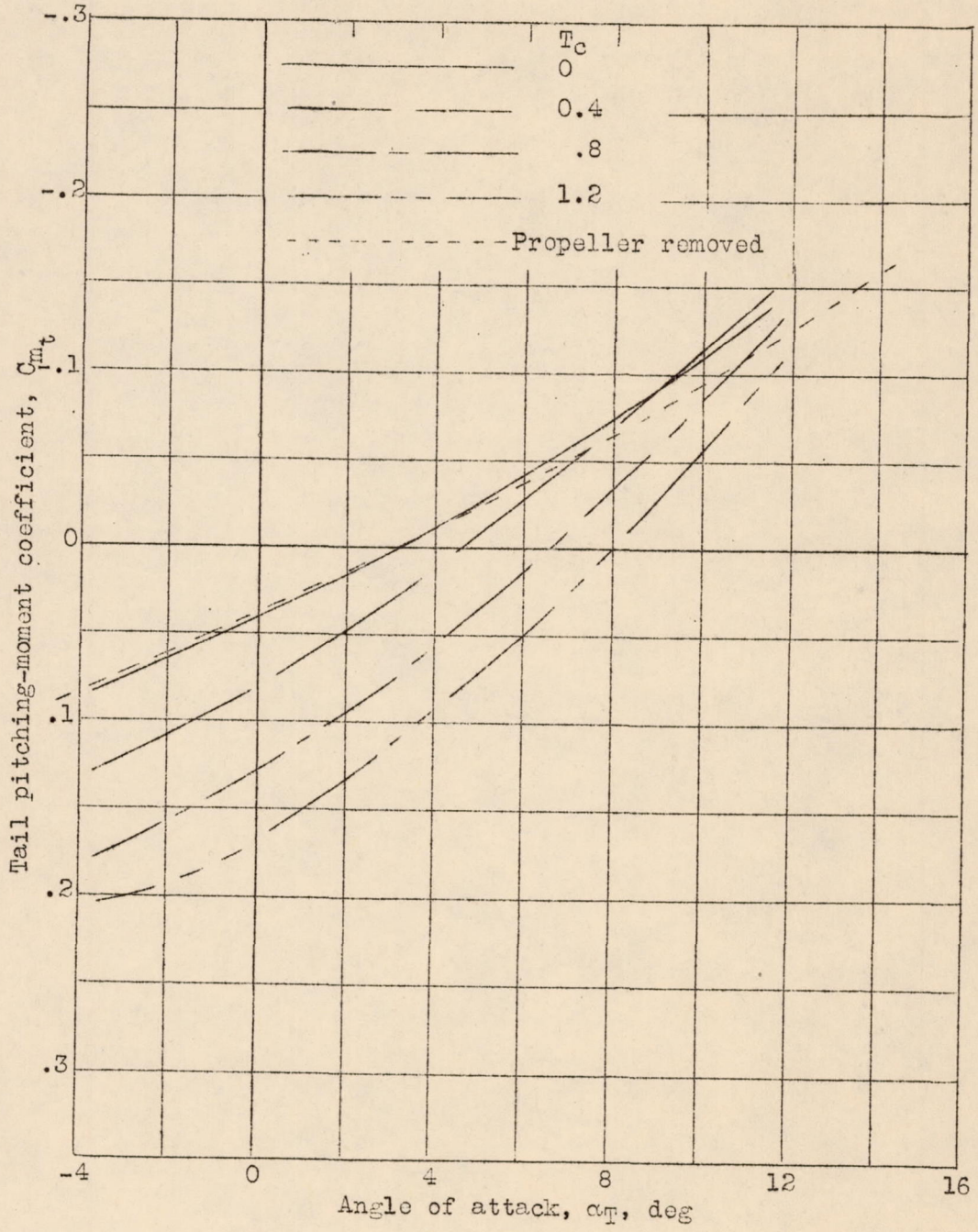

Figure 49.- Variation of tail pitching-moment coefficient with angle of attack. Nacelles off; $\delta_t = 0^\circ$.

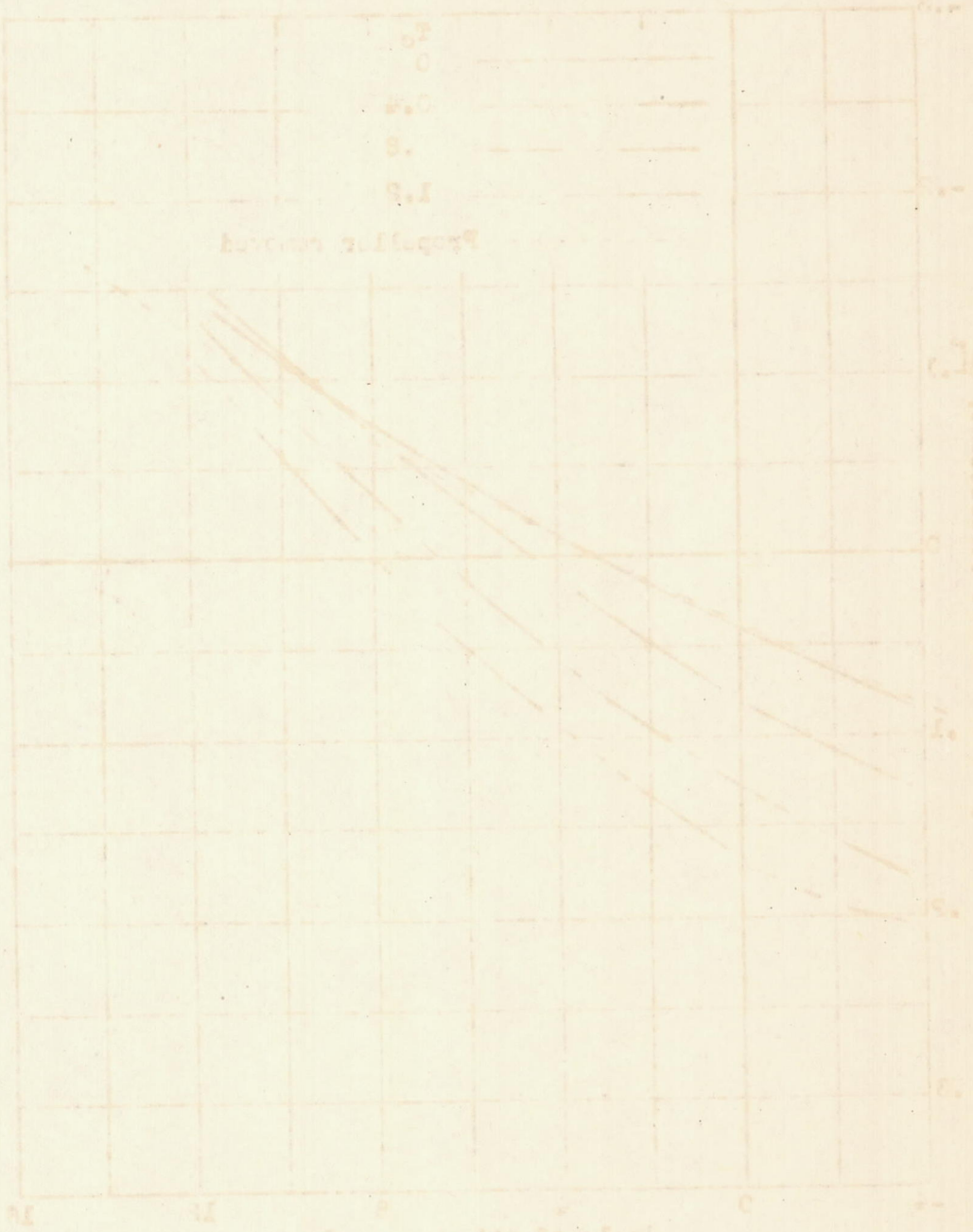

L-425

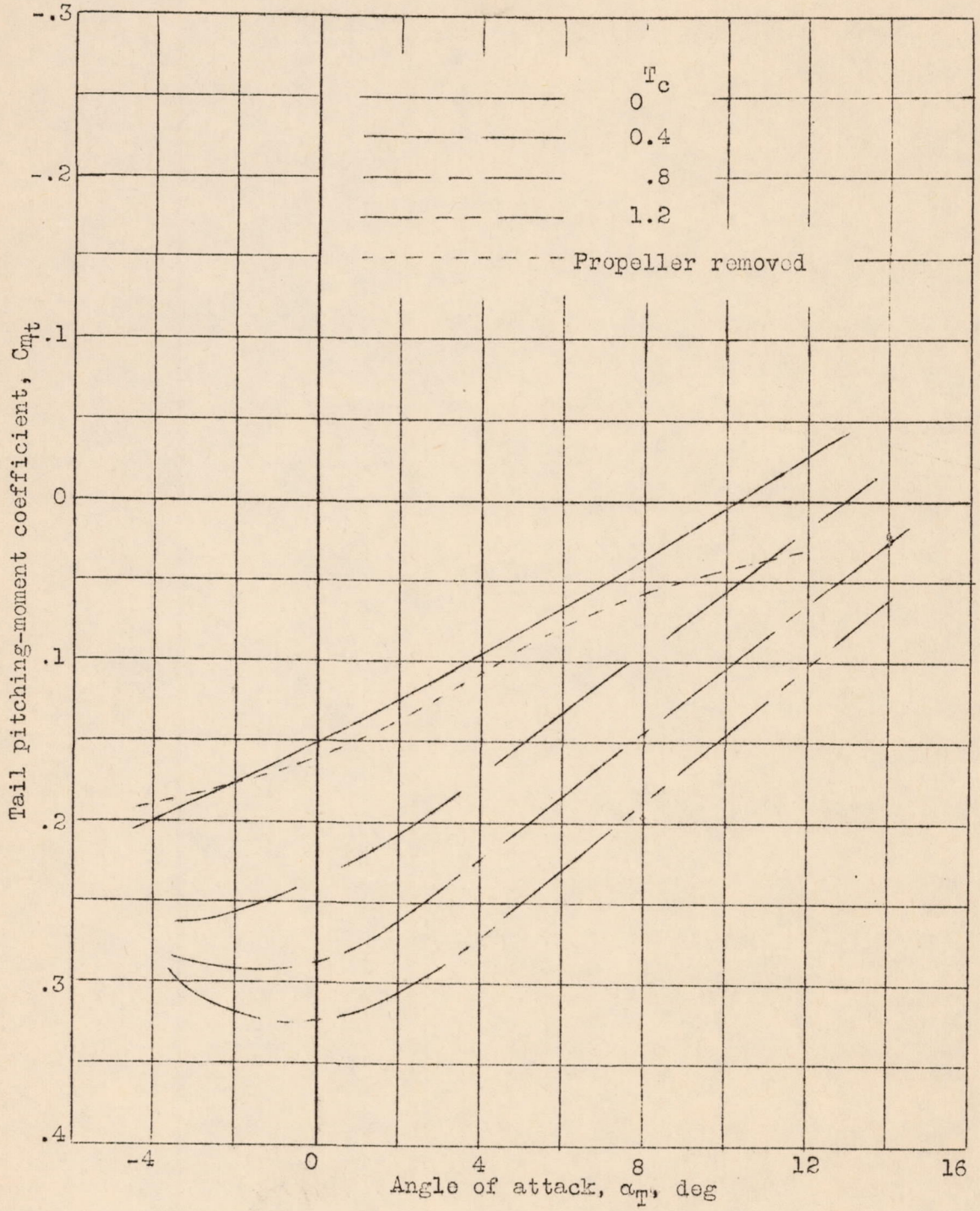

Figure 50.- Variation of tail pitching-moment coefficient with angle of attack. Nacelles off; $\delta_t = 50^\circ$.